Metal silsesquioxanes as precursors to microporous metallosilicates

Metal Silsesquioxanes as Precursors to Microporous Metallosilicates

PROEFSCHRIFT

ter verkrijging van de graad van doctor aan de Technische Universiteit Eindhoven, op gezag van de Rector Magnificus, prof.dr. R.A. van Santen, voor een commissie aangewezen door het College voor Promoties in het openbaar te verdedigen

op woensdag 3 april 2002 om 16.00 uur

door

Nicolae Maxim

geboren te Medias, Roemenië

Dit proefschrift is goedgekeurd door de promotoren:

prof.dr. R.A. van Santen
en
prof.dr. G. de With

Copromotor:
dr. H.C.L. Abbenhuis

CIP-DATA LIBRARY TECHNISCHE UNIVERSITEIT EINDHOVEN

Maxim, Nicolae

Metal silesquioxanes as precursors to microporous metallosilicates / by Nicolae Maxim. - Eindhoven : Technische Universiteit Eindhoven, 2002.
Proefschrift. - ISBN 90-386-2683-5
NUGI 813
Trefwoorden: heterogene katalyse / microporeuze materialen; silicaten / silsequioxanen / katalysatoroppervlak / metaaloxiden; nanodeeltjes
Subject headings: heterogeneous catalysis / microporous materials; silicates / silsesquioxanes / catalytic surface area / metal oxides; nanoparticles

The work described in this thesis has been carried out at the Schuit Institute of Catalysis (part of the Netherlands School for Catalysis Research), Laboratory of Inorganic Chemistry and Catalysis, Eindhoven University of Technology, The Netherlands

Druk: Universiteitsdrukkerij, Technische Universiteit Eindhoven

to Monica, Andra

and

my parents

Contents

1

Introduction

In this chapter the importance of catalysis for society is outlined. A brief introduction is given to the preparation methods for oxide catalysts. Several characteristics of heterogeneous metal catalysts essential for catalysis and their relation with the preparation procedure are mentioned. Silsesquioxanes and their applications are shortly described as a new methodology for preparation of microporous metallosilicate catalysts derived from these compounds is to be reported. In the end, the general scope of this thesis is presented.

1.1 Catalysis and catalyst development

The development of society and chemistry are closely related. The chemistry provides society with prosperity by its contributions to health care, agriculture, transportation, etc., while society pushes chemistry forward by constantly presenting new demands to chemical processes, waste stream reductions, new product developments, etc. Catalysis is at the frontier of this quickly changing interface since it is the key to efficient chemical processing. Almost 80 % of all chemicals, including important compounds such as ammonia, sulfuric acid or petrochemical derivatives are obtained with the aid of one or more catalysts. Moreover, while only a very small portion of the world production is spent on catalysts, almost 25 % of the world production is achieved with the aid of catalysts. Therefore, catalyst development plays an important role in the relationship between society and catalysis.

Catalysts are substances that increase the rates of chemical reactions without affecting the equilibrium and, ideally, without being consumed. Catalysts work by forming chemical bonds with reactants and providing energetically favorable pathways for their conversion into products. Catalysis may occur in a single gas or liquid phase (homogeneous catalysis) or in a multiphase mixture such as gas–solid mixture (heterogeneous catalysis).

Catalyst developement is largely a matter of trial and error testing. The methodology was defined in the first half of the last century by Haber, Bosch and Mittasch in the development of the ammonia synthesis process.[1,2] They tested more than 20,000 samples as candidate catalysts. The results led to the identification of an iron-containing mineral that is similar to today's industrial catalysts for ammonia synthesis. The researchers recognized the need for porous catalytic materials and materials with more than one component, today identified as the support, the catalytic active component, and the promoter. Nowadays, catalyst design can take advantage of new preparation methods with added variability and flexibility and of materials that were not available in the past.

Catalyst testing and evaluation have been revolutionized by computers, automated test reactors and analytical methods. With modern equipment, researchers can systematically prepare and screen many catalysts in a short time and efficiently determine their catalytic activity, selectivity and stability.

1.2 Preparation of oxide catalysts

The activity and selectivity of heterogeneous catalysts generally depend on the state of metal dispersion (particle size), structure (shape and morphology), metal composition and metal-support interaction. Catalytically active metals are usually dispersed on supports in order to reduce the size of the active metal crystallites to a diameter from twenty to several hundred angstroms and thereby prevent further metal agglomeration that would reduce the surface area.

It has been long recognized that the properties of catalysts often depend on their preparation method. For example, the dispersion and size distribution of metal

crystallites, their spatial distribution on the support, the homogeneity of components in a multicomponent catalyst, the porosity, surface area and pore size distribution of a support are all sensitive functions of the precursors used and the preparation conditions.[3,4]

Various methods for the preparation of heterogeneous metal catalysts have been developed to achieve high activity and selectivity, the most common being the impregnation[5] and the sol-gel[6,7] methods.

In the impregnation method, typically, a solution of inorganic salt such as a metal nitrate or chloride is adsorbed ("impregnation") in a supporting material such as SiO_2, Al_2O_3, zeolite, or carbon, followed by oxidation ("calcination") which, results in formation of dispersed metal oxide crystallites. Depending on the reaction that has to be catalyzed, the catalysts are used in the oxidized state or they are further reduced (by hydrogen or hydride reagents) to form dispersed metal particles.

Multicomponent gels can also be used as precursors to prepare multicomponent oxides or metal supported on oxide over a large range of compositions. In the sol-gel method a mixture of metal alkoxides in an organic medium is hydrolyzed by addition of water, followed by polymerization of the hydrolyzed alkoxides through condensation of hydroxyl and/or alkoxy groups. The gel is further dried and calcined.

Although these methods are conventionally used for production of commercial catalysts, such as Cr/SiO_2 for ethylene polymerization, $Ag\text{-}Al_2O_3$ for selective ethylene oxidation or Ga-ZSM-5 for oligomerization of light olefins, sometimes, they do not provide a good control of particle size distribution and metal composition, mainly because of the complicated reactions involved in the catalyst preparation procedures. For example, the homogeneity of the multi-component gels, in terms of the distribution of various components, strongly affects the properties of the final oxide material. If the hydrolysis and condensation rates of the metal precursors are very different this will result in formation of a gel with inhomogeneous metal distribution and segregation of the metal oxides after calcination.[8]

The preparation methods such as coprecipitation, impregnation, solid state reaction, etc. used to prepare multimetallic catalysts rely on interdiffusion of

components during thermal treatment. Because of the slow solid state diffusion, often high temperatures are used, which results in low surface area materials. If preformed complexes, which already contain the desired ratio of components are used as precursors, it is possible to prepare homogeneous multicomponent catalysts with lower temperature treatments.[9,10] The use of these compound precursors guarantees that the different metal components are atomically mixed in the precursor. Thus, it is expected that homogeneous multicomponent oxides can be obtained subsequently with rather mild treatments. However, because these metal complexes are stoechiometric compounds the range of compositions is limited.

All these preparation methods have their advantages and limitations with respect to the chemical compositions, homogeneity, ease of control of stoechiometry, porosity and surface area of the final oxide catalyst, and cost.

This thesis deals with the development of a new methodology for preparation of silica based metal oxide catalysts that use metal silsesquioxanes as precursors. As described further the calcination of metal silsesquioxanes produces amorphous microporous materials characterized by high surface area, narrow pore size distribution and high metal oxide dispersion. Moreover, the calcination of mixtures of metalsilsesquioxanes allows the preparation of silica catalysts containing very small and well dispersed particles of mixed metal oxides.

1.3 Silsesquioxanes

Silsesquioxane is the general name for a family of molecular spherosilicates with the formula $[RSiO_{3/2}]_n$, where R is an inorganic or organic group and n can be between 4 and about 30, but typically 6, 8, 10 or 12. These **p**olyhedral **o**ligo**sil**s**e**squioxanes (also referred to as POSS) are usually formed by hydrolytic multiple condensation of $RSiY_3$ (where Y is a highly reactive substituent such as Cl or an alkoxide and R and alkyl group such as isobutyl, cyclopentyl or cyclohexyl) in an acetone/water mixture to form dimers, quadrimers, etc.[11] Examples of incompletely condensed materials are shown in Figure 1.1.

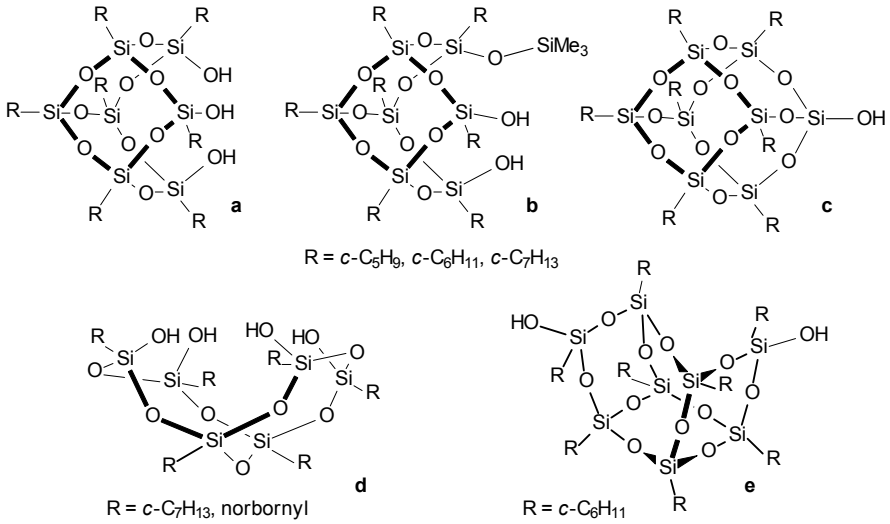

Figure 1.1 Incompletely condensed silsesquioxanes.

The preparation of incompletely condensed silsesquioxanes via hydrolytic condensation of trifunctional silanes is a slow process that normally takes months. However, the use of reflux methods reduces the synthesis time to days.[12] Moreover, it was recently shown that incompletely condensed silsesquioxanes can be prepared in high yield within hours by base–mediated cleavage of fully condensed [$RSiO_{3/2}$] frameworks which are instead easily available.[13]

Silsesquioxanes are used in various applications such as precursors for highly defined SiO_2 films (used for electrical insulation, anti reflective coatings and optical filters), in the production of specialized silicon oxi carbide ceramics or in the formation of inorganic/organic hybrid materials.[14-19] These structurally well defined materials have been extensively used as model compounds to mimic silica surfaces and as ligands for catalytic active metals to model the active sites of heterogeneous catalysts.[20,21]

Metal substituted silsesquioxanes result from the reaction of an incompletely condensed silsesquioxane with a metal precursor. An example of such a reaction is

the, so-called, corner capping reaction of a silsesquioxane trisilanol with a trifunctional metal reagent. Nowadays, the metals incorporated into the Si/O skeleton of silsesquioxanes include main group, early and late transition metals, as well as chalcogens (see Figure 1.2).[22-29]

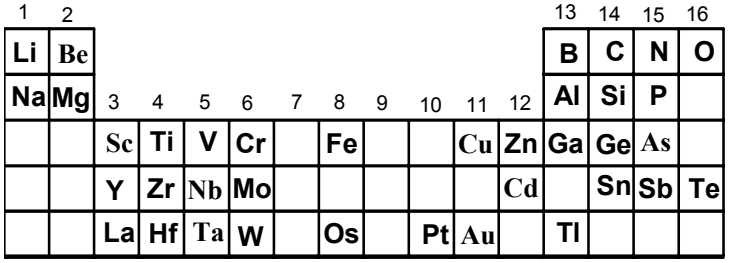

Figure 1.2 Known metal silsesquioxanes.

Lately, the metal-containing silsesquioxanes were proven to be convenient precursors for potentially catalytic microporous amorphous metallosilicates, so-called M-Si-O, which are characterized by high surface area, uniformly-controlled micropores and high metal oxide dispersion. The known literature already involves the calcination of Ti and Ga silsesquioxanes.[30-31] Calcination of Cr, Mg, Al and Fe silsesquioxanes is described in the present thesis. This development has also been stimulated by the fact that over the last decade a large number of metal silsesquioxane complexes have become available.

1.4 Scope of this thesis

The need of chemical industry for more efficient catalysts promotes the research to find new synthesis procedures resulting in catalysts with an optimum combination of properties. This thesis describes the development of a novel method for the synthesis of microporous metallosilicate catalysts based on calcination of metal silsesquioxane precursors. The characterization of the resulting materials was mainly directed towards features, which are essential for catalysis such as surface

area, pore size distribution, metal speciation and dispersion. The catalytic properties are only briefly investigated to prove the catalytic activity and help to illustrate some principles. The research plan was structured on three phases, which are exploring ways to make the proposed methodology more flexibile.

In the first phase different metal silsesquioxanes were calcined and the resulting materials were characterized by various complementary techniques. Chapter 2 investigates the properties of a Cr-Si-O material prepared from a chromium silsesquioxane precursor. Thermogravimetry and mass spectrometry methods are used to get insights into the transformation mechanism of this molecular precursor into a heterogeneous catalyst. The textural properties are investigated via N_2 physisorption and surface area and pore size distribution are estimated with different models. Chapter 3 describes Mg-Si-O and Al-Si-O materials derived from Mg and Al silsesquioxanes. The possibility to adjust the texture of metallosilicates and their metal dispersion by changing the calcination conditions is evaluated. Metal speciation and dispersion are estimated from x-ray photoelectron spectroscopy (XPS), energy dispersive x-ray analysis (EDX), ^{29}Si and ^{27}Al solid-state magic-angle spinning nuclear magnetic resonance (MAS NMR) and high resolution transmission electron microscopy (HRTEM). The possibility to prepare metallosilicates that are Lewis or Brönsted acids is examined by in situ infrared (IR) spectroscopy of adsorbed CD_3CN.

In the second phase a succesfull attempt is made to prepare M-Si-O materials with tailored metal content. Thus, a series of Fe-Si-O materials with iron contents in 1 – 11 wt % range prepared by calcination of mixtures of iron silsesquioxane and metal-free silsesquioxane is investigated in detail in chapter 4. A combination of techniques including difusse reflectance of ultraviolet and visible light (DRUV-Vis), Raman, IR of adsorbed NO, XPS, Mössbauer and TEM was used to follow the variation of the textural properties, metal dispersion and metal speciation with the iron content along the whole mixing series.

In the third phase a series of bimetallic M-Si-O catalysts are prepared from calcination of iron, chromium and metal-free silsesquioxane mixtures. This is described in chapter 5, where a careful investigation of the metal speciation is

performed. A comparison is made here between the developed methodology and the impregnation method.

References

1. A. Mittasch, *Kurze Geschichte der Katalyse in Praxis und Theorie,* J. Springer-Verlag, Berlin, Germany, 1939.
2. S. A. Topham, *Catalysis – Science and Technology*, 1984, 5, 119.
3. J. A. Schwarz, C. Contescu and A. Contescu, *Chem. Rev.*, 1995, 95, 477.
4. H. H. Kung and E. I. Ko, *Chem. Eng. J.*, 1996, 64, 203.
5. F. Pinna, *Catal. Today*, 1998, 129.
6. M. A. Cauqui and J. M. Rodriguez-Izquierdo, *J. Non-Cryst. Solids*, 1992, 147/148, 724.
7. D. A. Ward and E. I. Ko, *I&EC Res.*, 1995, 34, 421.
8. H. Hutter, T. Mallat and A. Baiker, *J. Catal.*, 1995, 153, 177.
9. E. Boellaard, A. M. van der Kraan and J. W. Geus, *Stud. Surf. Sci Catal.*, 1995, 91, 931.
10. J. B. Miller, L. J. Mathers and E. I. Ko, *J. Mater. Chem.*, 1996, 5, 1759.
11. J. F. Brown and L. H. Vogt, *J. Am. Chem. Soc.*, 1965, 87, 4313.
12. F. J. Feher, T. A. Budzichowski, R. L. Blanski, K. J. Weller and J. W. Ziller, *Organometallics*, 1991, 10, 2526.
13. F. J. Feher, R. Terroba and J. W. Ziller, *Chem. Commun.*, 1999, 2309.
14. P. G. Harrison, *J. Org. Met. Chem.*, 1997, 542, 141.
15. P. A. Agaskar, *Chem. Commun.*, 1992, 1024.
16. R. H. Baney, M. Itoh, A. Sakakibara and T. Suzuki, *Chem. Rev.*, 1995, 95, 1409.
17. D. A. Loy and K. J. Shea, *Chem. Rev.*, 1995, 95, 1431.
18. K. J. Shea, D. A. Loy and O. Webster, *J. Am. Chem. Soc.*, 1992, 114, 6700.
19. C. Zhang, F. Babonneau, C. Bonhomme, R. M. Laine, C. L. Soles, H. A. Hristov and A. F. Yee, *J. Am. Chem. Soc.*, 1998, 120, 8380.
20. F. J. Feher, D. A. Newman and J. F. Walzer, *J. Am. Chem. Soc.*, 1989, 111, 1741.
21. F. J. Feher and T. A. Budzichowski, *Polyhedron*, 1995, 14, 3239.
22. M. G. Voronkov and V. I. Lavrent'yev, *Top. Curr. Chem.*, 1982, 102, 199.
23. V. Lorenz, A. Fischer, S. Giebmann, J. W. Gilje, Y. Gun'ko, K. Jacob and F. T. Edelmann, *Coord. Chem. Rev.*, 2000, 206-207, 321.

24. H. C. L. Abbenhuis, *Chem. Eur. J.*, 2000, 6, 25.
25. K. Wada, M. Nakashita, M. Bundo, K. Ito, T. Kondo and T. Mitsudo, *Chem. Lett.*, 1998, 659.
26. V. Lorenz, A. Fischer and F. T. Edelmann, *Z. Anorg. Allg. Chem.*, 2000, 626, 1728.
27. F. T. Edelmann, S. Giebmann and A. Fischer, *Inorg. Chem. Comm.*, 2000, 3, 658.
28. V. Lorenz, A. Fischer and F. T. Edelmann, *Inorg. Chem. Comm.*, 2000, 3, 292.
29. L. Abis., L. Armelao, D. B. Dell'Amico, F. Calderazzo, F. Garbassi, A. Merigo and E. A. Quadrelli, *J. Chem. Soc., Dalton Trans.*, 2001, 2704.
30. K. Wada, M. Nakashita, M. Bundo, K. Ito, T. Kondo and T. Mitsudo, *Chem. Lett.*, 1998, 659.
31. K. Wada, K. Yamada, T. Kondo and T. Mitsudo, *Chem. Lett.*, 2001, 12.

2

Chromium silsesquioxane based synthesis and characterisation of a microporous Cr-Si-O material

Abstract

The controlled calcination of the chromium containing silsesquioxane (c-$C_5H_9)_7Si_7O_9(OSiMe_3)O_2CrO_2$, **3b**, monitored by MS analysis of the evolved gases and by thermogravimetry measurements, led to the formation of a microporous amorphous Cr-Si-O mixed oxide containing 10.2 wt % of chromium. The textural properties of the material as well as the speciation and dispersion of the chromium oxide on the silica surface were investigated by the use of nitrogen physical adsorption, XRD, XPS as well as DRS, RS and IR techniques. The nitrogen physical adsorption indicates a high surface area, a rather large pore volume and a very narrow pore size distribution around 6 Å diameter. The spectroscopic analysis of the material suggests a good dispersion of the chromium oxide species on the silica surface mainly as monochromate and to a certain extend as dichromate and clusters of Cr_2O_3. The material was briefly tested in the ammonia oxidation reaction and found to be an active catalyst.

Published as: N. Maxim, H. C. L. Abbenhuis, P. J. Stobbelaar, B. L. Mojet and R. A. van Santen, *Phys. Chem. Chem. Phys.*, 1999, 18, 4473.

2.1 Introduction

Chromium containing silsesquioxanes such as compound (c-$C_6H_{11})_7Si_7O_9(OSiMe_3)O_2CrO_2$, **3a,** (see Scheme 2.1) have been proposed as homogeneous models[1] for the active surface sites of silica supported chromium oxide, a well known ethylene polymerization catalyst[2]. The silyl-chromate complex **3a** catalyzed ethylene polymerization in the presence of Me_3Al and readily oxidized stilbene to benzaldehyde.

The surface chemistry of chromium oxide supported on silica has attracted a widespread interest and has been reviewed extensively.[3] The identification of the molecular structures of surface chromium species was many times controversial[4] (e.g. chromate vs. dichromate) therefore requiring the combination of different characterization techniques like X-ray photoelectron spectroscopy (XPS), extended X-ray absorption fine structure (EXAFS), diffuse reflectance spectroscopy (DRS), Raman spectroscopy (RS), infrared spectroscopy (IR), electron spin resonance (ESR), thermogravimetry (TG). It was shown that on calcined silica surfaces the polymerization of the chromium oxide species and the amount of Cr_2O_3 clusters increases with chromium loading.[5]

Metal silsesquioxanes like [(c-$C_5H_9)_7Si_7O_{12}$]Ti(η^5-C_5H_5) were recently reported[6] to be convenient precursors for microporous M-Si-O amorphous materials with high surface areas and relatively uniform pore size distributions. Moreover there were indications for a rather good dispersion of the titanium oxide on the silica surface.

In this chapter, we report a detailed extension of this methodology to chromium containing materials. This resulted in the preparation of a microporous Cr-Si-O amorphous mixed oxide with a high chromium loading and a good dispersion of the chromium species on the silica surface, through controlled calcination of the chromium containing silsesquioxane **3b**. The material was carefully characterized both with regard to the textural properties and to the chromium surface chemistry by

the use of a set of different complementary techniques including nitrogen physical adsorption, XRD, XPS as well as DRS, RS, IR and TG.

2.2 Experimental

2.2.1 Synthesis of the Cr-Si-O material

The incompletely condensed silsesquioxane **1b**, which was prepared by the hydrolytic condensation of cyclopentyltrichlorosilane, was silylated with Me_3SiCl using a procedure reported elsewhere to give white crystals of disilanol **2b**.[7] The reaction of **2b** with CrO_3, which was carried out as described in the literature for **3a**[1], gave an orange powder in 78 % yield which was identified on the basis of NMR data as compound **3b**.

Small portions of 0.5 g of chromium containing silsesquioxane **3b** were heated by 5 °C/min to 450 °C and 550 °C for 4 h in a continuous plug flow reactor of 27 mm internal diameter flushed with a 20 % O_2 in Ar gas mixture.

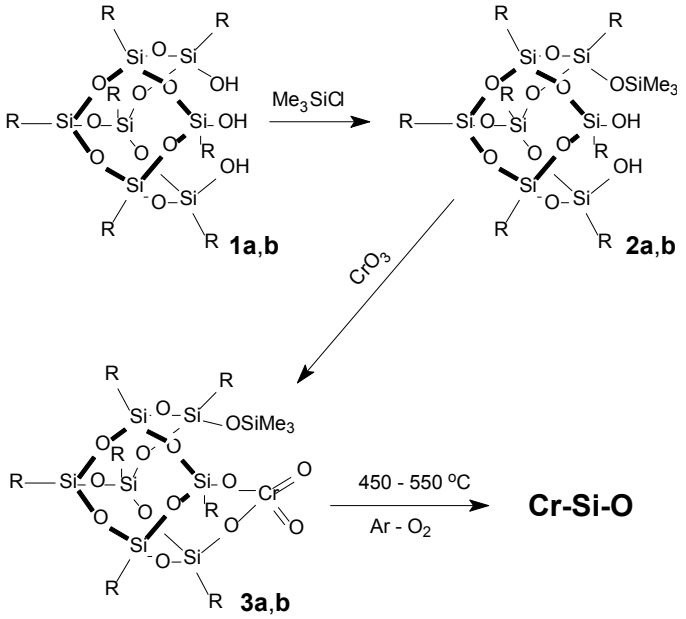

*Scheme 2.1 Schematic view of calcined **3b** synthesis (**a** stands for R = c-C_6H_{11} and **b** stands for R = c-C_5H_9).*

The resultant oxides were further designated as **3b**-550 and **3b**-450 where the suffix number is the calcination temperature in °C. Samples of trisilanol **1b** and disilanol **2b** were calcined for reference under the same conditions.

2.2.2 Analysis methods

The chromium content of the Cr-Si-O material obtained from calcination of **3b** was determined by atomic absorption spectrometry (AAS) after dissolution in a $HF:HNO_3:H_2O$ = 1:1:1 mixture. The carbon content of the Cr-Si-O material was measured by heating the samples at 925 °C on a Perkin Elmer automated analyzer.

The calcination of compound **3b** was monitored by mass spectrometry analysis of the evolved gases using a Balzers QMG-420 quadruple mass spectrometer. Samples of 0.05 g of **3b** were calcined in a continuous plug flow reactor of 4 mm internal diameter. The same temperature program and flow rates were applied but helium was used instead of argon. CO, CO_2, H_2, cyclopentene and cyclopentane were monitored using the ratios m/e = 28, 44, 2, 67 and 69 respectively. The signals of m/e = 12, 14 and 16 were used to distinguish between carbon containing and nitrogen containing fragments.

Samples of 0.012 g of compound **3b** were calcined in ambient air on a Shimadzu TGA-50 thermogravimetric analyzer using also the same temperature programs.

For the nitrogen physical adsorption analysis all the samples were pretreated before the measurement in vacuum at 200 °C for 2 h. The measurements were performed on an ASAP 2000 Micromeritics apparatus using an equilibriation interval of 5 seconds and a low pressure dose of 3.00 cm^3/g STP. Information about surface area, pore volume and pore size distribution was derived from Horvath-Kawazoe (H-K)[8a], Dubinin-Radushkevich (D-R)[8b], Brunauer-Emmett-Teller (BET)[8c] and Brunauer[8d] (based on the t-plot of de Boer et al[8e]) methods.

X-ray powder diffraction data were collected on a Rigaku diffractometer in the range $1.0° < 2\theta < 100°$ using Cu Kα radiation under continuous scanning at a scan speed of 0.2 deg/min.

X-ray Photoelectron Spectroscopy measurements were performed on a VG CLAM 2 spectrometer equipped with a Mg-Kα source and a hemispherical analyzer. Measurements were done at 20 eV pass energy and charging was corrected using the Si 2p signal at 103.3 eV. The samples were ground and pressed in indium foil, which was placed on a stainless-steel stub. The error in the binding energy was 0.2 eV. Elemental ratios were calculated from the peak areas with correction for the cross-sections.[9]

Diffuse reflectance UV spectra were taken at room temperature on a UV-2401PC Shimadzu spectrophotometer equipped with a diffuse reflectance unit. Powdered samples were loaded between 0.3 mm Suprasil windows. Spectra were recorded against a $BaSO_4$ reflectance standard in the range 190-1000 nm. The computer processing of the spectra consisted of the following steps: subtraction of the baseline, conversion to wavenumber and calculation of the Kubelka-Munk (KM) function.[10]

Raman spectra were recorded with a Labram from Dilor S.A.. A Spectra Physics Millenium II Nd:YVO_4 laser at 532 nm was used as the excitation source. The initial laser power was 0.20 W. All spectra were taken under ambient conditions.

Infrared spectroscopy was performed under ambient conditions on a Nicolet Protégé 460 FTIR Spectrometer E.S.P. equipped with a MCT/A detector and a Golden Gate Single Reflection Diamond sampling unit. An automatic baseline correction of the spectra was used.

Transmission electron microscopy was performed using a Philips CM30UT high resolution electron microscope. Samples were mounted on a microgrid carbon polymer supported on a copper grid by placing a few droplets of a suspension of ground sample in hexane on the grid followed by drying at ambient conditions.

Ammonia oxidation tests with **3b**-550 catalyst were carried out at 200 and 250 °C. 95 mg of catalyst, a flow rate of 50 ml/min and concentrations of 1000 ppm NH_3 and 10 % O_2 in the flow were used.

2.3 Results and discussion

2.3.1 Investigations on the calcination mechanism

In the chromium complex **3b** the chromium atoms are atomically dispersed since there is one chromate group per molecule of complex. We suppose that during the calcination treatment most of the chromium atoms remain bonded or at least stay close to their original silsesquioxane cube ligands, their mobility being low and thus restricting the agglomeration of chromate species with the concomitant formation of polychromates and Cr_2O_3 particles.

The mass spectra analysis data of the gases evolved during the calcination of **3b** at 550 °C are shown in Figure 2.1 (cyclopentene and cyclopentane are not shown because they were formed in very small amounts).

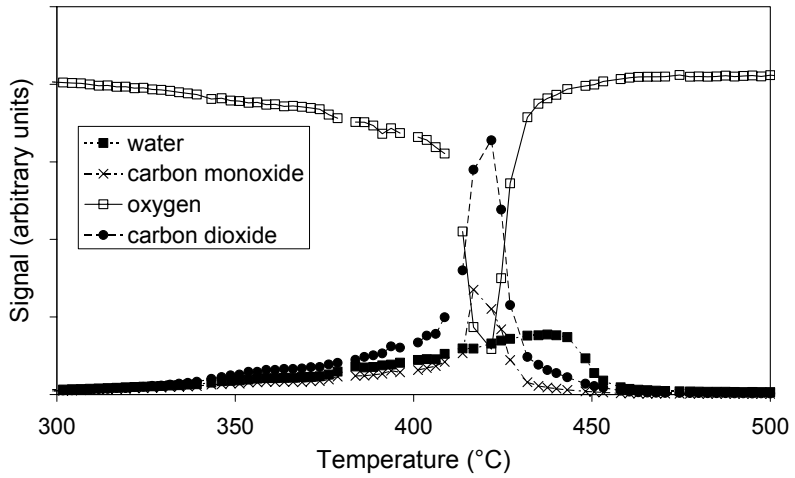

*Figure 2.1 Evolution of gases during the calcination of **3b** at 550 ºC monitored by mass spectra analysis.*

Small amounts of CO, CO_2 and water were released starting at around 250 °C and a slight consumption of oxygen was observed simultaneously. At 420 °C the amount of CO and CO_2 strongly increased while oxygen was consumed completely. The expected concomitant water evolution, however, occurred in a retarded fashion. This

retarded release of water suggests that its removal from the catalyst nascent pores and surfaces is rather difficult probably due to diffusion limitations. The total mass decrease of the complex during the calcination at 550 °C, estimated from thermogravimetric analysis, was 52.5 %, which is higher than the theoretical decrease of 43.6 % (this was calculated assuming a complete combustion of the cyclopentyl groups from the precursor and a Si : O atomic ratio of 1 : 2 as well as the oxidation state VI for Cr in the final Cr-Si-O material). Moreover the measurement of the chromium content by AAS for the calcined complex gave 10.2 wt % which is also somewhat higher than the expected 9 wt % value. The carbon content of this sample was about 0.1 wt%. Similar results were obtained for the sample calcined at 450 °C indicating that the 450-550 °C calcination temperature range is appropriate for the complete combustion of the organic groups as well as for the development of good textural properties. The higher weight loss and the slightly higher metal content were attributed to the contribution of a evaporation/sublimation effect that interferes with the combustion process. Note that some silsesquioxanes were reported to be extremely volatile.[11] Melting point measurements showed also that many metalsilsesquioxanes melt generally at temperatures lower than 250 °C. Moreover, when we tried to calcine a 3g sample of **3b** instead of a 0.5 g sample, under identical conditions, a black material was obtained and a white powder condensed on the walls of the reactor indicating that the availability of the oxygen inside the material bed and the easy removal of water out of it were critical. Higher calcination temperatures in exces of 550 °C are not desired since it was noted that for an oligomeric silsesquioxane-siloxane copolymer the use of calcination temperatures above 600 °C led to materials with a reduced surface area.[12]

2.3.2 Texture analysis

Conventionally, nitrogen adsorption isotherm measurements represent the most widely used way to determine the surface area and to characterize the porous texture of solids.[13] Regardless of the calcination temperature and the presence of the chromium in the samples, all the adsorption isotherms, shown in Figure 2.2, are Type

Ib characteristic for microporous materials.[13d] Note also that there were reports on the synthesis of microporous ceramics from polymeric precursors including siloxane cage structures.[14]

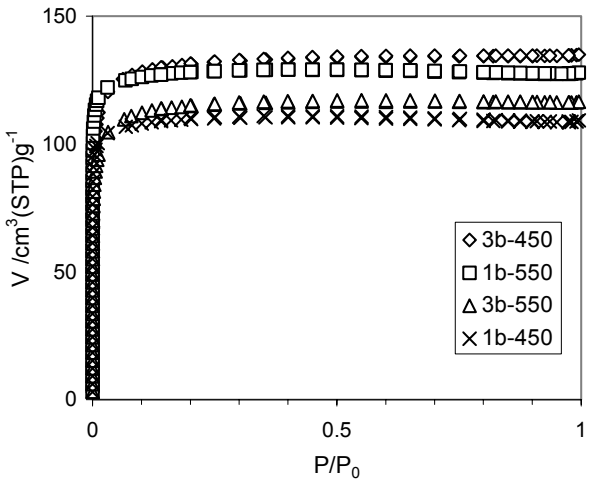

*Figure 2.2 N_2 adsorption/desorption isotherms of **3b** and **1b** calcined at 450 ºC and 550 ºC, respectively.*

Various computation treatments can be applied to the adsorption isotherm in order to determine the microstructure parameters of the solid. Surface area, pore volume and average pore size were estimated from Horwath-Kawazoe, Dubinin-Radushkevich, Brunauer-Emmett-Teller and Brunauer (t-plot of de Boer et al) equations and are compared in Table 2.1.[8]

*Table 2.1 Nitrogen sorption data for the **3b** and **1b** calcined at 450 ºC and 550 ºC, respectively.*

Sample	Surface area (m^2/g)		Pore volume (ml/g)			Average pore diameter (Å)	
	(D-R)	(BET)	(D-R)	(H-K)	(Brunauer)	(H-K)	(Brunauer)
3b-550	519	459	0.18	0.18	0.17	6.9	7.8
3b-450	614	521	0.21	0.21	0.20	6.8	7.9
1b-550	609	522	0.21	0.20	0.19	6.2	7.8
1b-450	499	445	0.17	0.17	0.16	6.1	7.6

*D-R: Dubinin-Radushkevich model; H-K: Horwath-Kawazoe model; BET: Brunauer-Emmett-Teller model.

The D-R, H-K and Brunauer (t-plot of de Boer et al) methods are commonly used for analysis of microporous solids. The Brunauer method[8d] is an extension of the t-plot method developed by de Boer et al.[8e] In the Brunauer method, the volumes and pore radii are calculated from the downward deviations of the straight line in the de Boer t-plot. The BET theory is usually applied for meso and macroporous solids but, as shown recently, it can give good results also in the case of microporous materials.[15] The data presented in Table 2.1 indicate a good agreement among the textural parameters estimated from different models. The BET method gives slightly lower surface areas while the H-K and Brunauer (t-plot) methods give very close average pore diameters. The nitrogen sorption measurements for **1b** and **3b** calcined at 450 °C and 550 °C indicate the formation of truly microporous materials characterized by high surface areas, rather large pore volumes and a very narrow pore size distribution with an average pore size diameter around 6-7 Å.

The calcination temperature and the presence of chromium have a certain influence over the surface areas and pore volumes of these materials while the average pore diameter is only slightly influenced by these parameters.

A typical pore size distribution, estimated from the H-K model is given in Figure 2.3 for **3b**-550. The plot shows a discrete number of pores around 6 Å diameter with a slight tailing up to 18 Å.

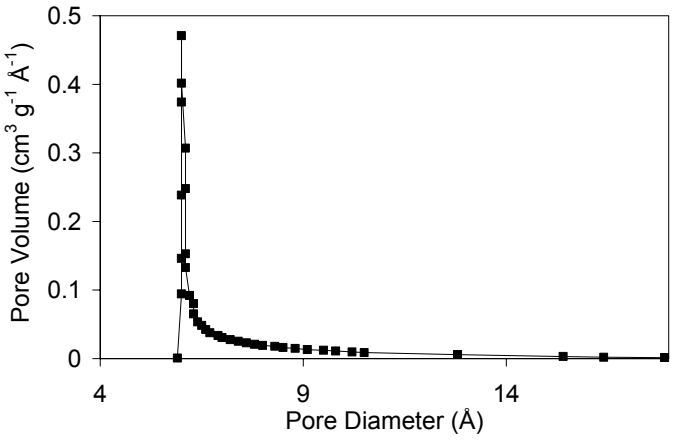

*Figure 2.3 Pore size distribution of **3b**-550 estimated by Horwath-Kawazoe model.*

The calculation from the adsorption isotherms of the maximum amounts of nitrogen adsorbed on **3b**-550 and **3b**-450 materials led to the values 4.79 and 5.69 mmoles N_2 per g, respectively. These values gave a good fit with the value of 5.71 mmoles N_2 per g, which is typical for the HZSM-5 zeolite[16], a well-known MFI type zeolite with similar pore size diameters, thus suggesting a good accessibility and utilization of the pore volume. However, in spite of the very narrow pore size distribution and good pore volume utilization derived from the sorption data, indicating a certain degree of structural organization of the calcined **3b** materials, they proved to be amorphous as shown by powder x-ray diffraction. The XRD spectra shown in Figure 2.4 present only one broad band around 23° 2θ angle which is usually assigned to amorphous silica.[17]

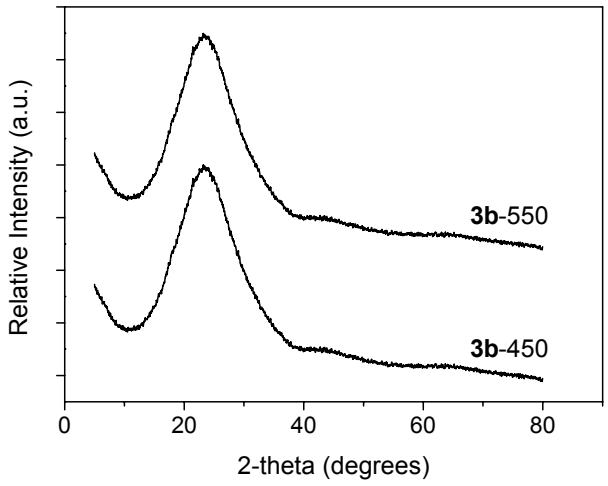

*Figure 2.4 X-ray diffraction diagrams of **3b**-450 and **3b**-550.*

2.3.3 Spectroscopic investigation of the chromium state

The Cr/Si atomic ratio calculated from the composition of chromium containing silsesquioxane **3b** is 0.125. This bulk Cr/Si atomic ratio was compared with the Cr/Si atomic ratio determined by XPS analysis. Since the photoelectrons excited by the X-ray radiation can only travel a few nanometers through a solid oxide material, the

XPS data contain surface sensitive information. If we assume that all the chromium species are homogeneously distributed into material then the surface and bulk ratios should be the same. The XPS measurements of the **3b**-550 and **3b**-450 materials revealed a Cr/Si atomic ratio of 0.175, suggesting a small chromium enrichment of the silica surface compared to the bulk. We also found that during the measurements the original Cr^{6+} species were significantly reduced since the ratio Cr^{3+}/Cr^{6+} increased. This is feasible since it was mentioned that highly dispersed Cr^{6+} and Cr^{5+} are readily reduced under high vacuum in the XPS chamber and/or under influence of X-ray irradiation.[18] However, the estimation of the Cr^{3+}/Cr^{6+} ratio at the start of the measurements still indicates the presence of a small amount of Cr^{3+} species in the samples. These are formed during the calcination of **3b** complex and should in any case appear as amorphous particles or small clusters of Cr_2O_3 undetectable by XRD. These clusters are probably of sub-nanometer size since no particles were observed on the surface of **3b**-550 sample, when examined in high resolution transmission electron microscope.

The IR spectrum of **3b**-550 material, shown in Figure 2.5, presents a peak at 910 cm^{-1} normally assigned to Cr-O vibrations of Cr^{6+} species.[19] For comparison reasons we also recorded the spectrum of **2b**-550.

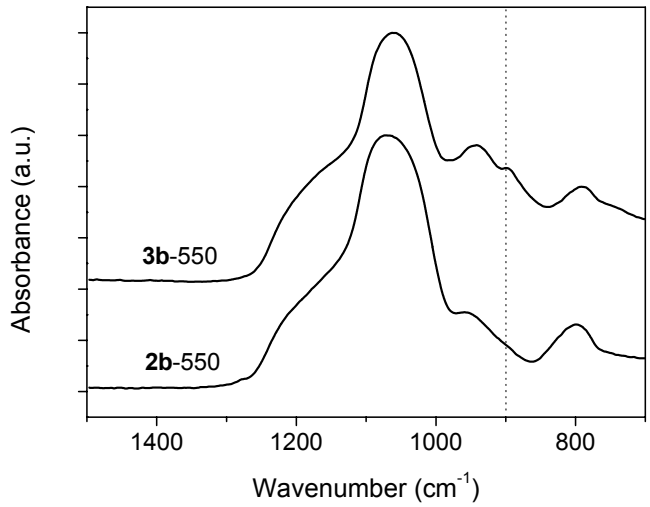

*Figure 2.5 Infrared spectra of **3b**-550 and **2b**-550.*

The collection of the Raman spectra for the calcined **3b** materials strongly suffered from fluorescence. However, as shown in Figure 2.6, in the case of **3b**-450 we could identify a well shaped Raman band at 986 cm^{-1} associated with the symmetric stretching mode of the terminal Cr=O bond of the dehydrated monomeric surface cromium oxide species on the silica support. A broad and weak band could also be observed around 550 cm^{-1} indicative for Cr_2O_3 formation. The presence of minor amounts of chromium oligomer species such as dimers or even trimers cannot be completely ruled out because of the mentioned fluorescence disturbing effect originating from the background of the samples.[5,20] The Raman spectra of the calcined **2b** materials also suffered from fluorescence but we were able to record the spectrum of a Ti-Si-O material[6] obtained by calcination of a titanium containing silsesquioxane, $[(\underline{c}\text{-}C_5H_9)_7Si_7O_{12}]Ti(\eta^5\text{-}C_5H_5)$, at 550 °C (labeled as Ti-Si-O-550). Assuming that Cr-Si-O and Ti-Si-O materials posses a similar silica matrix the comparison of the spectra shows that the two bands from **3b**-450 are not due to Si-O vibrations which may appear in the same wavenumber region.[21]

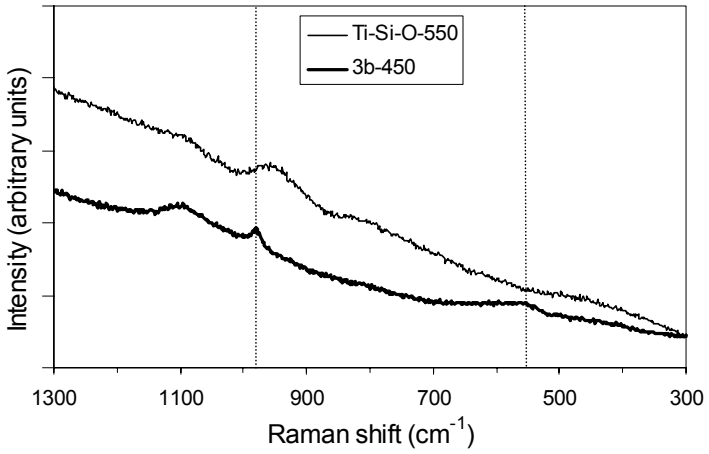

*Figure 2.6 Raman spectra of **3b**-450 and Ti-Si-O 550.*

The DRS spectra of the calcined and non-calcined **3b** materials shown in Figure 2.7 present the same bands around 27000-28000 cm^{-1} and 38000-39000 cm^{-1} characteristic for monochromates. Around 22000-23000 cm^{-1} a minor shoulder can be seen, which is indicative for the existence of some dichromates. The small absorptions

between 15000 – 17000 cm^{-1} are indicative for Cr_2O_3 formation but its concentration on silica surface is probably very low.[3c,5] At high chromium loadings, however, as for calcined **3b** materials**,** a quantitative analysis of the DRS spectra is not reliable[10].

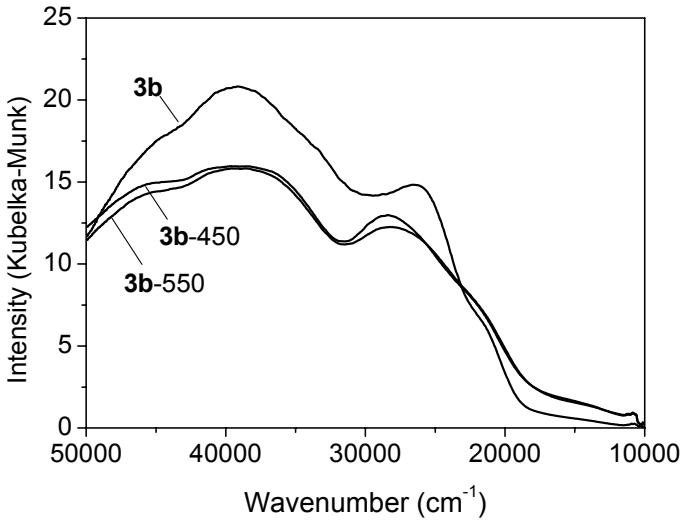

*Figure 2.7 Diffuse reflectance UV-Vis spectra of **3b**, **3b**-450 and **3b**-550.*

The highest surface coverage with Cr^{6+} species reported for silica supported chromium materials was between 1.8-2.3 Cr^{6+} per nm^2 for a sample calcined at 425 °C.[3a] Impregnation of silica at higher loadings was reported to result after calcination in decomposition of the CrO_3 excess to Cr_2O_3. The surface coverages by total chromium species calculated for **3b**-550 and **3b**-450 are 1.9 and 2.3 Cr per nm^2, respectively. However, at such high loadings the formation of some dichromates and Cr_2O_3 clusters is difficult to be avoided since the monochromate groups could be hydrolized by the water produced during the calcination treatment of complex **3b** and thus migrate onto the nascent silica surfaces.

2.3.4 Catalytic tests

The **3b**-550 was briefly tested in NH_3 oxidation to N_2 and O_2 at 200 and 250 °C. At 200 °C the **3b**-550 catalyst gave 56 % conversion and 68 % selectivity to N_2. When the temperature was raised to 250 °C the conversion increased to 100 % and selectivity to N_2 decreased to 51 %. Additional catalytic tests are described in chapter 5.

2.4 Conclusions

The calcination of compound **3b** over a 450-550 °C temperature range in an Ar-O_2 flow led to the formation of a microporous amorphous silica matrix that is highly loaded with chromium oxide. Under these conditions the formation of the microporous structure from the silsesquioxane Si/O skeleton proceeds well and is only slightly influenced by the presence of the transitional metal. During the calcination treatment, water removal appears to be slow suggesting the early formation of the microporous structure. The calcined **3b** materials, in spite of their amorphous nature, posses a rather well defined pore structure with a pore volume utilization comparable to that of MFI zeolites. Spectroscopic investigation of the material indicates a good dispersion of the chromium species over the formed silica surface mainly as monochromates and also to a certain degree as dichromates and Cr_2O_3 clusters. All these results clearly confirm the possibility of chromium silsesquioxane as excellent precursor for porous oxide catalysts.

References

1. F. J. Feher and R. L. Blanski, *J. Chem. Soc., Chem. Commun.*, 1990, 1614.
2. (a) M. P. McDaniel, C. H. Leigh and S. M. Wharry, *J. Catal.*, 1989, 120, 170; (b) J. P. Hogan, D. D. Norwood and C. A. Ayres, *J. Appl. Polym. Sci.*, 1981, 36, 49.
3. (a) B. M. Weckhuysen and R. A. Schoonheydt, *Catal. Today*, 1999, 51, 215; (b) M. P McDaniel, *Adv. Catal.*, 1985, 33, 47; (c) B. M. Weckhuysen, I. E. Wachs and R. A. Schoonheydt, *Chem. Rev.*, 1996, 96, 3327.
4. (a) D. S. Kim, J. M. Tatibouet and I. E. Wachs, *J. Catal.*, 1992, 136, 209; (b) M. A. Vuurman, F. D. Hardcastle and I. E. Wachs, *J. Mol. Catal.*, 1993, 84, 193; (c) B. Fubini, G. Ghiotti, L. Stradella, E. Garrone and C. Morterra, *J. Catal.*, 1980, 66, 200; (d) N. E. Fouad, H. Knozinger and M. I. Zaki, *Z. Phys. Chem.*, 1994, 186, 231.
5. B. M. Weckhuysen, R. A. Schoonheydt, J. M. Jehng, I. E. Wachs, S. J. Cho, R. Ryoo, S. Kijlstra and E. Poels, *J. Chem. Soc. Faraday Trans.*, 1995, 91 (18), 3245.
6. K. Wada, M. Nakashita, M. Bundo, K. Ito, T. Kondo and T. Mitsudo, *Chem. Lett.*, 1998, 659.
7. H. C. L. Abbenhuis, A. D. Burrows, H. Kooijman, M. Lutz, M. T. Palmer, R. A. van Santen and A. L. Spek, *Chem. Commun.*, 1998, 2627.
8. (a) G. Horwath and K. Kawazoe, *J. Chem. Eng. Japan*, 1983, 16, 470. (b) M. M. Dubinin and L. V. Radushkevich, *Proc. Acad. Sci. USSR*, 1947, 55, 331; (c) S. Brunauer, P. H. Emmett and E. Teller, *J. Am. Chem. Soc.*, 1938, 60, 309. (d) R. SH. Mikhail, S. Brunauer and E. E. Bodor, *J. Colloid and Interface Sci.*, 1968, 26, 45-61; A. J. Lecloux in *Catalysis: Science and Technology*, vol. 2, Springer: Berlin, 1981. (e) B. C. Lippens, B. G. Linsen and J. H. de Boer, *J. Catal.*, 1964, 3, 32-49; B. C. Lippens, B. G. Linsen and J. H. de Boer, *J. Catal.*, 1964, 3, 268-273; B. C. Lippens, B. G. Linsen and J. H. de Boer, *J. Catal.*, 1964, 4, 319-323; B. C. Lippens, B. G. Linsen and J. H. de Boer, *J. Catal.*, 1964, 4, 643-653.
9. J. H. Scofield, *J. Electron Spectrosc. Relat. Phenom.*, 1976, 8, 129.
10. (a) W. W. M. Wendlandt and H. G. Hecht, *Reflectance Spectroscopy*, Interscience Publishers, New York, 1966, 46; (b) B. M. Weckhuysen, I. E. Wachs and R. A. Schoonheydt, *Stud. Surf. Sci. Catal.*, 1995, 91, 151; (c) B. M. Weckhuysen and R. A. Schoonheydt, *Zeolites*, 1994, 14, 360.

11. P. Harisson and R. Kannengiesser, *J. Organomet. Chem.*, 1997, 542, 141.
12. R. A. Mantz, P. F. Jones, K. P. Chaffee, J. D. Lichtenhan and J. W. Gilman, *Chem. Mater.*, 1996, 8, 1250.
13. (a) S. J. Gregg and K. S. W. Sing in *Adsorption, Surface Area and Porosity*, 2nd ed., Academic Press: London, 1982. (b) S. Lowell and J. E. Shields in *Powder, Surface Area and Porosity*, Powder Technology Series: London, 1984. (c) M. Jaroniec and R. Madey in *Physical Adsorption on Heterogeneous Solids, Studies in Physical and Theoretical Chemistry*, vol. 59, Elsevier: Amsterdam, 1988. (d) F. Rouquerol, J. Rouquerol and K. Sing in *Adsorption by Powders & Porous Solids – Principles, Methodology and Applications*, Academic Press: London, 1999.
14. P. A. Agaskar, *J. Chem. Soc. Chem. Commun.*, 1992, 1024.
15. S. Blacher, B. Sahouli, B. Heinrichs, P. Lodewyckx, R. Pirard, J. P. Pirard, *Langmuir*, 2000, 16, 6754.
16. P. A. Jacobs, H. K. Beyer and J. Valyon, *Zeolites*, 1981, 1, 161.
17. C. Real, M. D. Alcala and J. M. Criado, *J. Am. Ceram. Soc.*, 1996, 79 (8), 2012.
18. (a) S. A. Best, R. G. Squires and R. A. Walton, *J. Catal.*, 1977, 47, 292; (b) A. Cimino, B. A. De Angelis, A. Luchetti and G. Minelli, *J. Catal.*, 1976, 45, 316.
19. M. A. Vuurman and I. E. Wachs, *J. Phys. Chem.*, 1992, 96, 5008.
20. F. D. Hardcastle and I. E. Wachs, *J. Mol. Catal.*, 1988, 46, 173.
21. B. Humbert, *J. of Non-Cryst. Solids*, 1995, 191, 29.

3

Microporous Mg-Si-O and Al-Si-O materials derived from metal silsesquioxanes

Abstract

Microporous amorphous metallosilicates designated as Mg-Si-O and Al-Si-O, with a very narrow pore size distribution around 6 Å diameter, typical surface areas ranging from 350 to 650 m^2/g, and loadings of well-dispersed metal oxide (up to about 10 wt% of metal) result from the controlled calcination of magnesium and aluminium silsesquioxane complexes $[(c\text{-}C_5H_9)_7Si_7O_{12}]_2Mg_4Cl_2{\cdot}2THF$, **1**, $\{[(c\text{-}C_5H_9)_7Si_7O_{12}]Al\}_n$, **2** and $[(c\text{-}C_5H_9)_7Si_7O_{11}(OSiMe_3)]Al[(c\text{-}C_5H_9)_7Si_7O_{10}(OSiMe_3)(OH)]$, **3**. Moreover, textural properties such as surface area and pore volume can be easily adjusted by varying the calcination conditions, while the pore size distribution remains practically unchanged. XPS, EDX, solid state MAS ^{29}Si and ^{27}Al NMR and HRTEM measurements suggest that the metal is present in M-Si-O materials mainly as isolated metal ions incorporated in the amorphous silica framework and also as small crystalline metal oxide particles of a few nanometers, which are well dispersed throughout the silica. SEM was employed as well to evaluate particle size and morphology. IR spectroscopy of adsorbed acetonitrile showed that both Al-Si-O materials are strong Lewis acids. Mg-Si-O and Al-Si-O were briefly tested as catalysts in 1-butanol dehydration. Mg-Si-O gave both dehydrogenation and dehydration, while on Al-Si-O only dehydration and cracking reactions occurred.

Published as: N. Maxim, P.C.M.M. Magusin, P.J. Kooyman, J.H.M.C. van Wolput, R.A. van Santen and H.C.L. Abbenhuis, *Chem. Mater.*, 2001, 13(9), 2958.

3.1 Introduction

Silsesquioxane chemistry spans more than half a century, but the interest in this field has increased dramatically over the last decade due to the applications of these compounds in materials science and catalysis. Silsesquioxanes have been found to be useful precursors for ceramic materials[1] while metallasilsesquioxanes have attracted attention from the view point of well-defined homogeneous models for the active surface sites of supported catalysts or metal-containing zeolites.[2] Moreover, titanium-containing silsesquioxanes are active catalysts for epoxidation of olefins[3] while titanium or zirconium-containing silsesquioxanes have been reported to be active catalysts for olefin polymerization.[4]

Recent studies focus on the application of metal-containing silsesquioxanes as convenient precursors for microporous amorphous M-Si-O materials.[5] These materials are characterized by a high surface area, uniformly-controlled micropores and good metal dispersion, being therefore potential heterogeneous catalysts. This development has also been stimulated by the fact that over the last decade a large number of metal silsesquioxane complexes have become available. Nowadays, the metals incorporated into the Si/O skeleton of silsesquioxanes include main group, early and late transition metals, as well as chalcogens[6]: Li, Na, Mg, Y, La, Ti, Zr, Hf, V, Cr, Mo, W, Fe, Os, Pt, Zn, B, Al, Ga, Tl, Ge, Sn, P, Sb, Te. The known literature involves the calcination of titanium silsesquioxane in order to form microporous mixed oxides.[5b] A Cr-Si-O material resulting from calcination of chromium silsesquioxane was also described in detail in the previous chapter.

Sol-gel methods can also be used to prepare mixed oxides or metal supported on silica. However, the homogeneity of the multi-component gels, in terms of the distribution of various components, strongly affects the properties of the final oxide.[7] For example, in the TiO_2-SiO_2 gel, titanium alkoxide hydrolyzes much faster than silicon alkoxide. Thus, hydrolysis of a liquid mixture of the two alkoxides would eventually result in the formation of titanium oxy-hydroxide clusters imbedded in the

silica gel, and segregation of TiO_2 and SiO_2 after calcination.[8] The use of the metal silsesquioxane precursors guarantees that the metal and silicon are atomically mixed. Assuming that the water formed during calcination causes only minor hydrolysis of the M-O-Si bonds and that the hydrolyzed metal species have low mobility, a uniform distribution of the metal throughout the silica is expected.

Thus, as described previously for chromium silsesquioxane, during calcination the organic groups attached to the silicon atoms are replaced by Si-O-Si linkages that seem to connect the initially isolated Si/O-cage structures. The resulting amorphous material had a very narrow pore size distribution centered at 6 Å. A relatively high loading (about 10 wt % of metal) of monodispersed metal oxide could be realized as well.[5c]

We have now started a detailed investigation into the use of silsesquioxane metal complexes as precursors for porous metallosilicates. In this chapter, we access aspects of this new methodology that are relevant to the area of catalysis. These involve the optimization and scope of the method of calcination and evaluation of the possibility to adjust the texture of metallosilicates and their metal dispersion by changing the calcination conditions.

Complex **3** can be considered as a model for both Brönsted and Lewis acidic zeolite sites while complex **2** has aluminium sites that are exclusively Lewis acidic.[9] It was reported that solid acidic catalysts active for 1-butene isomerization have been prepared from the silsesquioxane triol, $(c\text{-}C_5H_9)_7Si_7O_9(OH)_3$, deposited on alumina surface followed by calcination in air.[10] Therefore we examined also the possibility to prepare metallosilicates that are Lewis or Brönsted acids.

In order to develop and assess this methodology, the known magnesium and aluminium silsesquioxane complexes **1** – **3** were used (see Figure 3.1).[9,11]

The M-Si-O materials resulting from calcination of compounds **1**, **2** and **3** were carefully characterized both with regard to the textural properties and to the metal state and dispersion by the use of a set of different complementary techniques including nitrogen physical adsorption, XRD, XPS, EDX, solid state MAS ^{29}Si and ^{27}Al NMR as well as HRTEM and SEM.

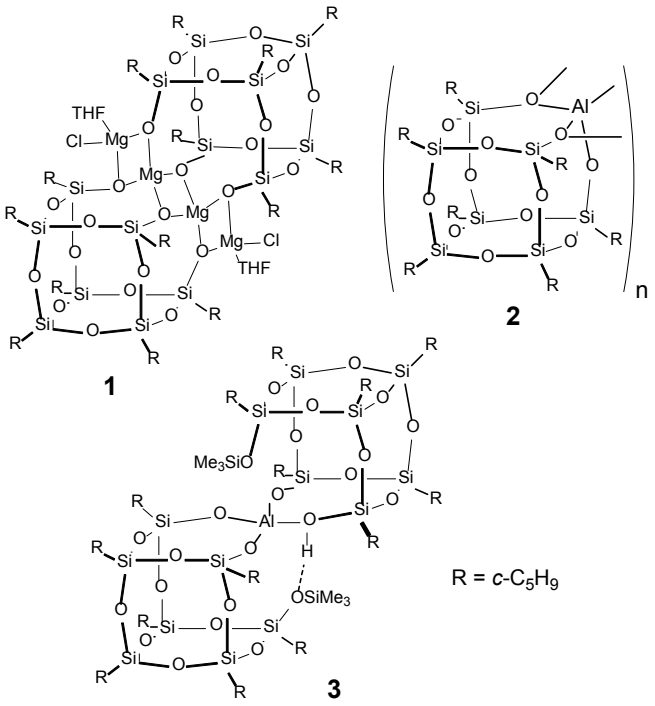

*Figure 3.1 Magnesium and aluminium silsesquioxane complexes **1** – **3** ($R = C_5H_9$).*

3.2 Experimental

3.2.1 Synthesis of the M-Si-O materials

The magnesium silsesquioxane complex **1** was prepared by reacting the trisilanol silsesquioxane[12] $(c\text{-}C_5H_9)_7Si_7O_9(OH)_3$ with the Grignard reagent CH_3MgCl in THF solvent.[11] The aluminium silsesquioxane complexes **2** and **3** were prepared by reacting $AlEt_3$ with this trisilanol silsesquioxane in THF and disilanol silsesquioxane[13] $(c\text{-}C_5H_9)_7Si_7O_9(OSiMe_3)(OH)_2$ in toluene, respectively.[9] Structures of magnesium and aluminium silsesquioxane complexes were verified by using ^1H and ^{13}C-NMR as well as solid state MAS ^{29}Si-NMR.

Calcination procedure. Small portions of 0.5 g of metal-containing oligosilsesquioxane **1**, **2** and **3** as well as metal-free silsesquioxane $(c\text{-}C_5H_9)_7Si_7O_9(OH)_3$ were heated at 5 °C/min to 500 °C for 4 h in a continuous plug-

flow reactor of 27 mm internal diameter flushed by an Ar-O_2 gas mixture flow of 30 ml/min containing 20 mol % of O_2. As reported earlier for calcination of chromium silsesquioxane, these conditions allowed an efficient carbon removal and led to large surface area materials.[5c] The resultant oxides are further designated as Mg-Si-O, Al-Si-O(I), Al-Si-O(II) and SiO_2. For other calcination conditions than the standard ones mentioned above additional suffixes are used for designations (e.g. Mg-Si-O 425 °C means that the sample was calcined at 425 instead of 500 °C but the gas flow and the calcination time were standard). The M-Si-O metal content, as calculated, is 9.7 wt% for Mg-Si-O, 5.7 wt% for Al-Si-O(I) and 2.6 wt% for Al-Si-O(II).

3.2.2 Analysis methods

The carbon content of the M-Si-O materials was measured by heating the samples at 925 °C on a Perkin Elmer automated analyzer Series II CHNS/O Analyzer 2400. The thermogravimetry was performed at 500 °C in ambient air on a Shimadzu TGA-50.

For nitrogen physisorption analysis, all samples were pretreated before the measurement in vacuum at 200 °C for 2 h. Surface area, pore volume and pore size distribution were calculated using the methods developed by Horvath-Kawazoe and Dubinin-Radushkevich.[14]

X-ray diffraction (XRD) data were collected on a Rigaku diffractometer in the range $5.0° < 2\theta < 80°$ using Cu Kα radiation and the step scan method at 0.1 deg/min scanning speed and 5 s dwelling time.

X-ray photoelectron spectroscopy (XPS) measurements were done using a VG CLAM 2 spectrometer equipped with a Mg Kα source and a hemispherical analyzer. Measurements were carried out at 20 eV pass energy. Charging was corrected by using the Si 2p peak of SiO_2 at 103.3 eV. The samples were ground and pressed in indium foil, which was placed on a stainless-steel stub. The error in the binding energy was 0.2 eV. Elemental ratios were calculated from the peak areas with correction for the cross-sections.[15]

Energy dispersive x-ray (EDX) elemental analysis was performed using a JEOL SUPERPROBE JXA-8600SX at an accelerating voltage of 10 kV. The powder

samples were coated with carbon before measurement in order to create a conductive film (~25 nm thickness) at the sample surface. The probe spotsize was about 40 nm.

Solid-state magic-angle spinning (MAS) ^{29}Si nuclear magnetic resonance (NMR) experiments were carried out on a Bruker MSL400 spectrometer operating at a ^{29}Si resonance frequency of 79.46 MHz. The peak of Q8M8 at 11.8 ppm was used as an external reference for the chemical shift. Magic-angle spinning at a sample rotation rate of 4 kHz was employed to eliminate the line broadening caused by the chemical-shift anisotropy. Chemical shift values were estimated from MAS ^{29}Si NMR spectra recorded with direct ^{29}Si excitation combined with high-power proton decoupling and relaxation delays of 30 s between subsequent scans. (Longer relaxation delays up to 300 s did not yield lineshape changes.) Typically 64 to 128 scans were recorded. MAS ^{27}Al NMR spectra were obtained on a Bruker DMX500 operating at a ^{27}Al NMR frequency of 130.32 MHz. A MAS rate of 12.5 kHz was employed and an echo synchronized with the sample rotation was recorded at $2\ \tau$ = 160 μs. The repetition time was 1 s, and the number of scans 6400.

Transmission electron microscopy (TEM) was performed using a STEM JEOL 2000 FX transmission electron microscope operated at 120 kV and a Philips CM30UT high resolution electron microscope with a field emission gun as a source of electrons operated at 300 kV. Samples were prepared in ethanol as described in the previous chapter.

Scanning electron microscopy (SEM) images were taken with a field emission gun (FEG) XL30 instrument operated at an accelerating voltage of 10 kV.

IR spectra were measured on a Bruker FTIR spectrometer (IFS 113v) equipped with a vacuum cell. Self-supporting discs with a thickness of 8 $mg \cdot cm^{-2}$ were used. The spectra were recorded by co-adding 500 scans at room temperature with a resolution of 4 cm^{-1}. Activation of the samples was performed at 720 K in high vacuum (10^{-6} mbar) for 2 h. After cooling down to room temperature, the spectrum of the unloaded sample was taken, followed by contacting the sample with deuterated acetonitrile for 30 min at a presure of 0.9 mbar and recording of a new spectrum. After this, the loading of the samples was reduced stepwise by lowering the equilibrium pressure to 0.05 mbar as well as by desorption for 30 min at 298, 353 and

573 K, respectively, followed by collecting room temperature spectra after each step. The spectrum of the unloaded sample was subtracted from the spectra of samples with different acetonitrile loadings.

Mg-Si-O and Al-Si-O samples were tested in 1-butanol dehydration. Catalytic tests were performed in a continuous plug-flow reactor at 200 °C and 300 °C using 0.7 g of catalyst. The reaction products were analyzed by gas chromatographic methods.

3.3 Results and discussion

3.3.1 Influence of calcination parameters on carbon removal and on textural properties of Mg-Si-O and Al-Si-O

Since the calcined magnesium and aluminium silsesquioxane complexes as well as the calcined silsesquioxane triol were brownish in color, indicating the presence of residual carbon in the M-Si-O materials, we measured the carbon content. The effect of O_2 flow, calcination time and calcination temperature on residual carbon content in Mg-Si-O materials is shown in Figure 3.2. Obviously the carbon removal can be improved by changing the calcination conditions. At low calcination temperature (425 °C) and 4 hours calcination time, the higher the O_2 flow the lower the residual C content. An increase in calcination time from 4 to 16 hours significantly diminishes the residual percentage of C but the effect of the O_2 flow becomes negligible. However, the most important factor seems to be the calcination temperature; high temperatures being necessary for complete carbon removal. Thus, a calcination temperature of 500 °C led to a Mg-Si-O material with a surface area of 347 m^2/g and only 0.6 wt % of C. Of course calcination temperatures as high as 550 °C can be used but higher temperatures may significantly decrease the surface area and pore volume of the samples.

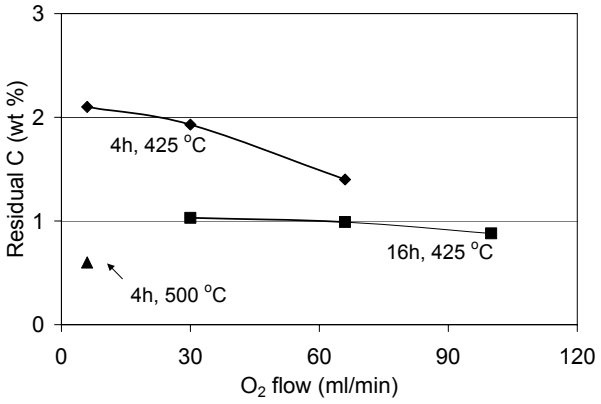

Figure 3.2 The effect of calcination conditions on the residual carbon content of M-Si-O materials (exemplified for Mg-Si-O).

It has been reported that for an oligomeric silsesquioxane – siloxane copolymer the use of pyrolysis temperatures above 600 °C led to materials with a reduced surface area.[16] As described in this reference the porosity, surface area and density measurements showed that char densification took place after the majority of mass loss from pyrolysis had occurred. Once the maximum density had been reached, pore closure occurred between 600 and 650 °C and the surface area decreased from 406 to 2.5 m^2/g. Therefore, appropriate temperatures for the calcination of the metallasilsesquioxane precursors range from 500 to 550 °C. Note also that the total weight losses of the metal complexes **1** and **2** during calcination, estimated from thermogravimetric analysis, were very close to the calculated values (**1**: measured 52%, calculated 51.27%; **2**: measured 47.1%, calculated 47.57%) indicating practically the absence of any evaporation/sublimation effect. A small effect was, however, observed for compound **3** (measured 51.8%, calculated 47.25%).

Typical values for surface area, pore volume and average pore diameter for Mg-Si-O and Al-Si-O as well as for SiO_2-450 °C materials are presented in Table 3.1. These results indicate the formation of microporous materials characterized by high surface area, rather large pore volume and a very narrow pore size distribution with an average pore size diameter around 6 – 7 Å.

Tabel 3.1 Nitrogen sorption data for Mg-Si-O, Al-Si-O and SiO_2.

Sample	Surface area[a] (m^2/g)	Pore volume[b] (ml/g)		Average pore diameter[c] (Å)
Mg-Si-O	347	0.12	0.12	6.0
Al-Si-O(I)	583	0.20	0.19	6.4
Al-Si-O(II)	641	0.22	0.21	6.3
SiO_2-450 °C	499	0.17	0.17	6.1

[a]estimated from Dubinin-Radushkevich equation; [b]estimated from Dubinin-Radushkevich (1st column) and Horvath-Kawazoe equations (2nd column); [c]estimated from Horvath-Kawazoe equation.

As reported earlier, the surface area and pore volume of the M-Si-O materials depended on the calcination temperature.[5b,c] Therefore for optimization of the proposed methodology here we have tried different calcination conditions in order to determine if it is possible to adjust the texture of the metallosilicates and their metal dispersion. Calcination conditions which have been tested included: temperature, which was varied in the range 425-550 °C, pure O_2 flows of 6-100 ml/min and a 30 ml/min flow of 20 mol% O_2 in Ar as well as a calcination time of either 4 or 16 hours.

Thus, the surface area of M-Si-O materials can be greatly changed by altering the O_2 flow, as we show in Figure 3.3 for Mg-Si-O, Al-Si-O(I) and Al-Si-O(II).

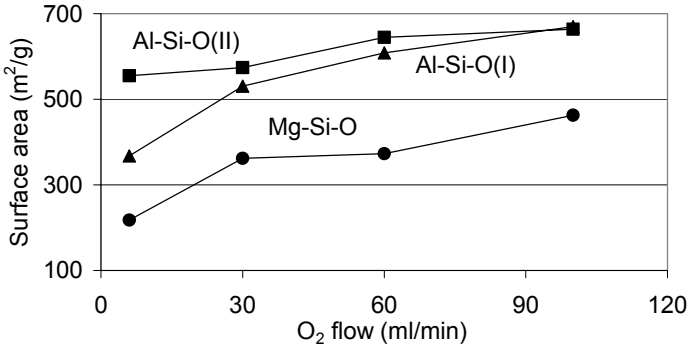

Figure 3.3 The effect of O_2 flow on the surface area of Mg-Si-O, Al-Si-O(I) and Al-Si-O(II) materials.

The surface area of all the samples increased with the O_2 flow. The lower surface areas for the Mg-Si-O sample might be attributed to a sintering process promoted by

the water resulting from combustion of organic part of silsesquioxane complex. It was reported that the surface area of active magnesia prepared by calcination procedures is significantly diminished due to sintering in the presence of water vapor. The greater effect of water on the sintering rate of magnesia compared with alumina and silica was attributed to the low charge and correspondingly high mobility of the magnesium ions.[17] One would also expect that surface area of M-Si-O materials to decrease with the increase of the O_2 flow because more water is produced. However, the observed variation (Fig. 3.3) could be explained by the fact that the increase of the O_2 flow speed up also the removal of the water from the M-Si-O materials and thus reduce the sintering effect. The difference found between the surface area of several duplo batches of M-Si-O was below 8 % indicating a rather good reproducibility of the data presented in Fig. 3.3.

There is also a significant temperature effect, since an increase in temperature from 425 to 475 °C diminished the Mg-Si-O surface area with *ca.* 25 % and reduced the residual carbon content with *ca.* 63%. From this point of view relatively low calcination temperatures are required in order to obtain high surface areas.

A longer calcination time can be effective for reducing the residual carbon content, especially at low temperatures like 425 °C, but it can also decrease slightly the surface area. However, at higher calcination temperatures of at least 500 °C, a 4 hours calcination time seems to be enough to remove the carbon almost completely from all the M-Si-O materials while large surface areas are obtained.

Pure O_2 flows can more efficiently remove residual carbon than diluted O_2 flows. They have usually little effect on textural properties of M-Si-O materials in comparison with Ar diluted O_2 flows but sometimes they can prevent mesopore formation. When an Ar diluted O_2 flow was used, all of the M-Si-O samples, excepting the Al-Si-O(I), yielded type Ib isotherms characteristic of microporous materials. Al-Si-O(I) afforded a type IIb curve associated with a steep increase in the adsorption amount at low p/p_0, indicative for the presence of both micro- and mesopores. When we used pure O_2, the isotherm was type Ib as well. Attribution of the M-Si-O material isotherms was made according to extended IUPAC classification.[18]

Whereas the surface area and pore volume can be adjusted rather well by changing the calcination conditions, the pore size distribution does not change significantly. However, since textural properties like surface area are very sensitive to the calcination conditions, the latter ones must be well controlled in order to achieve good reproducibility. For comparison, we chose a calcination temperature of 500 °C, a calcination time of 4 h, a heating rate of 5 °C/min and an Ar diluted O_2 flow of 30 ml/min 20 % O_2 as standard conditions.

3.3.2 Investigations on metal dispersion and speciation

The metal dispersion and state for Mg-Si-O and Al-Si-O materials were investigated by XPS, EDX, MAS ^{29}Si and ^{27}Al NMR and TEM techniques.

If we assume that all of the metal species are homogeneously distributed throughout the M-Si-O materials, then the surface and the bulk ratios should be similar. The M/Si atomic ratios calculated from the composition of silsesquioxane complexes **1**, **2** and **3** are 0.285, 0.142 and 0.062 respectively. These calculated bulk M/Si ratios are compared in Figure 3.4 with the surface M/Si ratios determined by XPS analysis.

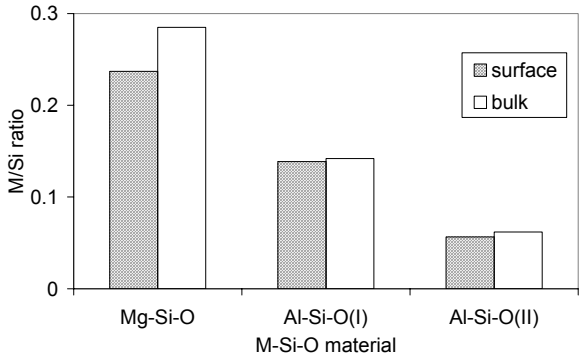

Figure 3.4 Comparison of bulk and surface (XPS data) M/Si atomic ratios for Mg-Si-O, Al-Si-O(I) and Al-Si-O(II) materials.

The surface and bulk M/Si ratios are almost the same for the Al-Si-O materials and only slightly different for Mg-Si-O material indicating a rather high dispersion of the metal throughout the silica and on its surface.

The homogeneity of the metal distribution inside the M-Si-O materials was also estimated from EDX spectra. It is known that emitted X-rays are characteristic for an element and measuring their intensities allows the quantification of the chemical composition of a selected part of the sample. Thus we measured the composition of Mg-Si-O and Al-Si-O in five different randomly selected areas of the samples, using a probe spot size of about 40 nm.

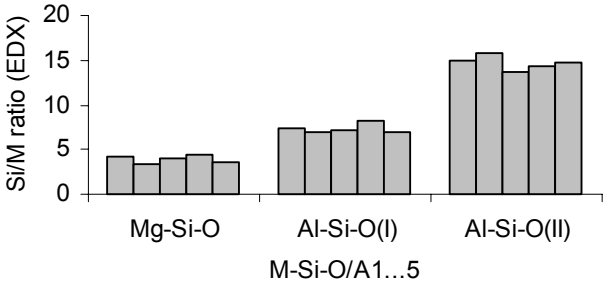

Figure 3.5 Si/M molar ratios for M-Si-O materials measured by EDX on five different areas.

As shown in Figure 3.5 the observed M/Si atomic ratios are fairly close to the expected bulk ratios indicating also a rather good distribution of the metal species inside the samples even if this distribution is not fully homogeneous.

It should be noted also that the XPS Al/Si ratio for Al-Si-O(I) did not change significantly when different O_2 flows in the range 6-100 ml/min were used, indicating a rather stable dispersion of aluminium species in the Al-Si-O material.

Solid state MAS ^{29}Si NMR spectra of the calcined magnesium and aluminium silsesquioxane complexes **1**, **2** and **3**, as well as of the calcined metal-free silsesquioxane ligand $(c\text{-}C_5H_9)_7Si_7O_9(OH)_3$ were recorded. We measured also the spectrum of a physical mixture of calcined metal-free silsesquioxane ligand (c-

$C_5H_9)_7Si_7O_9(OH)_3$ and MgO with the same content of Mg as in the Mg-Si-O material. All of these materials show a single, broad ^{29}Si resonance with a clearly defined maximum having a chemical shift value at –105.5 ± 0.5 ppm for M-Si-O materials and around –109.5 ± 0.5 ppm for pure silica, as shown in Table 3.2.

Tabel 3.2 Solid state MAS ^{29}Si-NMR chemical shift for Mg-Si-O, Al-Si-O and SiO_2.

Material	– δ (ppm)
Mg-Si-O[a]	105.44
SiO_2[a]	109.50
SiO_2[a] + MgO (physical mixture)	109.50
Al-Si-O(I)[b]	104.89
Al-Si-O(II)[b]	105.81
SiO_2[b]	108.76

[a]samples calcined at 425 °C/16h/30 $ml \cdot min^{-1}$ O_2

[b]samples calcined at 500 °C/4h/30 $ml \cdot min^{-1}$ 20%O_2 in Ar (standard conditions)

The observed chemical shift for the M-Si-O materials indicates a higher proportion of Q3 than Q4 environment in the second coordination sphere of Si atoms (Q3 stands for $MOSi(OSi)_3$ and Q4 stands for $Si(OSi)_4$). Thus, we can assume that the metal ions are mainly incorporated into the amorphous silica framework formed during the calcination process. Moreover, the physical mixture of pure silica and magnesium oxide presents the same chemical shift as pure silica. Therefore, the observed shift for the Mg-Si-O cannot be attributed to some susceptibility effect caused by the formation of a separate MgO phase.

Solid state MAS ^{27}Al NMR spectra of Al-Si-O(I) and Al-Si-O(II) materials, presented in Figure 3.6 , show two well defined peaks at *ca.* 0-3 and 52-54 ppm and a broad peak at 30 ppm. The peak at 0-3 ppm is assigned to octahedral Al and that at 52-54 pm to tetrahedral Al.[19] The less defined peak at 30 ppm has been attributed to distorted tetrahedral Al, five-coordinated Al or to both.[20] Thus, according to the assignment of the peaks at 52-54 and 30 ppm to tetrahedral and, respectively, distorted tetrahedral and/or pentacoordinated Al sites, NMR data suggest that Al is

mainly incorporated in the silica framework. The presence of the octahedral signal at 0 ppm indicates that a minor part of Al is forming small particles of Al_2O_3.

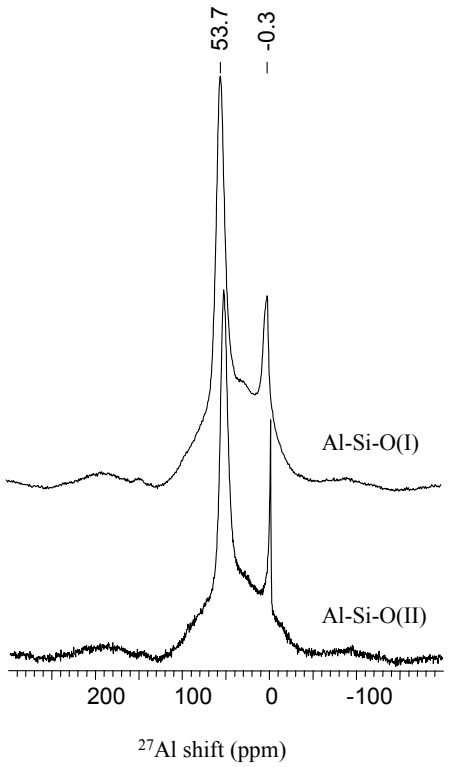

Figure 3.6 MAS ^{27}Al NMR spectra of Al-Si-O(I) and Al-Si-O(II).

Observing the metal dispersion with transmission electron microscopy requires sufficient contrast between the metal oxide and the support, and it can be difficult to detect small and highly dispersed metal oxide particles on the support surface. Nevertheless, Mg-Si-O and Al-Si-O materials were examined with HRTEM, which allowed us to get good images of thin areas of the samples as shown in Figure 3.7. In these micrographs well dispersed darker spots (Figure 3.7a,c) presenting lattice fringes (Figure 3.7b) can be seen on silica surface. The small size of these crystalline particles, around 5 nm, explains why they were not detected by XRD. Since the XRD patterns of the Mg-Si-O and Al-Si-O materials present only a broad band around 20-30° 2θ angle usually assigned to amorphous silica[21], identification of the nature of these particles is rather difficult.

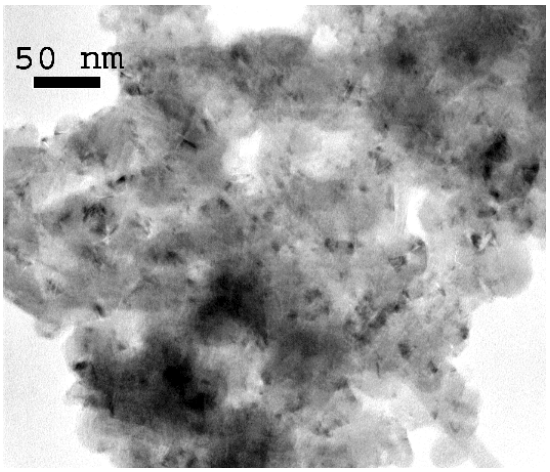

(a) Mg-Si-O 425 °C

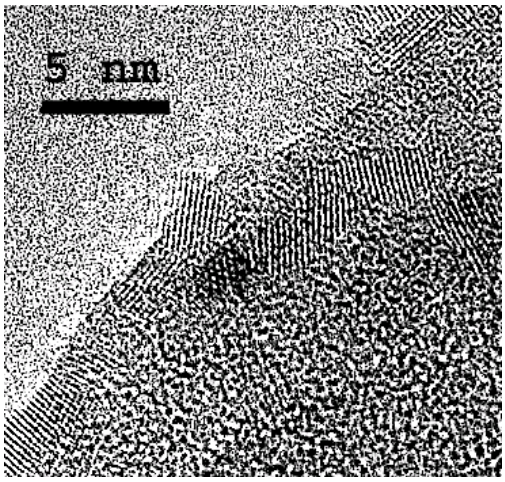

(b) Mg-Si-O

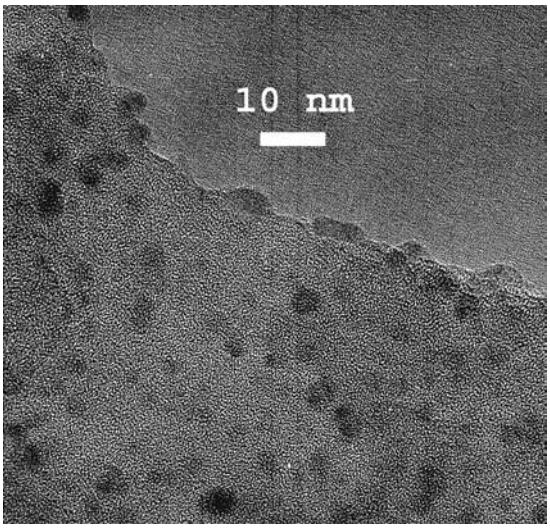

(c) Al-Si-O(II)

Figure 3.7 TEM micrographs of (a) Mg-Si-O-425 ℃, (b) Mg-Si-O and (c) Al-Si-O(II).

However, the measurements of lattice fringe spacings of the small crystalline phases (d = 1.49, 2.11 Å for Mg-Si-O and 1.73, 2.10, 2.37, 2.54 Å for Al-Si-O) and comparison with reference XRD data for MgO, Al_2O_3 and several metal silicates

indicated that they are more probably metal oxide than metal silicate particles. Thus, we assigned these particles to MgO in Mg-Si-O (d = 1.489, 2.106 Å, JCPDS file No. 78-0430) and to α-Al_2O_3 in Al-Si-O materials (d = 1.74, 2.085, 2.379, 2.550 Å, JCPDS file No. 46-1212).

This implies that during the calcination procedure some of the M-O-Si bonds can be hydrolyzed by the water formed from combustion of the organic part of the metal silsesquioxane complex and thus allows the migration of metal species on the nascent silica surface with the final formation of metal oxide particles.

Taking into account the results from XPS, EDX, NMR and TEM we can assume that the metal is present in M-Si-O samples mainly as isolated metal ions incorporated in the amorphous silica framework and also as small crystalline metal oxide particles of a few nanometers that are well dispersed throughout silica.

3.3.3 M-Si-O microtexture examined by SEM

The microtexture of M-Si-O materials was investigated by SEM. The Al-Si-O materials show agglomerates of cube-like particles, while Mg-Si-O and SiO_2 present smooth textures (see Figure 3.8). The particle size of the ground M-Si-O samples as estimated from SEM images (not shown here for sake of brevity) was roughly 5 – 20 μm.

The aggregates of cube-shape particles observed for Al-Si-O materials suggest a rather organized structure of these aluminosilicates. However, the XRD and the electron diffraction patterns obtained from Al-Si-O materials indicated only an amorphous phase. For comparison we collected SEM pictures of the non-calcined aluminium silsesquioxane **2** and found only agglomerates of cube-like particles. This indicates that the texture of Al-Si-O materials originates from one of the non-calcined aluminium silsesquioxane precursors, which seems to be maintained during calcination.

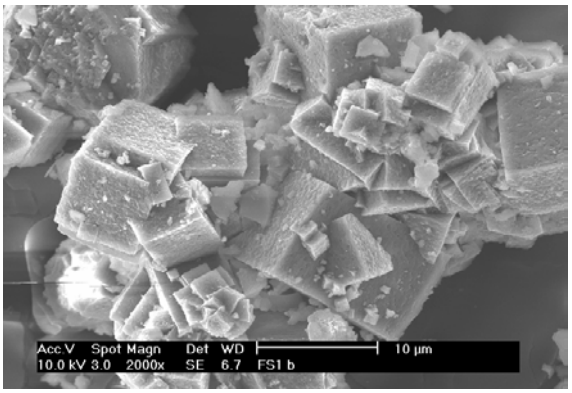

(a) Al-Si-O(I)

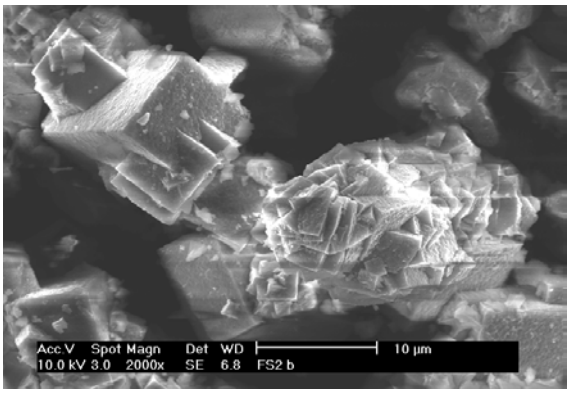

(b) Al-Si-O(II)

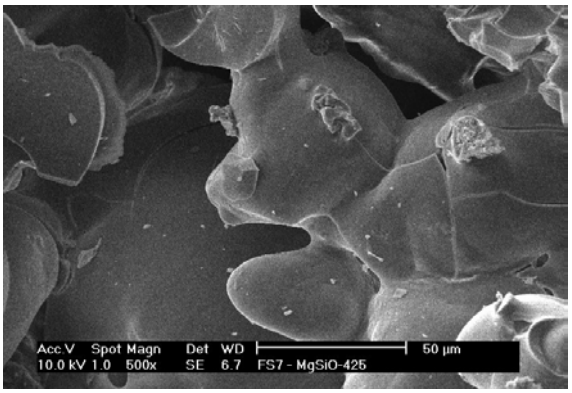

(c) Mg-Si-O 425 °C

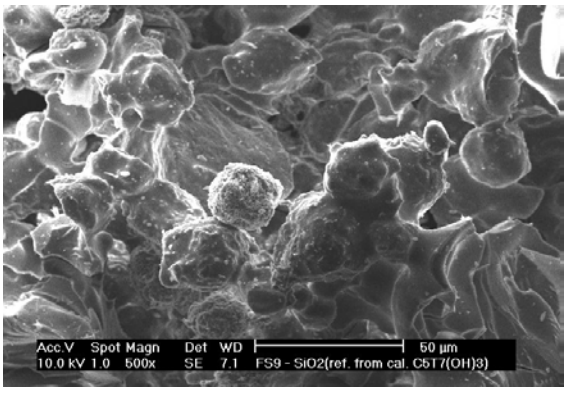

(d) SiO_2

Figure 3.8 SEM images of (a) Al-Si-O(I), (b) Al-Si-O(II), (c) Mg-Si-O 425 °C and (d) SiO_2.

3.3.4 The acid character of Al-Si-O(I) and Al-Si-O(II)

Complex **3** can be considered as a model for both Brönsted and Lewis acidic zeolite sites while complex **2** has aluminium sites that are exclusively Lewis acidic. Therefore we investigated the acid character of the calcined aluminium silsesquioxanes to determine if the resulting metallosilicates are Lewis or Brönsted acids. Thus, the aluminosilicates resulting from calcination of **2** and **3** were investigated with an in situ IR experiment involving sample treatment with deuterated acetonitrile. As described previously, this provides a good method to discriminate between Lewis and Brönsted acid sites.[22] The CN stretching frequency of CD_3CN can

be used efficiently to distinguish between different adsorbing sites on zeolites. IR measurements showed that both Al-Si-O materials posses only Lewis acid sites. Since both Al-Si-O materials gave similar CD_3CN adsorption spectra we discuss further only on the spectra of Al-Si-O(II) material presented in Figure 3.9.

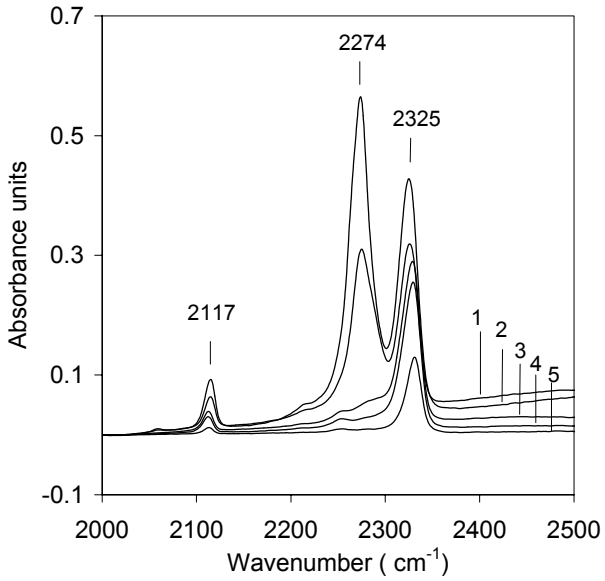

Figure 3.9 IR spectra of CD_3CN adsorbed on Al-Si-O(II): (1) at 298 K and 0.9 mbar; (2) at 298 K and 0.05 mbar; (3) after desorption at 298 K for 30 min.; (4) after desorption at 353 K for 30 min.; (5) after desorption at 573 K for 30 min.

When the sample is exposed to CD_3CN gas a band is observed at 2325 cm^{-1} which is attributed to CD_3CN adsorption on weak Lewis acid sites. When acetonitrile loading is reduced by desorption at 573 K this band evolves into a less intense one positioned at 2331 cm^{-1} which is assigned to CD_3CN adsorption on strong Lewis acid sites. The band at 2274 cm^{-1} is attributed to the adsorption of CD_3CN on the terminal Si-OH and disappeared after desorption because of the low acidity of this group. The interaction of CD_3CN gas with the terminal Si-OH groups produced also a shift of the Si-OH band from 3742 cm^{-1} to 3415 cm^{-1} (not shown here). However, after room temperature desorption, the Si-OH band came back to 3742 cm^{-1}. No band was

practically observed in the 2290 – 2300 cm^{-1} region indicative of the presence of Brönsted acid sites. Therefore we conclude that the Brönsted acid sites from compound **3** are removed probably by dehydration during calcination and that only Lewis acid sites are present.

3.3.5 Catalytic tests

The dehydration and dehydrogenation of alcohols over oxide catalysts have been previously studied.[23,24] Some oxides particularly tend to promote dehydration, whereas others have mainly dehydrogenating effects.

Mg-Si-O, Al-Si-O(I) and Al-Si-O(II) were briefly tested in the dehydrogenation – dehydration reaction of 1-butanol at 200 and 300 °C. On Mg-Si-O at 200 ºC, the 1-butanol conversion reached 45 % and at 300 ºC became 100 %. In the first 30 min at 200 ºC, butanal was the main product but afterwards butanal and 1-butene were formed in equal amounts. At 300 ºC only dehydration was observed. The color of the catalyst did not change during reaction suggesting no char building.

Al-Si-O(I) and Al-Si-O(II) were tested under similar conditions and gave at 200 ºC 100 % conversion. Dehydration to 1-butene is the main reaction that takes place but also cracking products are present. When the temperature is increased to 300 ºC the cracking reaction becomes predominant. The color of the catalyst turned black during the reaction.

3.4 Conclusions

Controlled calcination of silsesquioxane metal complexes leads to microporous amorphous metallosilicates with a narrow pore size distribution, high surface area and high loadings of well-dispersed metal oxide.

Oxidation of organic matter during calcination of the metal silsesquioxane complex precursor leaves a low amount of residual carbon in the resulting M-Si-O

materials. The amount of residual carbon can be significantly reduced by increasing the calcination temperature.

A standard calcination procedure can be generally applied for most of the metal silsesquioxane complex precursors. However, if necessary, calcination conditions like temperature or O_2 flow can be altered easily in order to adjust the textural properties of the M-Si-O, like surface area, while retaining the microporous matrix and the pore size distribution.

The spectroscopy and microscopy results show that the metal is present in M-Si-O materials mainly as isolated metal ions incorporated in the amorphous silica framework and also as small crystalline metal oxide particles of a few nanometers that are well dispersed throughout the silica and on its surface.

IR spectroscopy showed that both Al-Si-O materials posses only Lewis acid sites, both weak and strong, therefore concluding that the Bronsted acid sites from compound **3** are removed probably by dehydration during calcination and that only Lewis acid sites are present.

Mg-Si-O and Al-Si-O were active in 1-butanol conversion even at 200 °C. Mg-Si-O gave both dehydrogenation and dehydration while on Al-Si-O only dehydration and cracking reactions occurred.

References

1. (a) R. H. Baney, M. Itoh, A. Sakakibara and T. Suzuki, T., *Chem. Rev.*, 1995, 95, 1409. (b) P. A. Agaskar, *J. Chem. Soc., Chem. Commun.*, 1992, 1024.
2. (a) F. J. Feher and T. A. Budzichowski, *Polyhedron*, 1995, 14, 3239.
3. (a) T. Maschmeyer, M. C. Klunduk, C. M. Martin, D. S. Shephard, J. M. Thomas and B. F. G. Johnson, *Chem. Commun.*, 1997, 1847. (b) M. Crocker, R. H. M. Herold and A. G. Orpen, *Chem. Commun.*, 1997, 2411.
4. (a) R. Duchateau, H. C. L. Abbenhuis, R. A. van Santen, A. Meetsma, S. K. H. Thiele and M. F. H. van Tol, *Organometallics*, 1998, 17, 5663. (b) R. Duchateau, U. Cremer, R. J. Harmsen, S. I. Mohamud, H. C. L. Abbenhuis, R. A. van Santen, A. Meetsma, S. K. H. Thiele, M. F. H. van Tol and M. Kranenburg, *Organometallics*, 1999, 18, 5447.

5. (a) K. Wada, M. Nakashita, A. Yamamoto and T. Mitsudo, *Chem. Commun.*, 1998, 133. (b) K. Wada, M. Nakashita, M. Bundo, K. Ito, T. Kondo and T. Mitsudo, *Chem. Lett.*, 1998, 659. (c) N. Maxim, H. C. L. Abbenhuis, P. J. Stobbelaar, B. L. Mojet and R. A. van Santen, *Phys. Chem. Chem. Phys.*, 1999, 18, 4473. (d) K. Wada, M. Bundo, D. Nakabayashi, N. Itayama, T. Kondo and T. Mitsudo, *Chem. Lett.*, 2000, 628.
6. (a) M. G. Voronkov and V. I. Lavrent'yev, *Top. Curr. Chem.*, 1982, 102, 199. (b) V. Lorenz, A. Fischer, S. Giebmann, J. W. Gilje, Y. Gun'ko, K. Jacob and F. T. Edelmann, *Coord. Chem. Rev.*, 2000, 206-207, 321. (c) H. C. L. Abbenhuis, *Chem. Eur. J.*, 2000, 6, 25.
7. H. H. Kung and E. I. Ko, *Chem. Eng. J.*, 1996, 64, 203.
8. H. Hutter, T. Mallat and A. Baiker, *J. Catal.*, 1995, 153, 177.
9. R. Duchateau, R. J. Harmsen, H. C. L. Abbenhuis, R. A. van Santen, A. Meetsma, S. K-H. Thiele and M. Kranenburg, *Chem. Eur. J.*, 1999, 5, 3130.
10. Y. Imizu, K. Takahara, N. Okazaki, H. Itoh, A. Tada, R. Ohnishi and M. Ichikawa, *Stud. Surf. Sci. Catal.*, 1994, 90, 339.
11. R. W. J. M. Hanssen, A. Meetsma, R. A. van Santen and H. C. L. Abbenhuis, *Inorg. Chem.*, 2001, 40, 4049.
12. F. J. Feher, T. A. Budzichowski, R. L. Blanski, K. J. Weller and J. W. Ziller, *Organometallics*, 1991, 10, 2526.
13. H. C. L. Abbenhuis, A. D. Burrows, H. Kooijman, M. Lutz, M. T. Palmer, R. A. van Santen and A. L. Spek, *Chem. Commun.*, 1998, 2627.
14. (a) M. M. Dubinin and L. V. Radushkevich, *Proc. Acad. Sci. USSR*, 1947, 55, 331. (b) G. Horwath and K. Kawazoe, *J. Chem. Eng. Japan*, 1983, 16, 470.
15. J. H. Scofield, *J. Electron Spectrosc. Relat. Phenom.*, 1976, 8, 129.
16. R. A. Mantz, P. F. Jones, K. P. Chaffee, J. D. Lichtenhan and J. W. Gilman, *Chem. Mater.*, 1996, 8, 1250.
17. (a) P. J. Anderson and P. L. Morgan, *Trans. Faraday Soc.*, 1964, 60, 930. (b) C. R. Adams, *J. Phys. Chem.*, 1963, 67, 313. (c) W. G. Schlaffer, C. Z. Morgan and J. N. Wilson, *J. Phys. Chem.*, 1957, 61, 714. (d) I. Shapiro and I. M. Kolthoff, *J. Amer. Chem. Soc.*, 1950, 72, 776.
18. F. Rouquerol, J. Rouquerol and K. Sing in *Adsorption by Powders & Porous Solids – Principles, Methodology and Applications*, Academic Press: London, 1999.

19. (a) J. Livage, F. Babonneau, M. Chatry and L. Coury, *Ceram. Int.*, 1997, 23, 13. (b) K. Okada, T. Tomita, Y. Kameshima, A. Yasumori and K. J. D. MacKenzie, *J. Mater. Chem.*, 1999, 9, 1307.
20. (a) A. Samoson, E. Lippmaa, G. Engelhardt, U. Lohse and H-G. Jerschkewitz, *Chem. Phys. Lett.*, 1987, 134, 589. (b) J-P. Gilson, G. C. Edwards, A. W. Peters, K. Rajagopalan, R. F. Wormsbecher, T. G. Roberie and M. P. Shatlock, *J. Chem. Soc., Chem. Commun.*, 1987, 91. (c) J. Rocha, S. W. Carr and J. Klinowski, *Chem. Phys. Lett.*, 1991, 187, 401. (d) T-H. Chen, B. H. Wouters and P. J. Grobet, *Eur. J. Inorg. Chem.*, 2000, 281.
21. C. Real, M. D. Alcala and J. M. Criado, *J. Am. Ceram. Soc.*, 1996, 79, 2012.
22. (a) A. G. Pelmenschikov, R. A. van Santen, J. Janchen and E. Meijer, *J. Phys. Chem.*, 1993, 97, 11071. (b) M. Busio, J. Jänchen and J. H. C. van Hooff, *Microporous Mater.*, 1995, 5, 211.
23. K. Tanabe, M. Misono, Y. Ono and H. Hattori in *New Solid Acids and Bases*, *Stud. Surf. Sci. Catal.*, 51, 1989, Kodansha, Tokio.
24. H. Niiyama and E. Echigoya, *Bull. Chem. Soc. Japan*, 1970, 44, 1739.

4

Synthesis and characterisation of microporous Fe-Si-O materials with tailored iron content

Abstract

Calcination of mixtures of $(c\text{-}C_5H_9)_7Si_7O_9(OH)_3$, **1**, and $(c\text{-}C_5H_9)_7Si_7O_{12}Fe(tmeda)$, **2** (tmeda = N,N,N',N'-tetramethylethylenediamine), led to microporous amorphous Fe-Si-O materials with adjustable iron content in the range 1-11 wt%. A set of different complementary techniques including N_2 physisorption, XRD, XPS, DRUV-Vis, RS, IR, HRTEM and Mössbauer spectroscopy were used to follow the variation of the textural properties, metal dispersion and speciation with the iron content along the whole mixing series. The calcination of these mixtures produced Fe-Si-O materials having basically the same properties as those observed for the individually calcined iron silsesquioxane. The N_2 physisorption indicates high surface areas, rather large pore volumes and a very narrow pore size distribution with an average pore size diameter around 6-7 Å. The TEM and the spectroscopic analysis of the Fe-Si-O materials indicate that the iron is present mainly as small iron oxide particles highly dispersed throughout silica and to a minor extent as clustered and isolated species. The particle size distribution was estimated to be about 2-8 nm for 11 % Fe-Si-O and 2-4 nm for samples with lower iron content. These materials showed catalytic activity in NH_3 oxidation and N_2O decomposition.

N. Maxim, A. Overweg, P. J. Kooyman, R. W. J. M. Hanssen, R. A. van Santen, H. C. L. Abbenhuis, *J. Phys. Chem. B*, in press.

4.1 Introduction

The chemistry of silsesquioxanes receives considerable current interest as these organosilicon compounds offer numerous exciting applications in materials science and catalysis. Thus, metal-free silsesquioxanes are being used as precursors for ceramic materials[1] while metallasilsesquioxanes are suitable homogeneous model systems for silica-supported metal catalysts or metal-containing zeolites.[2] Moreover, they can even be active catalysts themselves[3,4]. Metal-containing silsesquioxanes also turn out to be convenient precursors for potentially catalytic microporous amorphous M-Si-O materials with high surface area, uniformly controlled micropores and high metal dispersion.[5] This development has also been stimulated by the fact that in recent years numerous main group, early and late transition metal silsesquioxane complexes have become available.[6] The known literature already involves the calcination of Ti, Cr, Mg, Al and Ga silsesquioxanes in order to form microporous mixed oxides with catalytic activity.[5]

As described in the previous chapters for chromium and aluminium silsesquioxanes, the calcination treatment resulted in the formation of metal oxide species highly dispersed throughout the amorphous silica.[5b,c] In both resulting M-Si-O materials the metal was mainly present in isolated sites. A minor amount of small metal oxide particles well dispersed throughout silica was observed as well. The resulting amorphous materials had a very narrow pore size distribution centered at 6 Å.

However, the metal content in the resulting M-Si-O materials (up to about 11 wt%) is fixed and depends on its concentration in the metal silsesquioxane precursors. In order to overcome this disadvantage for the potential catalytic applications of these materials we propose here a way to adjust the metal content in the metallosilicate synthesis. Thus, we confirmed that calcination of metal-free silsesquioxanes gave rise to the formation of a microporous amorphous silica with a similar pore size

distribution.[5a,b] In addition, metallasilsesquioxanes and silsesquioxanes are both soluble in solvents like tetrahydrofuran.

In this chapter, we report the first application of a calcination procedure to the synthesis of a series of Fe-Si-O materials differing in iron content resulting from mixing a metal-free silsesquioxane **1** and an iron silsesquioxane complex **2** in THF followed by removal of the solvent and calcination of the solid mixture.

We investigate here if the calcination of these mixtures leads to silica-based iron-containing materials having properties similar to those observed for the individually calcined iron silsesquioxane. Therefore, a set of different complementary techniques including N_2 physisorption, XRD, XPS, DRUV-Vis, RS, IR, HRTEM and Mössbauer spectroscopy were used to follow the variation of the textural properties, metal dispersion and speciation with the iron content along the whole mixing series.

4.2 Experimental

4.2.1 Synthesis of iron-containing silsesquioxane.

The iron silsesquioxane was prepared according to a procedure based on a synthesis reported recently for the analogous compound $(c\text{-}C_6H_{11})_7Si_7O_{12}Fe(tmeda)$.[7] The trisilanol silsesquioxane **1**[8] (6.23 g, 7.12 mmol) was dissolved in 125 ml of THF. Buthyl lithium (8.54 ml of a 2.5 M solution in hexane, 21.36 mmol) was added slowly to the solution of **1**. After mixing a white precipitate was formed. When $FeCl_3$ (1.15 g, 7.12 mmol) was added the white suspension changed its colour from white to brown and after 15 min transformed into a brown transparent solution. After removal of the solvent *in vacuo*, addition of 125 ml of hexane and hot filtration a dark brown clear solution was obtained. Tmeda (8 ml, 53 mmol) was added to the filtrate and resulted in rapid formation of a light yellow solution. Keeping this solution at –30 °C for 1 day produced crystals of **2** in 65 % yield. Elemental analyses were consistent with the calculated composition of complex **2**: calculated C 47.15, H 7.62, N 2.68; experimental C 47.13, H 7.69, N 2.61.

4.2.2 Synthesis of Fe-Si-O materials

Fe-Si-O materials with iron contents from 11 wt% of iron (calcined complex **2**) down to 1 wt% were prepared by using different mixing ratios of compounds **1** and **2** (see Scheme 4.1). The solvent removal was performed from warm solutions under controlled vacuum and using vigorous stirring in order to ensure a good homogeneity of the resulting solid mixtures. Samples were calcined in batches of 0.5 g at 500 °C, heating rate 5 °C/min, for 4 hours in a flow of 20 % O_2 in Ar. As reported earlier for calcination of chromium and magnesium silsesquioxane, these conditions allowed an efficient carbon removal and led to high surface area materials.[5b,c]

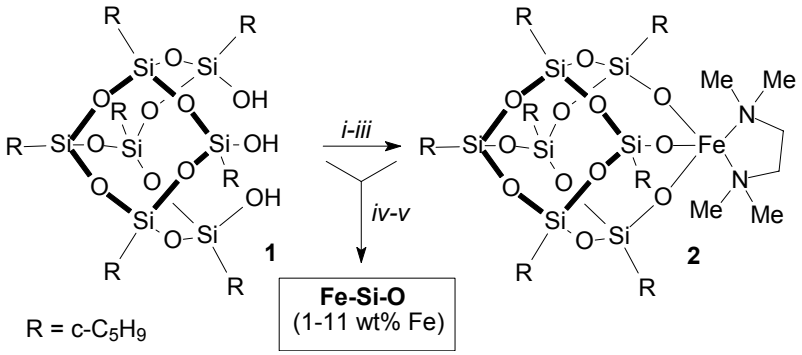

Scheme 4.1 A silsesquioxane route to Fe-Si-O materials with tailored iron content. Reagents and conditions. i: BuLi (3 equiv.), THF, 20 °C, 5 min; ii: $FeCl_3$ (1 equiv.), 15 min; iii: TMEDA (7.4 equiv.), Hexane, 18 h, 65 % yield; iv: mixture of 1 and 2, THF; v: calcination, O_2 / Ar, 500 °C, 4 h.

4.2.3 Analysis methods

The carbon content of M-Si-O materials was measured by heating the samples at 925 °C on a Perkin Elmer automated analyzer Series II CHNS/O Analyzer 2400. The thermogravimetry was performed at 500 °C in ambient air on a Shimadzu TGA-50.

Inductively coupled plasma optical emission spectrometry (ICP-OES) was used for the determination of the iron content in the Fe-Si-O materials. The measurements were performed with a SPECTRO CIROSCCD spectrometer. Before measurement the samples were dried at 110 °C for 1 hour and then dissolved in a mixture of HF and HNO_3 acids.

The nitrogen physisorption measurements, were performed as described in previous chapters. Surface area, pore volume and pore size distribution were calculated from Horvath-Kawazoe and Dubinin-Radushkevich models.[9]

X-ray diffraction data were collected on a Rigaku diffractometer in the range $5.0° < 2\theta < 80°$ using Cu Kα radiation and the step scan method at 0.1 deg/min scanning speed and 5 s dwelling time.

X-ray photoelectron spectroscopy data were obtained using the experimental procedure described in chapter 3. Elemental ratios were calculated from the peak areas with correction for the cross-sections.[10]

Transmission electron microscopy was performed using a Philips CM30UT high resolution electron microscope with a field emission gun as a source of electrons operated at 300 kV. Samples were mounted on a microgrid carbon polymer supported on a copper grid by placing a few droplets of a suspension of ground sample in ethanol on the grid followed by drying at ambient conditions.

^{57}Fe Mössbauer spectra were measured on a constant acceleration spectrometer in a triangular mode with a ^{57}Co:Rh source. Mössbauer spectra of all Fe-Si-O materials were recorded at 300 K. Additional measurements at 77 K and 4.2 K were carried out for the Fe-Si-O samples containing 3 wt%, 7 wt% and 11 wt% Fe, respectively. The overall spectra were deconvoluted with calculated Mössbauer spectra that consisted of Lorentzian-shape lines. In the case of quadrupole doublets the line widths and the absorption areas of the constituent lines were constrained equal. Positional parameters were not constrained in the fitting procedure. The isomer shift values are reported relative to sodium nitroprusside, $Na_2Fe(CN)_5NO$.

Diffuse reflectance UV-Vis spectra were taken at room temperature on a UV-2401PC Shimadzu spectrophotometer equipped with a diffuse reflectance unit. Powdered samples were loaded between 0.3 mm Suprasil windows. Spectra were

recorded against a $BaSO_4$ reflectance standard in the range 190-1000 nm. The computer processing of the spectra consisted of the following steps: subtraction of the baseline, conversion to wavenumber and calculation of the Kubelka-Munk (KM) function.[11]

Fourier transform infrared (FTIR) spectra of the Fe-Si-O samples were performed under ambient conditions on a Nicolet Protégé 460 FTIR Spectrometer E.S.P. equipped with a MCT/A detector and a Golden Gate Single Reflection Diamond sampling unit. Automatic baseline correction of the spectra was used.

FTIR spectra of NO adsorbed on 11% Fe-Si-O sample were measured on a Bruker FTIR spectrometer (IFS 113v) equipped with a vacuum cell. Self-supporting discs with a thickness of 8 $mg \cdot cm^{-2}$ were used. The spectra were recorded by co-adding 500 scans at room temperature with a resolution of 4 cm^{-1}. The samples were reduced in H_2 for 4 h at 673 K and evacuated in high vacuum (10^{-6} mbar) for 2 h. After cooling down to room temperature, the spectrum of the unloaded sample was taken, followed by exposing the sample to NO gas for 30 min at a pressure of 130 mbar and recording of a new spectrum. After this, the loading of the samples was reduced stepwise by lowering the equilibrium pressure to 0.1 mbar as well as by desorption for 30 min at 298, 373, 498 and 653 K, respectively, followed by collecting room temperature spectra after each step. The spectrum of the unloaded sample was subtracted from the spectra of samples with different NO loadings.

Raman spectra were recorded with a RFS 100/S FT-Raman Bruker spectrometer. A Nd:YAG laser at 1064 nm was used as the excitation source. Different laser powers in the range 40 –180 mW were used. All spectra were recorded under ambient conditions by co-adding 1024 scans with a resolution of 4 cm^{-1}.

Fe-Si-O samples were tested in NH_3 oxidation and N_2O decomposition. The catalytic tests were performed in continuous plug-flow reactors. Reaction conditions for NH_3 oxidation were: temperatures 200 – 400 °C; flow rate 50 Nml/min; NH_3 1 vol.%; O_2 10 vol.%; catalyst weight 0.1 g. Reaction conditions for N_2O decomposition were: temperature 500 °C; flow rate 16 Nml/min; N_2O 0.25 vol.%; catalyst weight 0.04 g. The reaction products were analyzed by mass spectrometry and chemiluminescence methods.

4.3 Results and discussion

4.3.1 Textural properties and composition of Fe-Si-O materials

The nominal and actual iron bulk contents of the Fe-Si-O materials are shown in Table 4.1.

Table 4.1 The textural properties and composition of Fe-Si-O materials.

Sample	wt%Fe (ICP)	Surface area[a] (m^2/g)	Pore volume[b] (ml/g)		Average pore diameter[c] (Å)	Fe/Si surface ratio (XPS)
11% Fe-Si-O	10.6	623	0.22	0.22	7.2	0.140
9% Fe-Si-O	8.3	662	0.24	0.23	7.1	0.110
7% Fe-Si-O	6.6	445	0.16	0.16	6.0	0.092
5% Fe-Si-O	4.9	561	0.20	0.19	6.3	0.063
3% Fe-Si-O	2.8	628	0.22	0.22	6.1	0.032
1% Fe-Si-O	0.9	548	0.19	0.19	5.9	0.011

[a]estimated from Dubinin-Radushkevich equation[9a]; [b]estimated from Dubinin-Radushkevich (left column)[9a] and Horvath-Kawazoe equations (right column)[9b]; [c]estimated from Horvath-Kawazoe equation[9b]

The actual iron contents of the Fe-Si-O samples were analysed by ICP-OES and are slightly in variance with the expected values. Unless otherwise notified, all iron loadings mentioned in the paper are refered to the nominal values. The carbon content of the samples determined by elemental analysis was about 0.2 – 0.4 wt%. Note also that the total weight loss of the complex **2** during calcination, estimated from thermogravimetric analysis, was very close to the calculated value (measured 52.14 %, calculated 52.09 %) indicating the absence of any sublimation effect.

The textural properties of the Fe-Si-O materials were determined by using N_2 physisorption. All of the Fe-Si-O samples, except the 11 % Fe-Si-O (calcined complex **2**), yielded type Ib isotherms characteristic of microporous materials. The 11 % Fe-Si-O sample showed a type IIb isotherm associated with a steep increase in the adsorption amount at low p/p_0, indicative for the presence of both micro- and mesopores. Attribution of the Fe-Si-O materials isotherms was made according to

extended IUPAC classification.[12] Typical values for surface area, pore volume and average pore diameter for Fe-Si-O materials are presented in Table 4.1. These results indicate the formation of microporous materials with large surface areas of about 500-600 m^2/g, rather large pore volumes of cca. 0.2 ml/g and a narrow pore size distribution with an average pore size diameter around 6 – 7 Å. Mesopore size distribution of the 11 % Fe-Si-O estimated from the desorption isotherm by using the Barrett-Joyner-Halenda (B-J-H) method[13] indicated the formation of a few mesopores with a diameter of about 4 nm. For the Fe-Si-O samples with lower iron content no mesopores were detected.

4.3.2 The investigation of iron dispersion and speciation

The metal dispersion was estimated from XPS data. The surface Fe/Si atomic ratios obtained by XPS analysis are also presented in Table 1. The surface Fe/Si ratios were plotted against the bulk Fe/Si atomic ratios calculated from the actual iron concentrations, as shown in Figure 4.1.

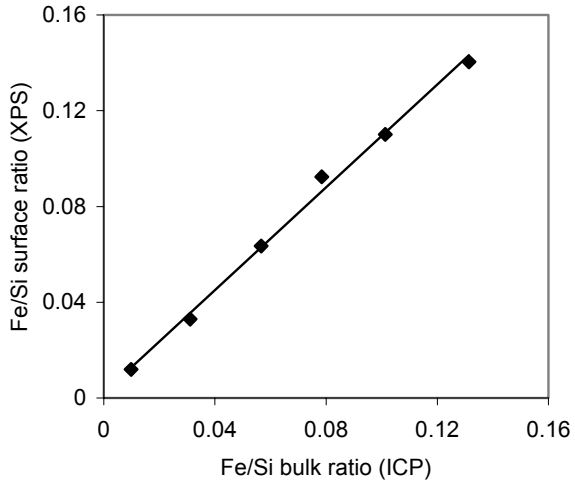

Figure 4.1 Fe/Si atomic bulk ratio versus Fe/Si atomic surface ratio.

It can be seen that the Fe/Si surface and bulk ratios have a linear relationship along the whole Fe-Si-O series. The regression coefficient (R^2 = 0.9955) and the slope of

the line (1.0726) are very close to 1 indicating a good dispersion of iron throughout the silica for all the iron samples.

DRUV-Vis spectroscopy is often used to identify the oxidation states and coordination environments of transition metal ions in supported metal oxide or zeolite catalysts.[11] The iron state in Fe-Si-O materials was investigated by DRUV-Vis spectroscopy. DRUV-Vis spectra of Fe-Si-O materials are shown in Figure 4.2. All of the Fe-Si-O samples show a strong and broad absorption extending from 50000 to 12000 cm^{-1}. The intensity of the absorption spectra increases with the iron loading of the samples. Pure tetrahedral or octahedral Fe^{3+} species are usually characterized by two distinct bands in the 50000 – 40000 cm^{-1} region.[14] The presence, in this case, of an unresolved absorption suggest that the Fe^{3+} species can also have distorted symmetries.

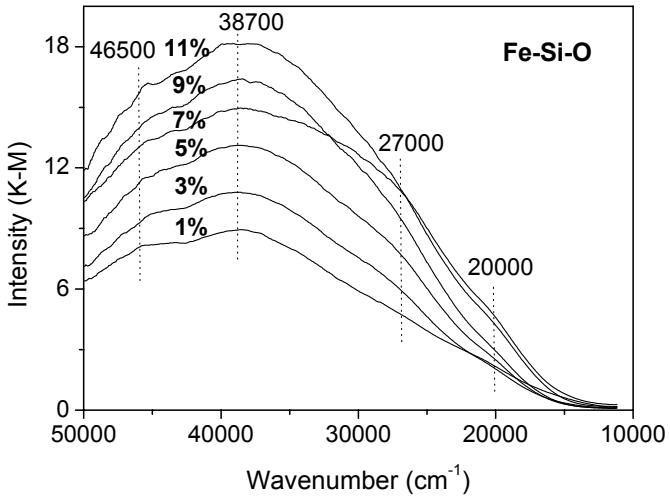

Figure 4.2 Diffuse Reflectance UV-Vis spectra of the Fe-Si-O materials with different loadings.

Two maxima can be distinguished in the DRUV-Vis spectra of all of the Fe-Si-O materials at about 46500 cm^{-1} and 38700 cm^{-1}. The band at 46500 cm^{-1} was also found for Fe-silicalite, Fe-ZSM-5 and Fe-mesoporous silica and is ascribed to ligand-to-metal Fe^{3+} charge transfer transitions involving isolated Fe^{3+} species with tetrahedral and/or octahedral coordination.[15] The band at 38700 cm^{-1} was also observed for Fe-

silicalite after thermal treatments and assigned to clustered octahedral Fe^{3+} formed by migration of framework tetrahedral Fe^{3+} towards extraframework positions.[15a] Besides the isolated and clustered Fe^{3+}, additional iron species are also present as indicated by the two shoulders at about 27000 cm^{-1} and 20000 cm^{-1}. The latter band is characteristic of Fe_2O_3 particles, while the former one is observed for example in γ-FeOOH diluted in silica.[16] The data for the 7 % Fe-Si-O sample noticeably deviate from the others in the low wavenumber region, where a stronger absorbtion and a broadening of the 27000 cm^{-1} band are observed. A newly prepared sample showed the same deviation, which we attributed to an increased contribution of ferric oxides particles for this sample. This could also result in blockage of some of the pores formed during calcination, explaining the somewhat lower surface area and pore volume of this sample. The origin of this deviation is not yet clearly understood but the extent of this effect seems to be rather limited since the other characterisation techniques used did not reveal significant differences between the 7 % Fe-Si-O and the other samples. Thus, DRUV-Vis spectra of Fe-Si-O materials indicate the presence in all the samples of both isolated and clustered Fe^{3+} species as well as of particles of iron oxide. A quantitative estimation of their concentration is however not reliable by reflectance spectroscopy.[11]

The Raman spectra of 11, 9 and 5 % Fe-Si-O materials and of silica, obtained by calcination of metal-free silsesquioxane **1**, were measured under ambient conditions and are compared in Figure 4.3. The silica possesses weak Raman bands at ~487, ~600, ~802 and 993 cm^{-1}. The 993 cm^{-1} band is associated with Si–OH stretching mode of the surface hydroxyls. The broad bands at 600 and 487 cm^{-1} are assigned to D2 and D1 defect modes which have been attributed to tri- and tetracyclosiloxane rings produced via the condensation of surface hydroxyls.[17] The band at ~802 cm^{-1} has been assigned to the symmetrical Si–O–Si stretching mode.[18] The changes in the silica Raman bands at ~600 and 487 cm^{-1} are not very significant for the Fe-Si-O materials. However, accurate determination of the position of these bands is hindered by the strong fluorescence arising from the background of the samples. The ~802 cm^{-1} band shifts downward to ~784 cm^{-1} and becomes less broad, suggesting that some Si–O–Si bridges are affected by the dispersed iron oxide.

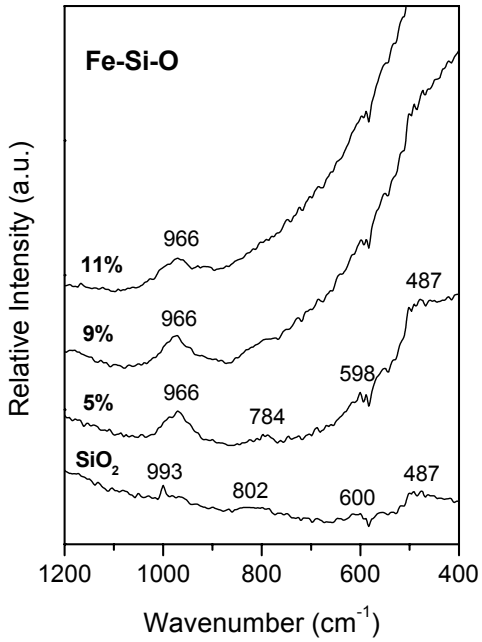

Figure 4.3 Raman spectra of the Fe-Si-O materials with different loadings.

A new silica band is observed at ~966 cm^{-1} while the sharp band at 993 cm^{-1} is not visible anymore. A similar behaviour observed for silica supported titania catalysts was attributed to the formation of Ti–O–Si bonds.[19] We also associated this 27 cm^{-1} shift with the presence of Fe–O–Si bonds. No bands characteristic for iron oxide or oxohydroxide particles are observed, probably because some of these compounds are poor light scatterers. For example, the γ-Fe_2O_3 (maghemite), in contrast to α-Fe_2O_3 (hematite) and Fe_3O_4 (magnetite), has broad and poorly defined Raman bands of which resolution depends on the degree of crystallinity of the material. This makes the observation of such a phase very difficult.[20]

The IR spectra of 7, 5, 3 and 1 % Fe-Si-O materials and of silica, obtained by calcination of metal-free silsesquioxane **1**, were measured under ambient conditions and are provided in Figure 4.4.

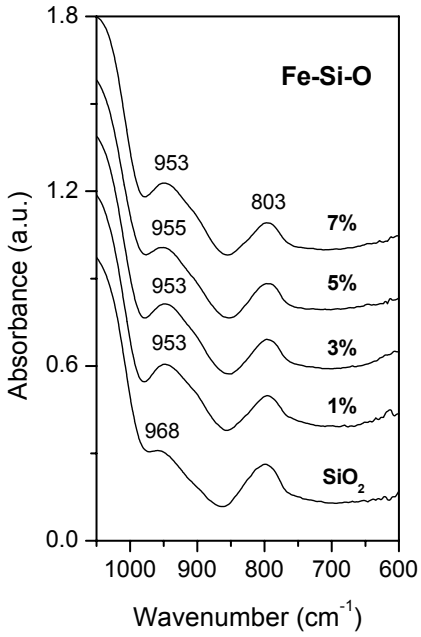

Figure 4.4 Infrared spectra of the Fe-Si-O samples.

Pure silica exhibits the symmetrical Si–O–Si stretching vibration at ~803 cm^{-1}, along with a band at ~968 cm^{-1} due to the symmetric stretch of Si–OH groups.[21] The ~968 cm^{-1} band is observed for highly hydroxylated (high surface area) silicas and its rather large half width is attributed to a hydrogen bonding perturbation. The slight downward shift of this band from ~968 cm^{-1} to ~953 cm^{-1}, observed for the Fe-Si-O samples, was assigned to the presence of some Fe–O–Si bonds in these materials.[19a] Thus, Raman and IR spectra of Fe-Si-O materials both suggest the presence of some Fe–O–Si bonds.

However, additional information can be obtained by means of adsorption of a probe molecule. NO is particularly attractive from this point of view since its uptake on Fe_3O_4 at 273 K and pressures near 10 kPa is ten times higher than that of CO under similar conditions.[22] In addition, the extent of nitric oxide adsorption on silica is small at 273 K and subatmospheric pressures.[23] NO adsorption has been used to investigate

iron speciation on silica supported iron oxide and iron containing zeolites.[24] Since NO adsorbs to very low extent on Fe^{3+} in comparison with Fe^{2+}, silica supported iron oxide catalysts are reduced in hydrogen before NO adsorption.

The IR spectra of NO adsorbed on reduced 11 % Fe-Si-O material (calcined **2**) are shown in Figure 4.5.

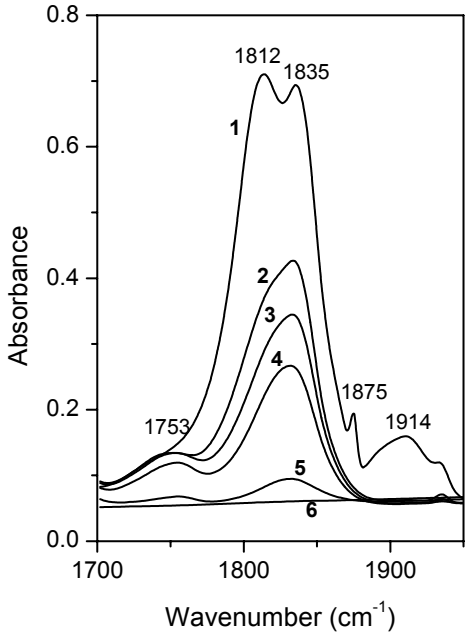

Figure 4.5 Room temperature infrared spectra of 11 % Fe-Si-O reduced in H_2 at 673 K, exposed to NO and evacuated at progressively higher temperatures: (1) at 298 K and 130 mbar; (2) at 298 K and 0.1 mbar; (3) after desorption at 298 K for 0.5 h; (4) after desorption at 373 K for 0.5 h; (5) after desorption at 498 K for 0.5 h; (6) after desorption at 653 K for 0.5 h.

Only the wavenumber range from 1700 to 1950 cm^{-1} is shown since all observable bands resulting from adsorbed NO were found within these limits. At maximum NO coverage, the spectrum is dominated by intense absorptions at 1812 and 1835 cm^{-1}. Less intense features appear at 1914, 1875 and 1753 cm^{-1}. Upon decreasing the NO

pressure, the bands at 1914, 1875 and 1812 cm^{-1} disappear. Only the 1835 and 1753 cm^{-1} bands survive at room temperature evacuation step. This doublet is not destroyed even after outgassing the sample under high vacuum at 498 K. It is worth noticing that the initial spectrum (curve 1) is recovered by readmission of NO. Similar bands have been reported for NO adsorption on silica supported iron oxide and Fe-silicalite.[24] These bands were attributed to nitrosyl complexes formed by NO adsorption on ferrous species present in two different coordinative states. In the Fe/SiO_2 case, the doublet appearing at 1914 and 1812 cm^{-1} and the single band at 1753 cm^{-1} were respectively assigned to di- and mononitrosyl species formed on fourfold coordinated Fe^{2+} centers strongly interacting with the support, while the band at 1835 cm^{-1} was assigned to a mononitrosyl complex on sixfold coordinated Fe^{2+} at the surface of small iron oxide particles. The disappearance of the 1914 and 1812 cm^{-1} bands upon evacuation was attributed to the conversion of dinitrosyl to mononitrosyl complexes that are more stable at low pressures.[24a]

In the Fe-silicalite case, the number of NO ligands involved in the formation of nitrosyl complexes and the equilibria between these complexes were rather differently interpretated. However, similar ferrous species were taken into consideration, namely, low-coordinated iron species present as isolated iron centers grafted to the framework, and high-coordinated iron species belonging to $(FeO)_n$ extraframework (or partially extraframework) clusters.[24c] According to these assignments, the IR spectra of NO adsorbed on 11 % Fe-Si-O indicate the presence of both isolated iron species and clusters or small particles of iron oxide. These findings are in agreement with the interpretation of DRUV-Vis, Raman and IR spectra.

Transmission electron microscopy is routinely used to investigate the dispersion and size of the metal oxide particles on the support surface. However, observing the metal dispersion with TEM requires sufficient contrast between the metal oxide and the support, and it can be difficult to detect small and highly dispersed metal oxide particles. Nevertheless, Fe-Si-O materials were examined with high resolution TEM, which allowed us to obtain good images of thin areas of the samples as exemplified in Figure 4.6 for the 7 % Fe-Si-O sample.

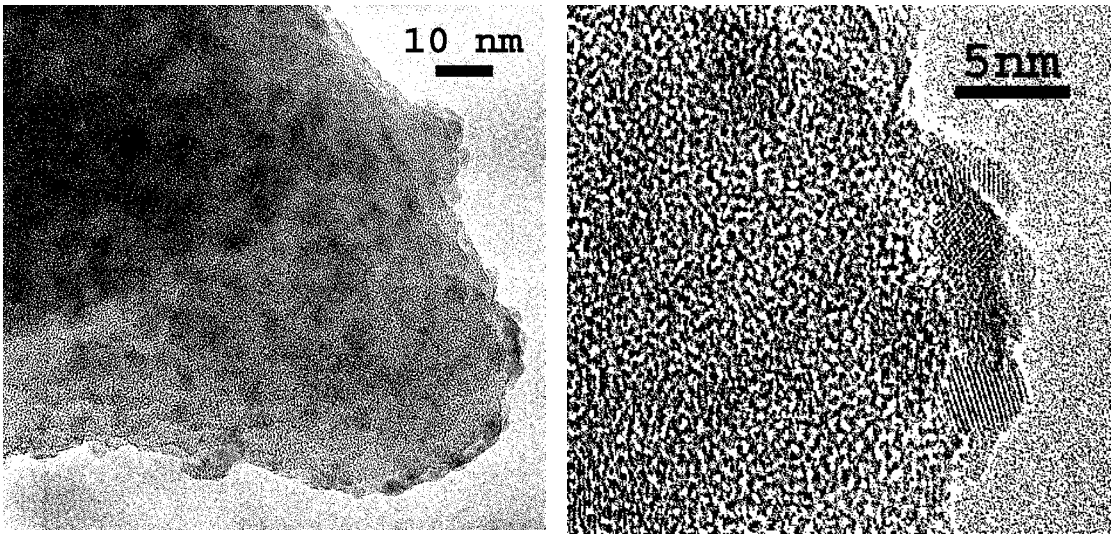

(a) 7 % Fe-Si-O (b) 7 % Fe-Si-O (enlargement)

Figure 4.6 TEM micrographs of (a) 7 % Fe-Si-O and (b) 7 % Fe-Si-O (zoom in).

In these micrographs well dispersed particles (Figure 4.6a) presenting lattice fringes, which indicate crystallinity (Figure 4.6b), can be seen on the silica surface. Similar pictures were obtained for the other Fe-Si-O samples (not shown here for sake of brevity). The particle size distribution seems to narrow with the decrease of the iron content. Thus, the particle size on the 11 % Fe-Si-O sample was in the 2 – 8 nm range while on the 3, 5 and 7 % Fe-Si-O samples mainly particles of 2 – 4 nm size were observed.

The small size of these crystalline particles explains why they were not detected by XRD. It should also be noted that some of the particles seem to be amorphous (no lattice fringe patterns are present). Since the XRD patterns of the Fe-Si-O materials present only a broad band around 20-30° 2θ angle usually assigned to amorphous silica[25], identification of the nature of these particles is rather difficult. However, the measurements of lattice fringe spacings of the small crystalline phases (d = 2.10, 2.52 and 2.95 Å) and comparison with reference XRD data for iron oxides and several iron silicates suggested that they are most probably γ-Fe_2O_3, maghemite (d = 2.09, 2.52 and 2.95 Å, JCPDS file No. 15-0615). The presence of such an iron

oxide phase would explain also why it could not be observed in the Raman spectra of Fe-Si-O materials. It is also known that γ-Fe_2O_3 is unstable versus α-Fe_2O_3 at high temperatures.[20a] However, the presence of a γ-Fe_2O_3 phase in the Fe-Si-O materials could be explained by a stabilizing effect of the water produced during calcination.[26]

TEM results are in good agreement with the DRUV-Vis and IR spectra of adsorbed NO. They clearly indicate the formation of iron oxide particles. This implies that during the calcination procedure, the Fe-O-Si bonds can be hydrolyzed by the water formed from combustion of the organic part of the silsesquioxanes. This allows the migration of the metal species on the nascent silica surface with the final formation of metal oxide particles. The tendency to form smaller iron oxide particles with the lowering of the iron content might be attributed to the fact that in the precursor mixtures containing less iron, the hydrolyzed iron species has to travel longer distances on the silica in order to form particles of iron oxide. This minimizes the chance to form large particles and favors the formation of smaller ones.

The chemical state of iron in Fe-Si-O materials was also investigated by means of Mössbauer spectroscopy**.** ^{57}Fe Mössbauer spectra of all Fe-Si-O materials were measured at 300 K. In all cases a single quadrupole doublet was obtained with isomer shifts (IS) of 0.61 ± 0.01 mm/s and quadrupole splittings (QS) ranging from 1.01 mm/s to 1.11 mm/s. These parameters are all very similar and indicate Fe^{3+} ions in a high-spin state for all Fe-Si-O materials.

Additional information on the particle size distribution of small iron oxide particles in these materials was obtained by studying the temperature dependence of the Mössbauer spectra. This information is based on the magnetic properties of the small iron oxide particles, which depend on both the temperature and the particle volume of these iron oxide particles.[27] Temperature dependent Mössbauer spectra of 3, 7 and 11 % Fe-Si-O samples are given in figures 4.7 (a) – (c). The corresponding Mössbauer parameters are given in Table 4.2. In all three figures, a temperature-related transition in the spectra can be observed from a quadrupole doublet to a sextuplet. This transition is related to a slowing down of the rate of fluctuation of the magnetization vector among the easy directions of the small iron oxide particles such

that the particles become magnetic on the time scale of the Mössbauer experiment. In that case a magnetically split Mössbauer spectrum, *i.e.* a sextuplet, is obtained.

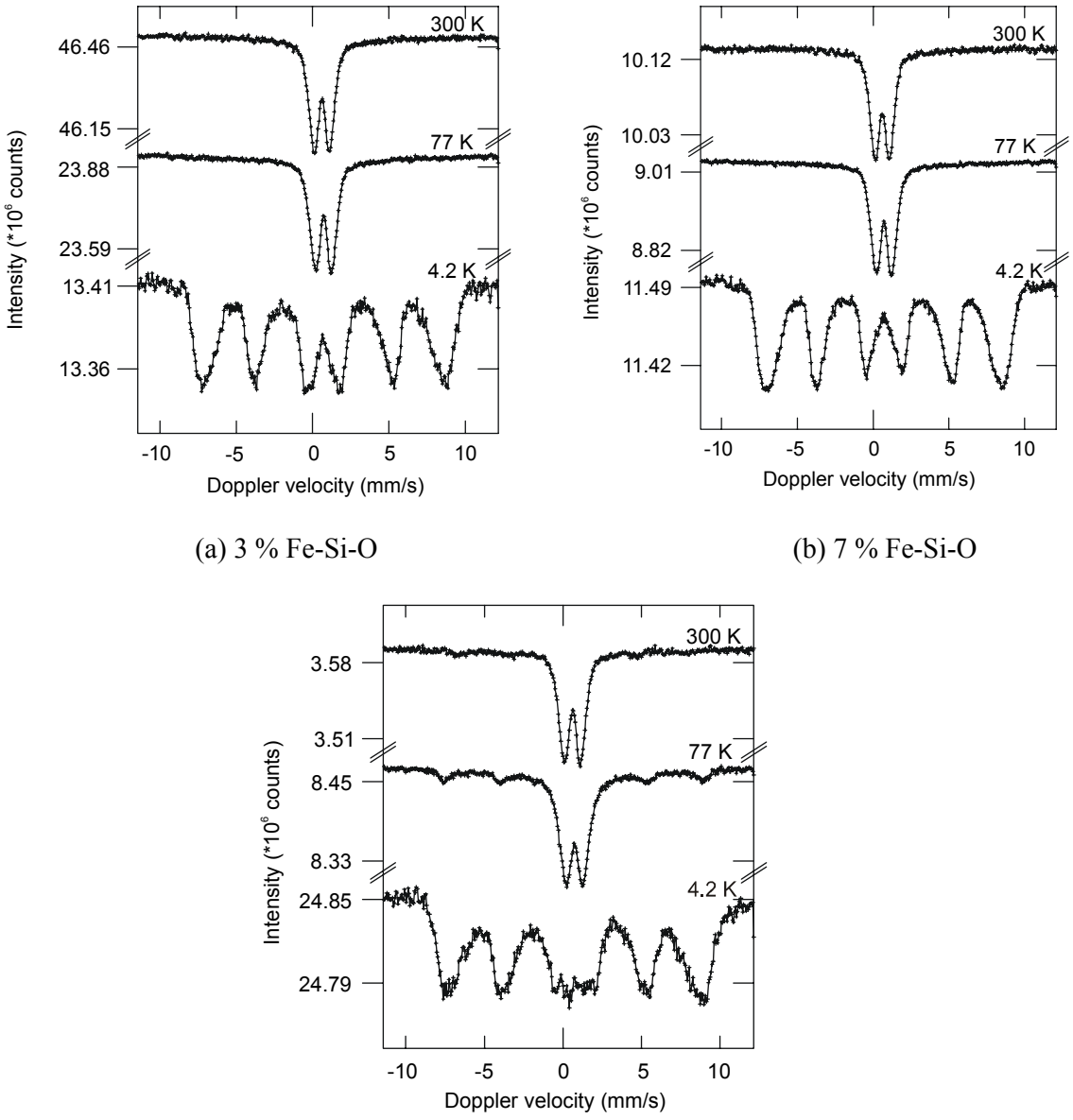

(a) 3 % Fe-Si-O

(b) 7 % Fe-Si-O

(c) 11 % Fe-Si-O

Figure 4.7 Mössbauer spectra of (a) 3 % Fe-Si-O, (b) 7 % Fe-Si-O and (c) 11 % Fe-Si-O recorded at 300 K, 77 K and 4.2 K.

Table 4.2 Parameters belonging to Mössbauer spectra of Fe-Si-O materials with different loadings.

Sample	Measurement condition	Isomer shift (mm/s)	Quadrupole splitting (mm/s)	Hyperfine field (T)	Spectral contribution (%)
3 % Fe-Si-O	300 K	0.61	1.05		100
	77 K	0.71	1.12		100
	4.2 K	0.72		47.2	82
		0.68		6.3	18
7 % Fe-Si-O	300 K	0.61	1.01		100
	77 K	0.71	1.07		100
	4.2 K	0.72		47.2	88
		0.74		7.0	12
11 % Fe-Si-O	300 K	0.62	1.06		100
	77 K	0.73	1.12		72
		0.72		50.6	28
	4.2 K	0.76		47.8	83
		0.72	1.08		17

For the 3 and 7 % Fe-Si-O samples, this transition takes place on lowering the temperature of the Mössbauer measurement from 77 K to 4.2 K. A more gradual transition is observed for the 11 % Fe-Si-O material. There, next to the quadrupole doublet, a sextuplet is already visible at 77 K that becomes more prominent at 4.2 K. In addition, the Mössbauer spectrum of the latter material still shows a quadrupole doublet at 4.2 K. Such a doublet is not observed in the 4.2 K Mössbauer spectra of the 3 and 7 % Fe-Si-O materials. Thus, the 11 % Fe-Si-O sample has an estimated particle size distribution ranging from smaller than 2 nm to about 6 nm. The samples containing less iron on the other hand have a much narrower particle size distribution, with an approximated particle size of ca. 2 nm. The absence of a quadrupole doublet at 4.2 K in the Mössbauer spectra of the 3 and 7 % Fe-Si-O samples indicates that no iron oxide clusters of sizes smaller than 2 nm (too small to give a sextuplet at 4.2 K) are detected. This could be related on one hand to the lower concentrations of iron in these samples, which makes more difficult to distinguish the quadrupole doublet from

the sextuplet at 4.2 K, and on the other hand to a low amount of isolated iron species and very small clusters of iron oxide compared with the larger iron oxide particles.

Summarizing we can conclude that Mössbauer spectra indicate that small iron oxide particles are the main iron species in the Fe-Si-O materials. The particle size distributions estimated from these spectra are very close to those observed with HRTEM and confirm the narrowing of the particle size range with the decrease of the iron content.

The predominance of iron oxide particles (oxidic aggregates) in the Fe-Si-O materials suggests a different behavior of the iron silsesquioxane during calcination in comparison with the aluminium or chromium silsesquioxane where mainly isolated metal oxide species were detected after calcination.[5b,c] This could be related to the different propensity to hydrolysis of M-O-Si bonds from different metallasilsesquioxanes. It is known that the large predisposition of iron precursors to hydrolysis restricts its incorporation in zeolite frameworks to very low concentrations.[28] The high dispersion of iron in Fe-Si-O materials should therefore be associated with a low mobility of the hydrolyzed iron species, which hamper the formation of bulk iron oxide and help to preserve the high dispersion from the initial precursors mixture.

4.3.3 Catalytic tests

Iron-based catalysts have been widely used in reactions like ammonia and Fischer-Tropsch synthesis and more recently for the hydroxylation of benzene and methane. Here the Fe-Si-O catalysts have been tested in ammonia oxidation and N_2O decomposition.

The Fe-Si-O catalysts have been tested in NH_3 oxidation at 400 °C. The 11 % Fe-Si-O sample catalysed the selective oxidation of NH_3 to N_2 and H_2O with 76 % conversion and 95 % selectivity. This catalyst, when pre-treated in H_2 before reaction, gave 84 % conversion and 97 % selectivity. The reduced 5 % Fe-Si-O sample gave 58 % conversion and 96 % selectivity. Related catalytic tests are described in chapter 5.

The reduced 11 % and 5 % Fe-Si-O catalysts were tested in N_2O decomposition to N_2 and O_2 at 500 °C and gave 20 % and 5 % conversion, respectively.

4.4 Conclusions

We proposed a successful way to prepare microporous amorphous Fe-Si-O materials with adjustable iron content in the range 1-11 wt% via calcination of mixtures of metal-free silsesquioxane **1** and iron silsesquioxane complex **2**.

Examination of the textural properties, metal dispersion and speciation along the whole mixing series showed that calcination of the silsesquioxane precursor mixtures led to Fe-Si-O materials having properties similar to those observed for the individually calcined iron silsesquioxane.

The N_2 physisorption indicates high surface areas, rather large pore volumes and a very narrow pore size distribution with an average pore size diameter around 6-7 Å. TEM and spectroscopic analysis showed that the iron is present mainly as small iron oxide particles highly dispersed throughout silica and to a minor extent as clustered and isolated species. Most of the iron oxide particles are crystalline but some amorphous particles seem to be present too. An increased formation of ferric oxides particles is indicated by DRUV-Vis spectra in the case of 7 % Fe-Si-O sample but the extent of this effect seems to be rather limited since the other characterisation techniques used did not reveal significant differences between this sample and the others. All these results recommend the iron silsesquioxane as an excellent precursor to prepare tiny iron oxide particles highly dispersed on silica.

Fe-Si-O materials catalyzed the selective oxidation of NH_3 to N_2 and H_2O. They also showed activity in N_2O decomposition.

In conclusion, we demonstrated the efficiency of this approach to overcome the disadvantage of the fixed metal content associated with calcination of individual metallasilsesquioxanes. This increases the applicability of the metallasilsesquioxane precursors for the synthesis of new microporous metallosilicate catalysts and it opens a way to prepare microporous mixed oxide catalysts containing more than one metal.

References

1. (a) R. H. Baney, M. Itoh, A. Sakakibara and T. Suzuki, T., *Chem. Rev.*, 1995, 95, 1409. (b) P. A. Agaskar, *J. Chem. Soc., Chem. Commun.*, 1992, 1024. (c) R. A. Mantz, P. F. Jones, K. P. Chaffee, J. D. Lichtenhan and J. W. Gilman, *Chem. Mater.*, 1996, 8, 1250.
2. (a) F. J. Feher and T. A. Budzichowski, *Polyhedron*, 1995, 14, 3239.
3. (a) T. Maschmeyer, M. C. Klunduk, C. M. Martin, D. S. Shephard, J. M. Thomas and B. F. G. Johnson, *Chem. Commun.*, 1997, 1847. (b) M. Crocker, R. H. M. Herold and A. G. Orpen, *Chem. Commun.*, 1997, 2411.
4. (a) R. Duchateau, H. C. L. Abbenhuis, R. A. van Santen, A. Meetsma, S. K. H. Thiele and M. F. H. van Tol, *Organometallics*, 1998, 17, 5663. (b) R. Duchateau, U. Cremer, R. J. Harmsen, S. I. Mohamud, H. C. L. Abbenhuis, R. A. van Santen, A. Meetsma, S. K. H. Thiele, M. F. H. van Tol and M. Kranenburg, *Organometallics*, 1999, 18, 5447.
5. (a) K. Wada, M. Nakashita, M. Bundo, K. Ito, T. Kondo and T. Mitsudo, *Chem. Lett.*, 1998, 659. (b) N. Maxim, H. C. L. Abbenhuis, P. J. Stobbelaar, B. L. Mojet and R. A. van Santen, *Phys. Chem. Chem. Phys.*, 1999, 18, 4473. (c) N. Maxim, P. C. M. M. Magusin, P. J. Kooyman, J. H. M. C. van Wolput, R. A. van Santen and H. C. L. Abbenhuis, *Chem. Mater.*, 2001, 13, 2958. (d) K. Wada, K. Yamada, T. Kondo and T. Mitsudo, *Chem. Lett.*, 2001, 12.
6. (a) M. G. Voronkov and V. I. Lavrent'yev, *Top. Curr. Chem.*, 1982, 102, 199. (b) V. Lorenz, A. Fischer, S. Giebmann, J. W. Gilje, Y. Gun'ko, K. Jacob and F. T. Edelmann, *Coord. Chem. Rev.*, 2000, 206-207, 321. (c) H. C. L. Abbenhuis, *Chem. Eur. J.*, 2000, 6, 25.
7. V. Lorenz, A. Fischer and F. T. Edelmann, *Z. Anorg. Allg. Chem.*, 2000, 626, 1728.
8. F. J. Feher, T. A. Budzichowski, R. L. Blanski, K. J. Weller and J. W. Ziller, *Organometallics*, 1991, 10, 2526.
9. (a) M. M. Dubinin and L. V. Radushkevich, *Proc. Acad. Sci. USSR*, 1947, 55, 331. (b) G. Horwath and K. Kawazoe, *J. Chem. Eng. Japan*, 1983, 16, 470.
10. J. H. Scofield, *J. Electron Spectrosc. Relat. Phenom.*, 1976, 8, 129.
11. B. M. Weckhuysen and R. A. Schoonheydt, *Catal. Today*, 1999, 49, 441.
12. F. Rouquerol, J. Rouquerol and K. Sing in *Adsorption by Powders & Porous Solids – Principles, Methodology and Applications*, Academic Press: London, 1999.

13. E. P. Barrett, L. G. Joyner and P. P. Halenda, *J. Am. Chem. Soc.*, 1951, 73, 373.
14. (a) S. Bordiga, F. Geobaldo, C. Lamberti, A. Zecchina, F. Boscherini, F. Genoni, G. Leofanti, G. Petrini, M. Padovan, S. Geremia and G. Vlaic, *Nucl. Instr. and Meth. B 97*, 1995, 23. (b) B. N. Figgis in *Introduction to Ligand Fields*, Wiley: New York, 1966.
15. (a) S. Bordiga, R. Buzzoni, F. Geobaldo, C. Lamberti, E. Giamello, A. Zecchina, G. Leofanti, G. Petrini, G. Tozzola and G. Vlaic, *J. Catal.*, 1996, 158, 486. (b) G. Centi and F. Vazzana, *Catal. Today*, 1999, 53, 683. (c) A. Tuel, I. Arcon and J. M. M. Millet, *J. Chem. Soc., Faraday Trans.*, 1998, 94, 3501.
16. R. Bongiovanni, E. Pellizzetti, E. Borgarello and D. Meisel, *Chim. Ind.*, 1994, 93, 261.
17. (a) B. A. Morrow and A. J. Mcfarlan, *J. Non-Cryst. Solids*, 1990, 120, 61. (b) C. J. Brinker, R. J. Kirkpatrick, D. R. Tallant, B. C. Bunker and B. Montez, *J. Non-Cryst. Solids*, 1988, 99, 418.
18. P. MacMillan, *Am. Mineral.*, 1986, 69, 622.
19. (a) X. Gao, S. R. Bare, J. L. G. Fierro, M. A. Banares and I. E. Wachs, *J. Phys. Chem. B*, 1998, 102, 5653. (b) S. Pei, G. W. Zajac, J. A. Kaduk, J. Faber, B. I. Boyanov, D. Duck, D. Fazzini, I. T. Morrison and D. S. Yang, *Catal. Lett.*, 1993, 21, 333.
20. (a) D. L. A. de Faria, S. V. Silva and M. T. de Oliveira, *J. Raman Spectrosc.*, 1997, 28, 873. (b) F. Perez-Robles, F. J. Garcia-Rodriguez, S. Jimenez-Sandoval and J. Gonzales-Hernandez, *J. Raman Spectrosc.*, 1999, 30, 1099.
21. (a) M. R. Boccuti, K. M. Rao, A. Zecchina, G. Leofanti and G. Petrini, *Stud. Surf. Sci. Catal.*, 1989, 48, 133. (b) E. F. Vansant, P. V. D. Voort and K. C. Vrancken, *Stud. Surf. Sci. Catal.*, 1995, 93. (c) A. Zecchina, S. Bordiga, S. Spoto, L. Marchese, G. Petrini, G. Leofanti and M. Padovan, *J. Phys. Chem.*, 1992, 96, 4985.
22. J. E. Kubsh, Y. Chen and J. A. Dumesic, *J. Catal.*, 1981, 71, 192.
23. A. Solbakken and L. H. Reyerson, *J. Phys. Chem.*, 1959, 63, 1622.
24. (a) S. Yuen, Y. Chen, J. E. Kubsh, J. A. Dumesic, N. Topsoe and H. Topsoe, *J. Phys. Chem.*, 1982, 86, 3022. (b) F. Boccuzzi, E. Guglielminotti, F. Pinna and M. Signoretto, *J. Chem. Soc. Faraday Trans.*, 1995, 91(18), 3237. (c) G. Spoto, A. Zecchina, G. Berlier, S. Bordiga, M. G. Clerici and L. Basini, *J. Mol. Catal. A*, 2000, 158, 107.
25. C. Real, M. D. Alcala and J. M. Criado, *J. Am. Ceram. Soc.*, 1996, 79, 2012.
26. F. E. DeBoer and P. W. Selwood, *J. Am. Chem. Soc.*, 1954, 76, 3366.
27. S. Mørup, *Hyperf. Int.*, 1990, 60, 959.
28. P. Fejes, J. B. Nagy, K. Lazar and J. Halasz, J. *Appl. Catal. A: General*, 2000, 190, 117.

5

Synthesis and characterisation of microporous bimetallic Fe-Cr-Si-O materials

Abstract

Calcination of silsesquioxane mixtures of $(c\text{-}C_5H_9)_7Si_7O_9(OH)_3$, **1**, $(c\text{-}C_5H_9)_7Si_7O_{12}Fe(CH_3)_2N(CH_2)_2N(CH_3)_2$, **2**, and $(c\text{-}C_5H_9)_7Si_7O_9(OSiMe_3)O_2CrO_2$, **3**, led to microporous amorphous bimetallic Fe-Cr-Si-O materials with different Fe/Cr ratios. A set of complementary characterization techniques including N_2 physisorption, XRD, XPS, RS, IR, HRTEM and Mössbauer spectroscopy were used to follow the variation of the textural properties, metal oxide dispersion and speciation with the metal content. Fe-Cr-Si-O materials possess high surface areas and uniformly controlled micropores with an average pore size diameter around 6-7 Å. Metal oxide speciation appears to be significantly different from the one observed for these metals in the individually calcined metal silsesquioxanes. The iron oxide and monochromates are the predominant species in the calcined **2** and **3** precursors while very small particles (2-4 nm) of bimetallic mixed oxides are the major species in Fe-Cr-Si-O materials. This suggests that the metal oxide species are highly interdispersed and can come in close contact with each other during the calcination procedure thus favoring the formation of the bimetallic mixed oxide phase. On the contrary, a reference catalyst containing 7 % Fe and 3 % Cr prepared via impregnation method showed only chromate species and large particles (10-30 nm) of iron oxide. A silsesquioxane-derived catalyst of similar composition was much more selective in ammonia oxidation than the reference catalyst. This recommends the metallasilsesquioxane mixtures as versatile precursors to silica based catalysts containing very small and well dispersed particles of mixed metal oxides.

To be submitted for publication: Nicolae Maxim, Arian Overweg, Patricia J. Kooyman, Anton Nagy, Rutger A. van Santen and Hendrikus C.L. Abbenhuis, *J. Mater. Chem.*

5.1 Introduction

Metal-containing silsesquioxanes are convenient precursors for potentially catalytic microporous amorphous M-Si-O materials with high surface area, uniformly controlled micropores and high metal dispersion.[1] We showed in the previous chapters that the calcination of Cr, Mg, Al and Fe silsesquioxanes produced microporous mixed oxides with catalytic activity.[1b-c,2] In addition, we showed for Fe that the metal content can be conveniently adjusted in the metallosilicate synthesis, in the range 0 – 11 wt%, by mixing the iron silsesquioxane and the metal-free silsesquioxane in tetrahydrofuran followed by solvent removal and calcination of the solid mixture.[2] The resulting Fe-Si-O materials showed the same good textural properties and metal dispersion as the individually calcined iron silsesquioxane. Remarkably, in this case small iron oxide particles were the predominant iron species while mainly isolated metal species were detected previously in the calcined chromium and aluminium silsesquioxanes[1b-c] This could be related to the different propensity to hydrolysis of the M-O-Si bonds from different metallasilsesquioxanes by the water formed during the calcination. Consequently, the high dispersion of the metal in M-Si-O materials is therefore associated with a low mobility of the hydrolyzed metal species, which hamper the formation of bulk metal oxide and help to preserve the high dispersion from the initial precursors. These results open a way to prepare microporous mixed oxide catalysts containing more than one metal.

Bimetallic oxide catalysts are used extensively in many important industrial processes and often they are better than their single-metal counterparts in terms of catalytic activity and/or selectivity. We report, in this chapter, the first application of a calcination procedure to the synthesis of a series of bimetallic Fe-Cr-Si-O materials with different Fe/Cr ratios resulting from mixing a metal-free silsesquioxane, **1**, an iron silsesquioxane, **2**, and a chromium silsesquioxane, **3**.

We investigate here how the textural properties, metal speciation and dispersion of the calcined mixtures differ on one hand compared with the individually

calcined metal silsesquioxanes and on the other hand compared with a silica supported iron-chromium material prepared via the classical impregnation method. In order to accomplish this, a set of complementary characterisation techniques including N_2 physisorption, XRD, XPS, RS, IR, HRTEM and Mössbauer spectroscopy were used. Both the silsesquioxane derived materials and the reference were tested as catalysts in ammonia oxidation reaction to nitrogen and water.

5.2 Experimental

5.2.1 Synthesis of Fe-Cr-Si-O materials

The incompletely condensed silsesquioxane, **1**, was prepared by the hydrolytic condensation of cyclopentyl-trichlorosilane.[3] Iron and chromium silsesquioxanes, **2** and **3**, were prepared from **1** according to procedures reported earlier.[1b,2]

Fe-Cr-Si-O materials with different Fe/Cr ratios and a total metal content of maximum 10.5 wt% were prepared by using different mixing ratios of metal silsesquioxanes **2** and **3** (see Scheme 5.1). The metal-free silsesquioxane **1** was added, when necessary, in order to achieve the desired metal to silicon ratio. Hexane and toluene were used as solvents in order to solubilize the silsesquioxane precursors. The solvent removal was performed from warm solutions under controlled vacuum and using vigorous stirring in order to ensure a good homogeneity of the resulting solid mixtures. Samples were calcined in batches of 0.5 g at 500 °C for 4 h in a flow of 20 % O_2 in Ar. As reported earlier for calcination of chromium and magnesium silsesquioxanes, these conditions allowed an efficient carbon removal and led to large surface area materials.[1b,c]

A reference sample was prepared by sequential incipient wetness impregnation of a conventional mesoporous silica SG-360 Grace (surface area 513 m^2/g and pore volume 0.95 cm^3/g). The silica was first evacuated at 200 °C for 2 h. $Fe(NO_3)_3 \cdot 9H_2O$ and CrO_3 were used as impregnation precursors. The impregnated sample was calcined under the same conditions as the silsesquioxane mixtures.

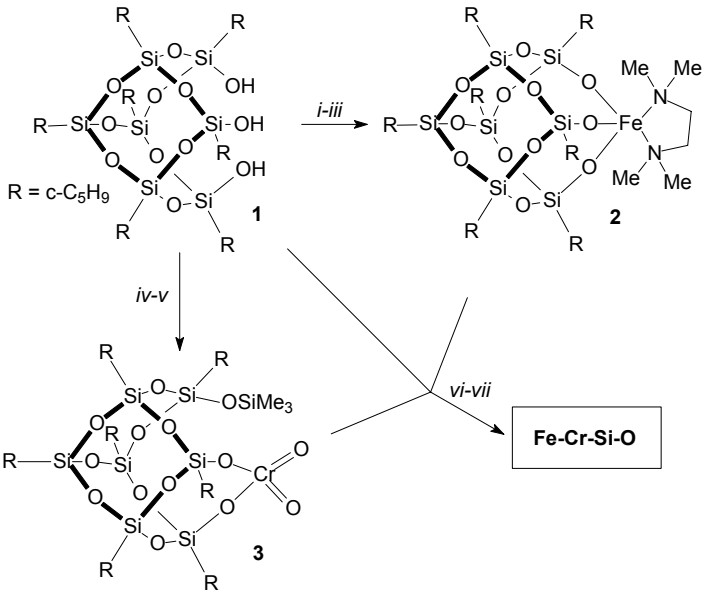

Scheme 5.1 A silsesquioxane route to Fe-Cr-Si-O materials with tailored metal content. Reagents and conditions. i: BuLi; ii: $FeCl_3$; iii: TMEDA (N,N,N',N'-tetramethylethylenediamine); iv: Me_3SiCl; v: CrO_3, ; vi: mixture of 1, 2 and 3, hexane/toluene; vii: calcination, O_2 / Ar, 500 ^oC, 4 h.

The silsesquioxanes derived samples were labeled using element symbols preceded by numbers, which indicate the approximate nominal metal contents. For example, 7/3 Fe-Cr-Si-O indicates a silica based material containing approximately 7 wt% Fe and 3 wt% Cr. The reference sample was labeled 7/3 Fe-Cr/SiO_2 (r). Fe-Si-O and Cr-Si-O indicate materials obtained from the separate calcination of iron and chromium silsesquioxanes or from mixtures of these complexes with metal-free silsesquioxane. For simplicity, the silica symbol was omitted from the labels used in the figures.

5.2.2 Analysis methods

The carbon content of M-Si-O materials was measured by heating the samples at 925 °C on a Perkin Elmer automated analyzer Series II CHNS/O Analyzer 2400.

Inductively coupled plasma optical emission spectrometry (ICP-OES) was used for the determination of the iron and chromium content in the Fe-Cr-Si-O materials. The measurements were performed with a SPECTRO CIROSCCD spectrometer. Before measurement the samples were dried at 110 °C for 1 h and then dissolved in an aqueous mixture of HF and HNO_3.

The nitrogen physisorption measurements were performed as described in previous chapters. Surface area, pore volume and pore size distribution were calculated from Horvath-Kawazoe and Dubinin-Radushkevich models.[4] For the reference 7/3 Fe-Cr (r) sample the BET and BJH models were used as well.[5]

X-ray diffraction (XRD) data were collected on a Rigaku diffractometer in the range $5.0° < 2\theta < 80°$ using Cu Kα radiation and the step scan method at 0.1 deg/min scanning speed and 5 s dwelling time.

X-ray photoelectron spectroscopy data were obtained using the experimental procedure described in the previous chapter. Elemental ratios were calculated from the peak areas with correction for the cross-sections.[6]

Transmission electron microscopy (TEM) was performed using a Philips CM30UT high resolution electron microscope with a field emission gun as a source of electrons operated at 300 kV. Samples were mounted on a microgrid carbon polymer supported on a copper grid by placing a few droplets of a suspension of ground sample in hexane on the grid followed by drying at ambient conditions.

^{57}Fe Mössbauer spectra were measured, on a constant acceleration spectrometer in a triangular mode with a ^{57}Co:Rh source, as described in chapter 4. Mössbauer spectra of Fe-Cr-Si-O materials (except for 3/3 Fe-Cr-Si-O) and of the reference 7/3 Fe-Cr/SiO_2 (r) were recorded at 300, 77 and 4.2 K.

Fourier transform infrared (FTIR) spectra of the Fe-Si-O samples were performed under ambient conditions on a Nicolet Protégé 460 FTIR Spectrometer E.S.P. equipped with a MCT/A detector and a Golden Gate Single Reflection Diamond sampling unit. An automatic baseline correction of the spectra was used.

Raman spectra were recorded with a RFS 100/S FT-Raman Bruker spectrometer. A Nd:YAG laser at 1064 nm was used as the excitation source.

Different laser powers in the range 40 –180 mW were used. All spectra were recorded under ambient conditions by co-adding 1024 scans with a resolution of 4 cm^{-1}.

All the Fe and/or Cr containing samples including the reference 7/3 Fe-Cr/SiO_2 (r) were tested in NH_3 oxidation. The catalytic tests were performed in continuous plug-flow reactors. Reaction conditions for NH_3 oxidation were: temperatures 200 – 400 °C; flow rate 50 N ml/min; NH_3 1 vol.%; O_2 10 vol.%; carrier gas He; catalyst weight 0.1 g. The samples were pretreated in a H_2-He flow containing 16 vol.% H_2 at 400 °C for 1h. The reaction products were analyzed by mass spectrometry and chemiluminescence methods.

5.3 Results and discussion

5.3.1 Textural properties and composition of Fe-Cr-Si-O materials

The nominal and actual metal bulk content of the Fe-Cr-Si-O materials and of the 7/3 Fe-Cr/SiO_2 (r) reference sample are shown in Table 5.1.

Table 5.1 The textural properties and composition of Fe-Cr-Si-O, Fe-Si-O, Cr-Si-O and Fe-Cr/SiO_2 (r).

Sample	Fe[a] (wt%)	Cr[a] (wt%)	Surface area[b] (m^2/g)	Pore volume[b] (ml/g)	Average pore diameter[c] (Å)
11% Fe-Si-O	10.6	0	623	0.22	7.0
7/3 Fe-Cr-Si-O	6.8	3.0	764	0.27	7.1
5/5 Fe-Cr-Si-O	5.4	4.9	569	0.20	6.7
3/6 Fe-Cr-Si-O	3.5	6.3	561	0.20	6.8
3/3 Fe-Cr-Si-O	2.9	2.6	467	0.16	6.0
10% Cr-Si-O	0	10.2	546	0.19	6.8
7/3 Fe-Cr/SiO_2 (r)[d]	6.0	2.8	449	0.94	80

[a]determined by ICP-OES; [b]estimated from Dubinin-Radushkevich equation; [c]estimated from Horvath-Kawazoe equation; [d]for this sample surface area was estimated from BET equation and pore volume and average pore diameter from BJH equation.

The actual metal contents were analysed by ICP-OES and are slightly in variance with the expected values. Unless otherwise notified, all metal loadings mentioned in the paper are referred to the nominal values. The carbon content of the Fe-Cr-Si-O materials determined by elemental analysis was about 0.1 wt%.

The textural properties of the Fe-Cr-Si-O materials and of the reference sample were determined by N_2 physisorption. All of the Fe-Cr-Si-O samples yielded type Ib isotherms characteristic of microporous materials. The reference sample showed a type IV isotherm associated with a small increase in the adsorption amount at low p/p_0. This indicates a mesoporous material containing also a small amount of micropores. The attribution of the materials isotherms was made according to extended IUPAC classification.[7]

Typical values for surface area, pore volume and average pore diameter for Fe-Cr-Si-O, Fe-Si-O, Cr-Si-O samples and the reference are presented in Table 1. These results indicate that the calcination of the metal silsesquioxanes mixtures produced microporous materials with large surface areas of about 450 – 750 m^2/g, rather large pore volumes of about 0.16 – 0.27 ml/g and a narrow pore size distribution with an average pore size diameter around 6 – 7 Å. These results are comparable with those observed for individually calcined metal silsesquioxanes. The reference sample showed a surface area of 450 m^2/g, a very large pore volume of 0.94 ml/g and an average pore diameter around 80 Å.

5.3.2 Investigations on metal dispersion and speciation

The metal dispersion in Fe-Cr-Si-O materials and in the reference 7/3 Fe-Cr/SiO_2 (r) was estimated from XPS data. The surface Fe/Si, Cr/Si and Fe/Cr atomic ratios obtained by XPS analysis are presented in Table 5.2. The surface Fe/Si ratios are close to the bulk ratios for all Fe-Cr-Si-O samples indicating a high dispersion of iron in these materials. The reference sample has a striking surface Fe/Si ratio, which is half of the bulk ratio. This means that in the reference sample the iron might be present in the form of large particles of probably iron oxide. The surface Cr/Si ratios of both the Fe-Cr-Si-O and the reference samples indicate a less uniform distribution

of the chromium. The surface Cr/Si ratios are higher than the bulk ratios indicating that the chromium resides preferentially on the silica surface than in the bulk.

Tabel 5.2 Surface (XPS) and bulk (ICP) atomic ratios for Fe-Cr-Si-O and Fe-Cr/SiO_2 (r).

Sample	Fe/Si		Cr/Si		Fe/Cr	
	surface	bulk	surface	bulk	surface	bulk
7/3 Fe-Cr-Si-O	0.075	0.086	0.068	0.041	1.102	2.11
5/5 Fe-Cr-Si-O	0.069	0.070	0.095	0.068	0.728	1.02
3/6 Fe-Cr-Si-O	0.048	0.045	0.130	0.087	0.371	0.51
3/3 Fe-Cr-Si-O	0.043	0.034	0.062	0.033	0.685	1.03
7/3 Fe-Cr/SiO_2 (r)	0.038	0.075	0.053	0.037	0.726	1.99

Consequently, the surface Fe/Cr ratios are lower than the expected bulk values for all the samples with a markedly decreased value for the reference sample, 0.726 instead of 1.99. The comparison between 7/3 Fe-Cr-Si-O sample and the reference indicate a better metal dispersion for the silesquioxane derived sample. It also suggests that the iron and chromium species are much better interdispersed in the Fe-Cr-Si-O samples compared to the reference.

Raman spectra of Fe-Cr-Si-O materials with various metal loadings, measured under ambient conditions, are presented in Figure 5.1. For comparison, Raman spectra of 5 % Fe-Si-O, 10 % Cr-Si-O and of silica obtained by calcination of metal-free silsesquioxane **1** are shown as well. The silica possesses weak Raman bands at ~487, ~600, ~802 and 993 cm^{-1}. The 993 cm^{-1} band is associated with Si–OH stretching mode of the surface hydroxyls. The broad bands at 600 and 487 cm^{-1} are attributed to vibration modes of tri- and tetracyclosiloxane rings produced via the condensation of surface hydroxyls.[8] The band at ~802 cm^{-1} has been assigned to the symmetrical Si–O–Si stretching mode.[9] The 5 % Fe-Si-O sample does not show any Raman bands characteristic to iron oxide. However, we showed in the previous chapter that such a sample contains very small and highly dispersed γ-Fe_2O_3 (maghemite) particles. This is explained by the fact that the Raman bands of maghemite are not well defined and their resolution seems to depend on the degree of crystallinity of the material. The Cr-Si-O sample shows two well-defined bands at 980 and 865 cm^{-1} assigned to

dehydrated and, respectively, hydrated monochromate species.[10] The Fe-Cr-Si-O samples show also the hydrated monochromate band which becomes less defined with the decrease of the chromium content. The band at 980 cm^{-1} is broadened and slightly shifted to 976 cm^{-1} and it could be due to both the dehydrated monochromate species and the silica.

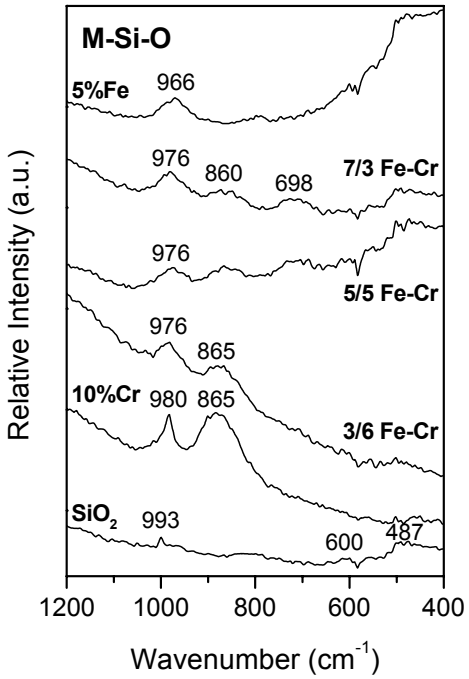

Figure 5.1 Raman spectra of the Fe-Cr-Si-O, Fe-Si-O and Cr-Si-O materials.

Remarkably, a new band is observed at ~698 cm^{-1} for the 7/3 and 5/5 Fe-Cr-Si-O samples. The intensity of this band is higher for the former sample that has the highest content of iron. This band is not present in the Raman spectra of Fe-Si-O and Cr-Si-O materials, suggesting that it might be attributed to an iron-chromium mixed oxide phase. Note that a band appearing in the 650 – 700 cm^{-1} range was reported in literature for iron-chromium mixed oxides of spinel type.[11] The 698 cm^{-1} band is not observed in the Raman spectrum of 3/6 Fe-Cr-Si-O sample.

Raman spectra of the reference 7/3 Fe-Cr/SiO_2 (r) sample and of the silica used for the impregnation, measured under ambient conditions, are shown in Figure 5.2. The reference sample also shows the dehydrated and hydrated monochromate bands at 980 and, respectively, 872 cm^{-1}. In addition, three sharp bands are observed at 409, 292 and 224 cm^{-1}, which are assigned according to previous reports to a α-Fe_2O_3 (hematite) phase.[12]

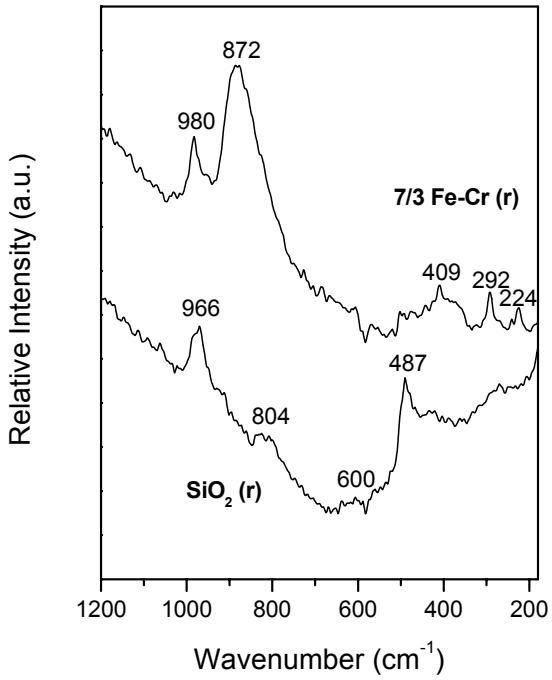

Figure 5.2 Raman spectra of Fe-Cr/SiO_2 (r) reference sample and of silica support.

Note that in contrast to maghemite the Raman spectrum of hematite is characterized by sharp and intense bands, which makes this phase easier to detect. Moreover, no band can be observed in the 650 – 700 cm^{-1} range where bimetallic mixed oxide phases were reported.[11]

The XPS and Raman spectra suggest that in the Fe-Cr-Si-O materials the metal oxide species are highly interdispersed and can come in close contact with each other during the calcination procedure thus favoring the formation of the bimetallic mixed oxide phase. The absence of such a phase in the reference sample might be attributed to a poor interdispersion of the chromium and iron oxide species.

Additional information about chromium speciation was obtained from IR spectroscopy. The IR spectra of 3/6, 5/5 and 7/3 Fe-Cr-Si-O, 7/3 Fe-Cr/SiO_2 (r) and of silica prepared by calcination of metal-free silsesquioxane **1**, were measured under ambient conditions and are provided in Figure 5.3.

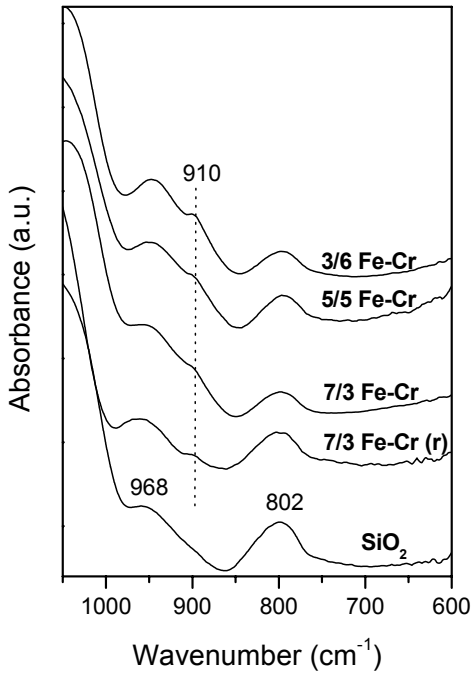

Figure 5.3 Infrared spectra of the Fe-Cr-Si-O materials and of Fe-Cr/SiO_2 (r) reference sample.

Pure silica exhibits the symmetrical Si–O–Si stretching vibration at ~803 cm^{-1}, along with a band at ~968 cm^{-1} due to the symmetric stretch of Si–OH groups.[13] The ~968 cm^{-1} band present a shoulder at about ~910 cm^{-1} for all the chromium containing

samples. This shoulder is not observed in the IR spectra of silica or Fe-Si-O sample (this spectrum is not shown for sake of brevity). Comparison with literature data suggests that dichromates are also present on the surface of the iron-chromium containing samples as these species alone absorb in the 900 – 950 cm^{-1} .[14]

The chemical state of iron in Fe-Cr-Si-O materials and the reference sample was also investigated by means of Mössbauer spectroscopy. Mössbauer spectra have been recorded at 300 K, 77 K and 4.2 K. For sake of brevity only the spectra recorded at 4.2 K are shown in Figure 5.4.

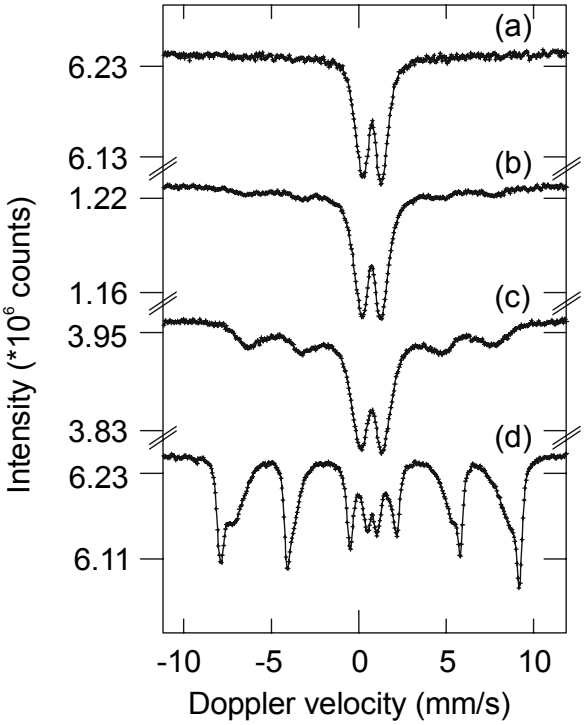

Figure 5.4 ^{57}Fe Mössbauer spectra recorded at 4.2 K for (a) 3/6 Fe-Cr-Si-O, (b) 5/5 Fe-Cr-Si-O, (c) 7/3 Fe-Cr-Si-O and (d) 7/3 Fe-Cr/SiO_2 (r).

The parameters of all Mössbauer measurements are included in Table 5.3. The Mössbauer spectra recorded at 300 K and 77 K of the Fe-Cr-Si-O materials all show a quadrupole doublet with spectral parameters that indicates a high-spin Fe^{3+} state. At

4.2 K, however, differences appear in the spectra. Whereas the 3/6 Fe-Cr-Si-O sample (Figure 5.4 a) shows only a quadrupole doublet, the 5/5 and 7/3 Fe-Cr-Si-O materials (Figure 5.4 b and c) reveal both a quadrupole doublet and a magnetic component, which is composed of six lines.

Table 5.3 Mössbauer parameters of the Fe-Cr-Si-O materials and 7/3 Fe-Cr/SiO_2 (r) reference.

Material	Temperature (K)	Isomer shift (mm/s)	Quadrupole splitting (mm/s)	Hyperfine field (T)	Spectral contribution (%)
3/6 Fe-Cr-Si-O	300	0.62	1.12		100
	77	0.73	1.12		100
	4.2	0.73	1.15		100
5/5 Fe-Cr-Si-O	300	0.61	1.10		100
	77	0.72	1.12		100
	4.2	0.73	1.19		24
		0.71	0.00	43.0	76
7/3 Fe-Cr-Si-O	300	0.60	1.09		100
	77	0.71	1.15		100
	4.2	0.71	1.31		48
		0.72	0.02	43.4	52
7/3 Fe-Cr/SiO_2	300	0.60	0.70		78
		0.63	0.10	48.7	22
	77	0.73	0.72		64
		0.74	0.10	52.3	36
	4.2	0.77	0.61		15
		0.75	0.11	53.1	28
		0.74	0.03	48.0	57

The Mössbauer spectra recorded for the reference material, 7/3-Fe-Cr/SiO_2 (r), (Figure 5.4 d) present a different view. Most significantly, the spectrum of this material, which was recorded at 300 K, shows a quadrupole doublet with spectral parameters that differs strongly from the parameters analyzed for the doublets found in the 300 K spectra of the Fe-Cr-Si-O materials. In addition to this quadrupole doublet, a sextuplet with well-defined lines is observed. This magnetic component,

which grows in intensity at lower temperature, has spectral parameters that strongly indicate the presence of large α-Fe_2O_3 particles. Moreover, a second magnetic component with less well-defined lines is observed at 4.2 K. This component with an average hyperfine field of *ca.* 48 T most likely belongs to small iron oxide particles, which vary in size from 2 to 4 nm and have more amorphous character than the aforementioned α-Fe_2O_3 particles.

These measurements clearly indicate that different iron-containing phases are formed, depending on the method of preparation. Whereas the method of impregnation of mesoporous silica leads to a rather inhomogeneous mixture of different iron oxide clusters, the method based on silsesquioxane precursors leads to a more homogeneous phase. This phase is most likely a solid solution of α-Fe_2O_3 and Cr_2O_3 oxides. It is known that the crystal structures of these phases are the same and that they can easily mix.[15] Such a mixed oxide is more likely to be formed than a spinel phase, since the latter would require Fe^{2+} ions, which have not been observed in the Mössbauer spectra. Note also that besides monochromate species very small clusters of Cr_2O_3 were detected by Raman spectroscopy in the calcined chromium silsesquioxane **3**.[1b] An indication for the formation of a mixed oxide is the presence of a magnetic component in the Mössbauer spectra of 5/5 Fe-Cr-Si-O and 7/3 Fe-Cr-Si-O materials that were measured at 4.2 K (Figure 5.4 b and c). This magnetic component has a hyperfine field close to 43 T, which is too small for an iron oxide phase. It is known that an increasing amount of Cr_2O_3 in a α-Fe_2O_3 phase leads to a reduction of the observed hyperfine field.[16] Because TEM indicates that there is no difference in the sizes of the metal oxide particles observed for the different Fe-Cr-Si-O materials, we attribute the differences in intensity of the magnetic component, found in the 4.2 K Mössbauer spectra, to variations in the Fe : Cr ratio in these oxides. This could also explain the disappearance of the 698 cm^{-1} Raman band for the 3/6 Fe-Cr-Si-O sample.

High resolution transmission electron microscopy is a widely used technique that can provide information about the dispersion and size of the metal oxide particles on the support surface. Examination of the Fe-Cr-Si-O materials and of the 7/3 Fe-Cr/SiO_2 (r) reference with high resolution TEM, yielded images that confirm the

presence of metal oxide particles on the silica surface. The Fe-Cr-Si-O samples showed very small and well dispersed metal oxide particles of about 2 – 4 nm size as exemplified in Figure 5.5 a for 7/3 Fe-Cr-Si-O. On the contrary, large and non-uniformly dispersed crystalline particles of about 10 – 30 nm can be observed on the reference sample, as shown in Figure 5.5 b.

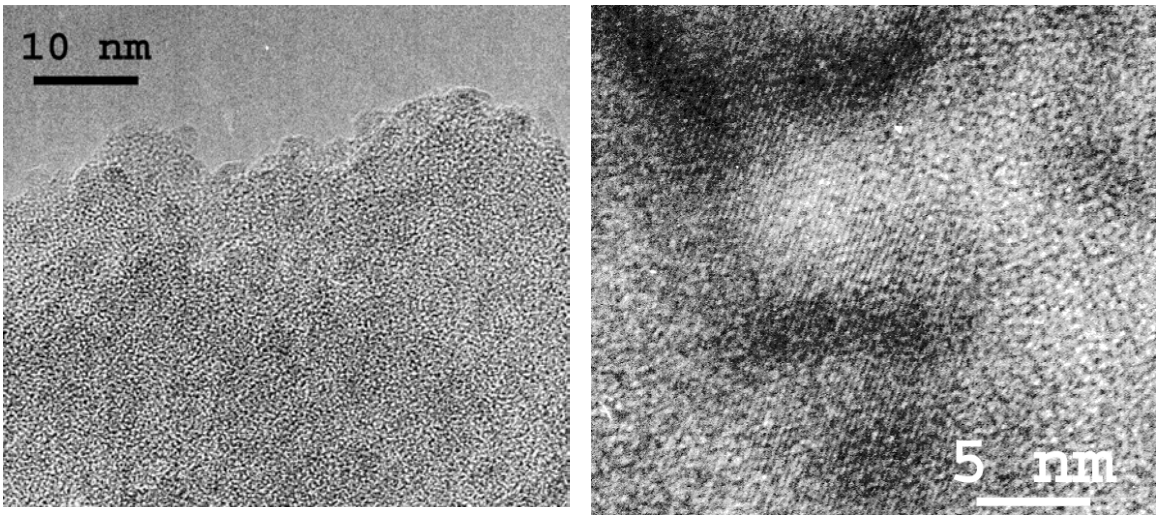

(a) 7/3 Fe-Cr-Si-O (b) 7/3 Fe-Cr/SiO_2 (r)

Figure 5.5 TEM micrographs of (a) 7/3 Fe-Cr-Si-O and (b) 7/3 Fe-Cr/SiO_2 (r).

No lattice fringes could be observed for the metal oxide particles present on 7/3 Fe-Cr-Si-O sample suggesting that they have an amorphous character. According to Raman and Mössbauer spectra these small particles should consist of a bimetallic mixed oxide phase. The presence of particles on 3/6 Fe-Cr-Si-O sample (not shown here for sake of brevity) and the absence of a magnetic sextuplet in the 4.2 K Mössbauer spectrum of this sample indicate that the particles consist in this case of a non-magnetic metallic oxide phase. This phase is probably also a bimetallic mixed oxide since no particles were observed by TEM on the surface of a 10 % Cr-Si-O material and a 3 % Fe-Si-O material did show a magnetic sextuplet in the 4.2 K Mössbauer spectrum.

The large crystalline particles present on the surface of the reference sample allowed us to measure the lattice fringe spacings and the obtained values (d = 1.59, 2.68, 3.70 Å) indicate a good fit with a α-Fe_2O_3 (hematite) phase (d = 1.59, 2.69, 3.68 Å, JCPDS file No. 86-0550). This finding is in agreement with Raman and Mössbauer spectra of the reference sample. As expected, these large hematite particles were also visible in the XRD pattern of the reference sample, as shown in Figure 5.6.

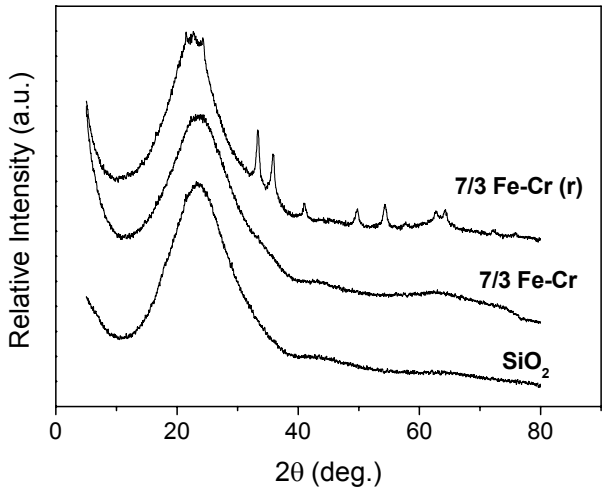

Figure 5.6 XRD patterns of 7/3 Fe-Cr-Si-O, 7/3 Fe-Cr/SiO_2 (r) and of SiO_2.

The average diameter of these particles estimated from line broadening analysis is 21 nm, which is in the size range observed with TEM. The XRD patterns of 7/3 Fe-Cr-Si-O and of silsesquioxane derived silica, shown also in Figure 5.6 for comparison, present only a broad band around 20-30° 2θ angle usually assigned to amorphous silica.[17] This is to be expected for the 7/3 Fe-Cr-Si-O sample since the bimetallic mixed oxide particles observed with TEM are too small anyway to generate diffraction patterns even if they would be crystalline.

Summarizing we can conclude that TEM and XRD results are in good agreement with Raman and Mössbauer spectra. Together, they clearly indicate the formation of bimetallic mixed oxide particles in the silsesquioxane derived Fe-Cr-Si-

O materials and the formation of separate phases of iron oxide and chromates in the impregnated Fe-Cr/SiO_2 (r) reference sample.

5.3.3 Catalytic tests

Transition metal oxides supported on silica, alumina or zeolites have been found to be active catalysts in gas phase ammonia oxidation with oxygen to nitrogen and water, an environmentally important process.[18] It was also shown that CrO_3/SiO_2 catalyst is very active but not very selective in this reaction giving 100 % conversion with only 51 % selectivity at 250 °C.[1b] On the other hand, the iron-exchanged Y zeolite showed little activity but very high selectivity in this reaction giving 13 % conversion with 96 % selectivity at 400 °C.[18]

The silsesquioxane derived Fe-Cr-Si-O catalysts have been tested in ammonia oxidation and compared with the reference catalyst prepared via impregnation method. The reactions were performed in the 200 – 400 °C temperature range. The conversion and selectivity to N_2 versus temperature obtained on Fe-Cr-Si-O catalysts with various compositions, Fe-Si-O and Cr-Si-O are plotted in Figure 5.7.

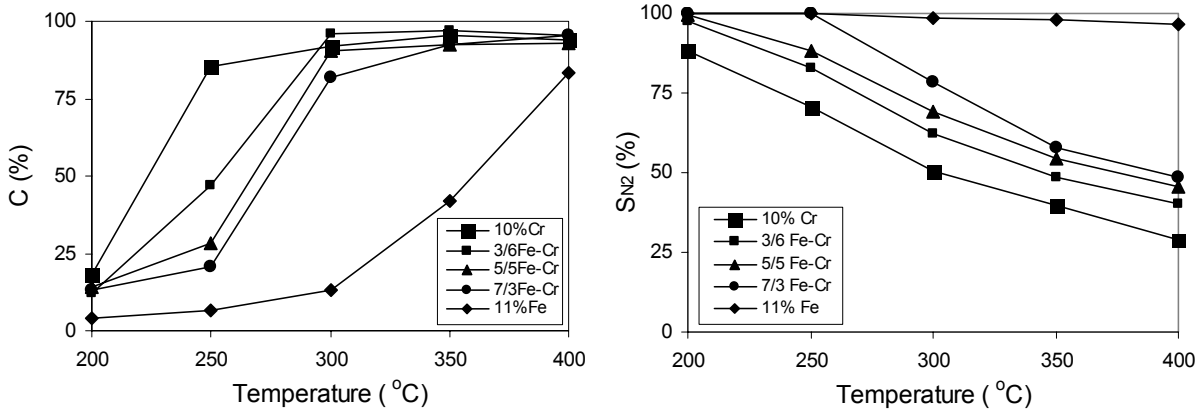

Figure 5.7 NH_3 conversion and selectivity to N_2 versus temperature on Fe-Cr-Si-O, Cr-Si-O and Fe-Si-O catalysts: (a) conversion (b) selectivity.

It can be noticed that at 250 °C the conversions of the Fe-Cr-Si-O catalysts are situated between the conversions of Fe-Si-O and Cr-Si-O samples and they increase with the chromium loading. The conversions increase also with the temperature and above 300 °C the Fe-Cr-Si-O and the Cr-Si-O catalysts have similar conversions. The selectivities of the Fe-Cr-Si-O catalysts show an opposite variation, the best selectivity being observed for the sample with the highest iron loading, namely 7/3 Fe-Cr-Si-O. It was also observed that at 250 °C the 10 % and 5 % Cr-Si-O catalysts have different conversions but the same selectivity, which indicates that at this temperature the selectivity does not depend on conversion or chromium content. Accordingly, the higher selectivities observed for Fe-Cr-Si-O catalysts, compared to the 10 % Cr-Si-O sample, should be attributed to other catalytic species than those present on chromium only containing catalyst. On the other hand, the activity of iron only containing catalyst, 11 % Fe-Si-O, is too small at 250 °C to attribute the higher selectivities of the Fe-Cr-Si-O samples to a simple additive effect of isolated iron and chromium species. Thus, the major catalytic species on the Fe-Cr-Si-O catalysts are most probably bimetallic iron-chromium mixed oxides. This interpretation is supported by the catalytic tests performed with the reference catalyst.

The conversion and selectivity to nitrogen versus temperature obtained on 7/3 Fe-Cr-Si-O, 5 % Cr-Si-O and 7/3 Fe-Cr/SiO_2 (r) catalysts are presented in Figure 5.8.

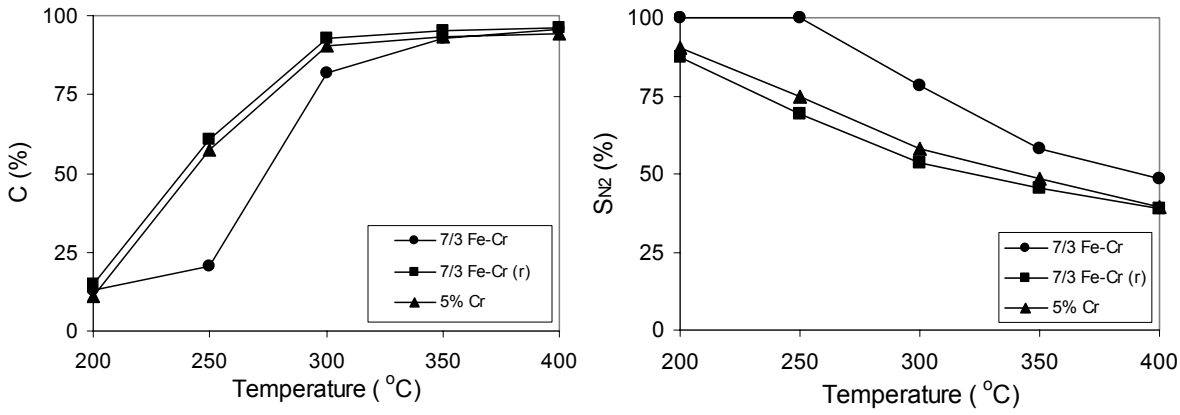

Figure 5.8 NH_3 conversion and selectivity to N_2 versus temperature on 7/3 Fe-Cr-Si-O, 7/3 Fe-Cr/SiO_2 (r) and 5 % Cr-Si-O catalysts: (a) conversion (b) selectivity.

The results show that the 7/3 Fe-Cr-Si-O catalyst is less active but much more selective than the reference sample which has the same composition. At 250 °C, the selectivity of the 7/3 Fe-Cr-Si-O sample is 100 %, while it is only 69 % for the 7/3 Fe-Cr/SiO_2 (r) reference. Moreover, the selectivity of the reference catalyst is almost identical to that of a 5 % Cr-Si-O sample that contains only chromium. Thus, the behavior of the reference catalyst correlates well with the characterization data of this sample, which indicates the severe segregation of the iron and chromium species.

This recommends the metallasilsesquioxane mixtures as versatile precursors to silica based catalysts containing very small and well dispersed particles of bimetallic mixed metal oxides.

5.4 Conclusions

Microporous amorphous bimetallic Fe-Cr-Si-O materials with different metal ratios were prepared by calcination of silsesquioxane mixtures of **1**, **2**, and **3**. The variation of the textural properties, metal dispersion and speciation with the metal content were investigated by various complementary techniques.

Fe-Cr-Si-O materials possess high surface areas and uniformly controlled micropores with an average pore size diameter around 6-7 Å. Metal oxide speciation appears to be significantly different from the one observed for these metals in the individually calcined metal silsesquioxanes. Iron oxide and monochromates, respectively, are the predominant species in the calcined **2** and **3** precursors while very small particles (2-4 nm) of bimetallic mixed oxides are the major species in Fe-Cr-Si-O materials. This suggests that the metal oxide species are highly interdispersed and can come in close contact with each other during the calcination procedure thus favoring the formation of the bimetallic mixed oxide phase.

A reference catalyst containing 7 % Fe and 3 % Cr prepared via impregnation showed only chromate species and large particles (10-30 nm) of iron oxide. A silsesquioxane-derived catalyst of similar composition was much more selective in ammonia oxidation than the reference catalyst. This recommends the

metallasilsesquioxane mixtures as versatile precursors to silica based catalysts containing very small and well dispersed particles of mixed metal oxides.

References

1. (a) K. Wada, M. Nakashita, M. Bundo, K. Ito, T. Kondo and T. Mitsudo, *Chem. Lett.*, 1998, 659. (b) N. Maxim, H. C. L. Abbenhuis, P. J. Stobbelaar, B. L. Mojet and R. A. van Santen, *Phys. Chem. Chem. Phys.*, 1999, 18, 4473. (c) N. Maxim, P. C. M. M. Magusin, P. J. Kooyman, J. H. M. C. van Wolput, R. A. van Santen and H. C. L. Abbenhuis, *Chem. Mater.*, 2001, 13, 2958. (d) K. Wada, K. Yamada, T. Kondo and T. Mitsudo, *Chem. Lett.*, 2001, 12.
2. N. Maxim, A. Overweg, P. J. Kooyman, J. H. M. C. van Wolput, R. W. J. M. Hanssen, R. A. van Santen and H. C. L. Abbenhuis, *J. Phys. Chem. B*, in press.
3. F. J. Feher, T. A. Budzichowski, R. L. Blanski, K. J. Weller and J. W. Ziller, *Organometallics*, 1991, 10, 2526.
4. (a) M. M. Dubinin and L. V. Radushkevich, *Proc. Acad. Sci. USSR*, 1947, *55*, 331. (b) G. Horwath, and K. Kawazoe, *J. Chem. Eng. Japan*, 1983, *16*, 470.
5. (a) S. Brunauer, P. H. Emmett and E. Teller, *J. Am. Chem. Soc.*, 1938, 60, 309. (b) E. P. Barrett, L. G. Joyner and P. P. Halenda, *J. Am. Chem. Soc.*, 1951, 73, 373.
6. J. H. Scofield, *J. Electron Spectrosc. Relat. Phenom.*, 1976, 8, 129.
7. F. Rouquerol, J. Rouquerol and K. Sing in *Adsorption by Powders & Porous Solids – Principles, Methodology and Applications*, Academic Press: London, 1999.
8. (a) B. A. Morrow and A. J. Mcfarlan, *J. Non-Cryst. Solids*, 1990, 120, 61. (b) C. J. Brinker, R. J. Kirkpatrick, D. R. Tallant, B. C. Bunker and B. Montez, *J. Non-Cryst. Solids*, 1988, 99, 418.
9. P. MacMillan, *Am. Mineral.*, 1986, 69, 622.
10. (a) B. M. Weckhuysen, I. E. Wachs and R. A. Schoonheydt, *Chem. Rev.*, 1996, 96, 3327. (b) F. D. Hardcastle and I. E. Wachs, *J. Mol. Catal.*, 1988, 46, 173. (c) D. S. Kim, J. M. Tatibouet and I. E. Wachs, *J. Catal.*, 1992, 136, 209.
11. (a) S. C. Tjong, *Mater. Characteriz.*, 1991, 26, 29. (b) P. Fabis, R. Heiderbach, C. Brown and T. Rockett, *Corrosion*, 1981, 37, 700.

12. (a) D. L. A. de Faria, S. V. Silva and M. T. de Oliveira, *J. Raman Spectrosc.*, 1997, 28, 873. (b) F. Perez-Robles, F. J. Garcia-Rodriguez, S. Jimenez-Sandoval and J. Gonzales-Hernandez, *J. Raman Spectrosc.*, 1999, 30, 1099.
13. (a) M. R. Boccuti, K. M. Rao, A. Zecchina, G. Leofanti and G. Petrini, *Stud. Surf. Sci. Catal.*, 1989, 48, 133. (b) A. Zecchina, S. Bordiga, S. Spoto, L. Marchese, G. Petrini, G. Leofanti and M. Padovan, *J. Phys. Chem.*, 1992, 96, 4985.
14. (a) A. Zecchina, E. Garrone, G. Ghiotti, C. Morterra and E. Borello, *J. Phys. Chem.*, 1975, 79, 966. (b) H. Stammreich, D. Sala and K. Kawai, *Spectrochim. Acta*, 1961, 17, 226.
15. T. C. Gibb and N. N. Greenwood in *Mössbauer Spectroscopy*, Chapman and Hall Ltd., 1971.
16. G. Shirane, D. E. Cox and S. L. Ruby, *Phys. Rev.*, 1962, 125, 1158.
17. C. Real, M. D. Alcala and J. M. Criado, *J. Am. Ceram. Soc.*, 1996, 79, 2012.
18. (a) L. Gang, B. G. Anderson, J. van Grondelle and R. A. van Santen, *Catal. Today*, 2000, 61, 179. (b) E. T. C. Vogt, A. Boot, J. W. Geus and F. J. J. G. Janssen, *J. Catal.*, 1988, 114, 313. (c) Y. Li and J. N. Armor, *Appl. Catal. B*, 1997, 13, 131.

Summary

The activity and selectivity of heterogeneous catalysts generally depend on the state of metal dispersion (particle size), structure (shape and morphology), metal composition and metal-support interaction. Catalytically active metals are usually dispersed on supports in order to dilute the size of the active metal crystallites to a diameter from twenty to several hundred angstroms and thereby prevent further metal agglomeration that would reduce the surface area. On the other hand, the properties of catalysts often depend on their preparation method. For example, the dispersion and size distribution of metal crystallites, their spatial distribution on the support, the homogeneity of components in a multicomponent catalyst, the porosity, surface area and pore size distribution of a support are all sensitive functions of the precursors used and the preparation conditions. Various methods for the preparation of heterogeneous metal catalysts have been developed to achieve high activity and selectivity, such as impregnation, sol-gel, coprecipitation, solid state reaction, etc. Although these methods are conventionally used for production of commercial catalysts, sometimes they do not provide a good control of particle size distribution and metal composition, mainly because of the complicated reactions involved in the catalyst preparation procedures. If preformed complexes, which already contain the desired ratio of components, are used as precursors it is possible to prepare highly homogeneous multicomponent catalysts. The use of these compound precursors guarantees that the different metal components are atomically mixed in the precursor. In spite of the promising features of this preparation method only a few examples of catalysts prepared via this way are present in literature.

This thesis describes the development of a novel methodology for synthesis of microporous metallosilicate catalysts based on calcination of metal silsesquioxane precursors (preformed complexes). Metal silsesquioxanes are compounds from a well-known class of soluble nanostructured silicon based metal complexes. Nowadays, the metals incorporated into the Si/O skeleton of silsesquioxanes include main group, early and late transition metals. As showed in this thesis, the calcination of metal silsesquioxanes produces amorphous microporous materials characterized by high surface area, narrow pore size distribution and high metal oxide dispersion being therefore promising catalysts.

The characterization of the resulting materials was mainly directed towards features, which are essential for catalysis such as surface area, pore size distribution, metal speciation and dispersion, etc. The catalytic properties were only briefly investigated to prove the catalytic activity and help illustrate some principles. The research was developed on three phases, which explored ways to make the proposed methodology more flexibile.

In the first phase different metal silsesquioxanes were calcined and the resulting materials were investigated by various complementary characterisation techniques. Chapter 2 investigates the properties of a Cr-Si-O material prepared from

a chromium silsesquioxanes precursor. Thermogravimetry and mass spectrometry methods were used to get insights into the transformation mechanism of this molecular precursor into an heterogeneous catalyst. It is showed that, during the calcination, the nearly complete combustion of the organic alkyl groups takes place while an amorphous microporous silica matrix is formed. The textural properties were measured via N_2 physisorption and evaluated from different models. They indicate high surface areas of about 400 – 600 m^2/g and an average pore diameter around 6 – 7 Å. The main species were monochromates like in the non calcined precursor. Chapter 3 describes Mg-Si-O and Al-Si-O catalysts derived from silsesquioxanes of earthy-alkaline and earthy metals. We showed here that textural properties such as surface area and pore volume can be easily adjusted by varying the calcination conditions, while the pore size distribution remains practically unchanged. Metal state and dispersion estimated from XPS, EDX, solid state MAS ^{29}Si and ^{27}Al NMR and HRTEM measurements suggest that the aluminum is present in Al-Si-O materials mainly as isolated metal ions incorporated in the amorphous silica framework and also as small crystalline metal oxide particles of a few nanometers (< 5 nm) which are well dispersed throughout the silica. IR spectroscopy of adsorbed acetonitrile showed that both Al-Si-O materials are strong Lewis acids. Mg-Si-O and Al-Si-O were briefly tested as catalysts in 1-butanol dehydration. Mg-Si-O gave both dehydrogenation and dehydration, while on Al-Si-O only dehydration and cracking reactions occurred.

The individually calcined metal silsesquioxanes have a fixed metal content. In order to overcome this disadvantage for the potential catalytic applications of these materials, in the second phase, we made a successful attempt to adjust the metal content in the metallosilicate synthesis. Thus, chapter 4 investigate in detail a series of Fe-Si-O materials with iron contents in 1 – 11 wt% range prepared via calcination of mixtures of iron silsesquioxane and metal-free silsesquioxane. A good homogeneity of the precursor mixture was ensured by solubilization in THF and subsequent drying. A combination of techniques including DRUV-Vis, Raman, IR of adsorbed NO, XPS, Mossbauer and TEM was used to follow the variation of the textural properties, metal dispersion and speciation with the iron content along the whole mixing series.

The calcination of these mixtures produced Fe-Si-O materials having basically the same properties as the individually calcined iron silsesquioxane. The N_2 physisorption indicates high surface areas and the same narrow pore size distribution as observed for Cr-Si-O, Mg-Si-O or Al-Si-O, while the XPS show that iron is homogeneously distributed throughout the materials. The TEM and the spectroscopic analysis of the Fe-Si-O materials indicate that the iron is present mainly as small iron oxide particles highly dispersed throughout silica and to a minor extent as clustered and isolated species. The particle size distribution was estimated to be about 2-8 nm for 11 % Fe-Si-O and 2-4 nm for samples with lower iron content. The predominance of iron oxide particles in the Fe-Si-O materials suggests a different behavior of the iron silsesquioxane during calcination in comparison with the aluminium or chromium silsesquioxane where mainly isolated metal oxide species were detected after calcination. This was attributed to the different propensity to hydrolysis of M-O-Si bonds from different metallasilsesquioxanes. It is known that the large predisposition of iron precursors to hydrolysis restricts its incorporation in zeolite frameworks to very low concentrations. The high dispersion of iron in Fe-Si-O materials should therefore be associated with a low mobility of the hydrolyzed iron

species, which hamper the formation of bulk iron oxide and help to preserve the high dispersion from the initial precursors mixture. These materials showed catalytic activity in NH_3 oxidation and N_2O decomposition.

Bimetallic oxide catalysts are used extensively in many important industrial processes and often they are better than their single-metal counterparts in terms of catalytic activity and/or selectivity. Therefore, in the third phase, a series of bimetallic M-Si-O catalysts are prepared from calcination of iron, chromium and metal-free silsesquioxane mixtures. This is described in chapter 5 where a careful investigation of the metal speciation is performed. Metal oxide speciation appears to be significantly different from the one observed for these metals in the individually calcined metal silsesquioxanes. The iron oxide and monochromates are the predominant species in the calcined iron and chromium precursors, while very small particles (2-3 nm) of bimetallic mixed oxides are the major species in Fe-Cr-Si-O materials. This suggests that the metal species are highly interdispersed and can come in close contact with each other during the calcination procedure thus favoring the formation of the bimetallic mixed oxide phase. On the contrary, a reference catalyst containing 7 % Fe and 3 % Cr prepared via impregnation method showed only chromate species and large particles (10-30 nm) of iron oxide. A silsesquioxane-derived catalyst of similar composition was much more selective in ammonia oxidation than the reference catalyst. This recommends the metallasilsesquioxane mixtures as versatile precursors to silica based catalysts containing very small and well dispersed particles of mixed metal oxides. Moreover, this novel synthesis method seems to be suitable for automatization.

Samenvatting

De activiteit en selectiviteit van heterogene katalysatoren hangt in het algemeen samen met de mate van metaal dispersie (deeltjesgrootte), structuur (vorm en morfologie), samenstelling en metaal-drager interactie. Katalytisch actieve metalen worden meestal verdeeld over een drager om de grootte van de actieve metaal kristalletjes te beperken tot een diameter variërend van twintig tot honderden ångstroms om metaalagglomeratie te voorkomen, die het actieve oppervlak zou verminderen. De eigenschappen van katalysatoren hangen vaak samen met de manier van bereiden. Bijvoorbeeld, de dispersie en grootteverdeling van metaal kristallietjes, hun ruimtelijke verdeling op de drager, de homogeniteit van componenten in een uit meerdere componenten bestaande katalysator, drager oppervlak, en poriegrootteverdeling van een drager zijn allemaal zeer gevoelig voor de gebruikte precursors en de condities waaronder de katalysator bereid wordt. In het verleden zijn verscheidene methodes ontwikkeld om een zo actief en selectief mogelijk katalysator te bereiden, zoals impregnatie, sol-gel methodes, coprecipitatie, vaste-stof reacties, etc. Hoewel deze methodes al wijd en zijd toegepast worden in de productie van commerciële katalysatoren, geven ze soms geen goede controle over de deeltjesgrootteverdeling en metaal verdeling, meestal vanwege de gecompliceerde reacties die tijdens de katalysatorbereiding plaatsvinden. Als van tevoren bereide complexen, die al de gewenste verhouding van componenten bevatten, worden gebruikt als precursor, is het mogelijk om zeer homogene multi-component katalysatoren te bereiden. Het gebruik van deze precursor-verbindingen garandeert dat de verschillende metalen op atomaire schaal gemengd zijn in deze precursors. Ondanks het feit dat deze bereidingswijze veelbelovend lijkt, zijn er uit de literatuur nog maar weinig voorbeelden bekend, waarbij katalysatoren op deze manier bereid werden.

Dit proefschrift beschrijft de ontwikkeling van een nieuwe methode om microporeuze metallosilicaat katalysatoren te bereiden, gebaseerd op het calcineren van metaal silsesquioxaan precursors (van tevoren gesynthetiseerde complexen). Metaal silsesquioxaan complexen zijn verbindingen van een bekende klasse van oplosbare nano-gestructuureerde metaal complexen, gebaseerd op silicium. Heden ten dage zijn er metaal silsesquioxaan complexen bekend met metalen uit de hoofdgroep, en vroege en late overgangsmetalen. Zoals beschreven in dit proefschrift, wordt na het calcineren van metaal silsesquioxanen materialen verkregen die gekarakteriseerd worden door hoge specifieke oppervlaktes, nauwe poriegrootteverdelingen en hoge metaaloxide dispersies, waardoor deze veelbelovende katalysatoren zouden kunnen zijn.

De karakterisatie van de verkregen materialen was vooral gericht op eigenschappen, die essentieel zijn voor de katalyse zoals specifiek oppervlak, poriegrootteverdeling, metaal speciatie en dispersie, etc. De katalytische eigenschappen werden verkend om de katalytische activiteit aan te tonen, en om

enkele principes te verduidelijken. Het onderzoek werd verdeeld in drie fases, die manieren onderzochten om de voorgestelde methodologie flexibeler te maken.

Tijdens de eerste fase werden verschillende metaal silsesquioxaan complexen gecalcineerd en de verkregen materialen werden onderzocht met meerdere, elkaar aanvullende karakteriseringmethodes. Hoofdstuk 2 beschrijft de eigenschappen van een Cr-Si-O materiaal, verkregen uit een silsesquioxaan chroom precursor. Thermogravimetrische en massaspectrometrische methodes werden gebruikt om inzicht te verkrijgen in het omvormingsmechanisme van deze moleculaire precursor in een heterogene katalysator. Er werd aangetoond dat tijdens de calcinering de organische zijgroepen bijna geheel worden verbranden, terwijl tegelijkertijd een amorfe microporeuze silica matrix wordt gevormd. De textuureigenschappen werden gemeten met stikstof-fysisorptie en de resultaten werden geïnterpreteerd met meerdere modellen. Deze gaven hoge specifieke oppervlakken (400 tot 600 m^2/g) en een gemiddelde poriediameter tussen de 6 en 7Å. De meest voorkomende chroom species waren monochromaten, net zoals in de niet-gecalcineerde precursor. Hoofdstuk 3 beschrijft Mg-Si-O en Al-Si-O katalysatoren, bereid uit aardalkali- en hoofdgroepmetalen. We toonden in dit hoofdstuk aan dat textuureigenschappen zoals specifiek oppervlak en porievolume eenvoudig aangepast kunnen worden door de calcinerings-omstandigheden te veranderen, terwijl de poriegrootteverdeling nagenoeg onveranderd blijft. De oxidatietoestand en de chemische omgeving van het metaal en dispersie, bepaald uit XPS, EDX, vaste-stof MAS ^{29}Si en ^{27}Al NMR, en HRTEM metingen gaven aan dat het aluminium in deze materialen voornamelijk aanwezig is als geïsoleerde metaalionen, die ingebed zijn in een amorfe silica matrix, en als kleine kristallijne metaaloxide deeltjes ter grootte van een paar nanometer (<5 nm) die goed verspreid zijn door de silica. Infrarood spectroscopie van geadsorbeerd acetonitril toonde aan beide Al-Si-O materialen sterk Lewis-zuur zijn. Mg-Si-O and Al-Si-O werden kort getest als katalysator in de dehydratatie van 1-butanol. Mg-Si-O gaf zowel dehydrogenatie als dehydratatie, terwijl op Al-Si-O alleen dehydratatie en kraakreacties plaatsvonden.

De individueel gecalcineerde silsesquioxaan metaal complexen hebben een vast metaalgehalte. Om dit nadeel voor de potentiële katalytische toepasbaarheid te overwinnen, hebben we in de tweede fase een succesvolle stap genomen om het metaalgehalte te variëren in de metallosilicaat bereiding. In Hoofdstuk 4 wordt tot in details een serie Fe-Si-O materialen onderzocht met een ijzergehalte variërend van 1 tot 11 gewichtsprocent. Deze materialen werden bereid door mengsels van silsesquioxaan ijzer complexen en vrij ligand te calcineren. De homogeniteit van het precursor mengsel wordt verzekerd door het oplossen van beide precursors in THF en dit mengsel vervolgens in te dampen. Een combinatie van technieken (DRUV-Vis, Raman, infrarood absorptie van geadsorbeerd NO, XPS, Mossbauer en TEM) werd gebruikt om de afhankelijkheid van de textuureigenschappen, metaaldispersie en -speciatie te volgen van het ijzergehalte over de gehele serie.

Door het calcineren van deze mengsel werden Fe-Si-O materialen bereid die over het algemeen soortgelijke eigenschappen hadden als de apart gecalcineerde silsesquioxaan ijzer complexen. Stikstoffysisorptie gaf hoge specifieke oppervlaktes en dezelfde nauwe poriegrootteverdeling aan, net zoals voor Cr-Si-O, Mg-Si-O en Al-Si-O werden geobserveerd, terwijl XPS metingen aantoonden dat ijzer homogeen verdeeld was over de materialen. TEM en spectroscopische analyse van de Fe-Si-O

materialen geven aan dat ijzer voornamelijk aanwezig is als kleine metaaloxide deeltjes, die sterk verdeeld zijn door de silica matrix en ,in veel kleinere mate, als geclusterde en geïsoleerde species. Het veelvuldig voorkomen van ijzeroxide deeltjes in de Fe-Si-O materialen geeft een indicatie dat de ijzer silsesquioxaan verbinding zich anders dan de chroom of aluminium silsesquioxaan verbindingen gedraagt tijdens de calcinering, waar voornamelijk geïsoleerde metaaloxide species werden waargenomen. Dit werd toegeschreven aan de stabiliteit van de M-O-Si bindingen van de verschillende metaalsilsesquioxanen ten opzichte van hydrolyse. Uit de literatuur is bekend, dat door de sterke vatbaarheid van ijzer-precursors voor hydrolyse, het inbouwen van ijzer in zeolietstructuren beperkt is tot zeer lage concentraties. De hoge dispersie van ijzer in Fe-Si-O materialen zou veroorzaakt kunnen worden door de lage mobiliteit van de gehydrolyseerde ijzer species, waardoor de vorming van bulk ijzeroxide wordt verhinderd, en de oorspronkelijk hoge dispersie in de precursor behouden wordt. Deze materialen vertoonden activiteit in de katalytische oxidatie van ammoniak en de decompositie van N_2O.

Bimetallische metaaloxide katalysatoren worden wijd en zijd toegepast in vele belangrijke industriële processen en vaak zijn deze beter dan hun slechts één metaal bevattende tegenhangers in termen van katalytische activiteit of selectiviteit. De derde fase bestaat derhalve uit de bereiding van een serie van bimetallische M-Si-O katalysatoren, die bereid worden door calcinering van mengsel van silsesquioxaan-ijzer en –chroomcomplexen en vrij silsesquioxaanligand. In Hoofdstuk 5 wordt een nauwgezette studie van de metaal speciatie beschreven. De metaaloxide speciatie voor deze metalen lijkt significant anders te zijn dan in het geval van de individueel gecalcineerde complexen. De ijzeroxide deeltjes en monochromaten zijn de overheersende species in de gecalcineerde ijzer en chroom precursors, terwijl zeer kleine deeltjes (2-3 nm), bestaand uit bimetallisch gemengde oxides de meest voorkomende species zijn in Fe-Cr-Si-O materialen. Dit geeft aan dat de metaal species op atomaire schaal zeer goed gemengd zijn, en dat ze tijdens de calcineringsprocedure dicht bij elkaar in de buurt kunnen komen, hetgeen de vorming van bimetallisch gemengde oxide fasen bevordert. In scherp contrast hiermee toonde een referentiekatalysator met 7 % Fe en 3 % Cr, die werd bereid via een conventionele impregnatiemethode, alleen chromaat species en grote deeltjes ijzeroxide (10-30 nm). Een katalysator van vergelijkbare samenstelling die werd bereid met de silsesquioxaan-calcineringsmethode, was veel selectiever in de ammoniak oxidatie dan de eerdergenoemde referentiekatalysator. Dit maakt de metaalsilsesquioxaan mengsels veelzijdig toepasbare precursors voor op silica gebaseerde katalysatoren, die zeer kleine en goed verdeelde deeltjes van gemengde metaaloxides bevatten. Tevens lijkt deze nieuwe bereidingsmethode geschikt voor automatisering.

Publications

Cyclohexane oxidation over Zn-Cr-O catalysts

F. Patcas, N. Maxim, M. Alifanti, F. Buciuman,

Prog. Catal., 1999, 8(2), 54-60.

Chromium silsesquioxane based synthesis and characterization of a microporous Cr-Si-O material

N. Maxim, H.C.L. Abbenhuis, P.J. Stobbelaar, B.L. Mojet and R.A. van Santen,

Phys. Chem. Chem. Phys., 1999, 1, 4473-4477.

Development of a new combinatorial approach to multifunctional catalysts: metal silsesquioxanes as precursors to microporous metallosilicates

N. Maxim, H.C.L. Abbenhuis, P.C.M.M. Magusin and R.A. van Santen,

Chin. J. Chem., 2001, 19(1), 30-39.

Microporous Mg-Si-O and Al-Si-O Materials Derived from Metalsilsesquioxanes

N. Maxim, P.C.M.M. Magusin, P.J. Kooyman, J.H.M.C. van Wolput, R.A. van Santen and H.C.L. Abbenhuis,

Chem. Mater., 2001, 13(9), 2958.

Synthesis and Characterisation of Microporous Fe-Si-O Materials with Tailored Iron Content from Silsesquioxane Precursors

N. Maxim, A. Overweg, P.J. Kooyman, R.W.J.M. Hanssen, R.A. van Santen and H.C.L. Abbenhuis,

J. Phys. Chem. B, in press.

Synthesis and Characterisation of Microporous Bimetallic Fe-Cr-Si-O Materials from Silsesquioxane Precursors

N. Maxim, A. Overweg, P.J. Kooyman, A. Nagy, R.A. van Santen and H.C.L. Abbenhuis

J. Mater. Chem., to be submitted.

Acknowledgement

I would like first to express my gratitude to prof.dr. Rutger van Santen and dr. Erik Abbenhuis for the opportunity to work in this research group and on this attractive project. We had together many work meetings, which had an important role in my research and in my scientific development. I am also grateful to prof.dr. G. de With, for stimulating discussions and professional advice.

I would like to thank all other reading committee members, prof.dr. K. P. de Jong and prof.dr. G. J. Gruter, who reviewed the manuscript and made many valuable suggestions.

Many people from the SKA group have provided their invaluable help. I would like to acknowledge my colleagues Rob Hanssen, Danka Ptasinski, Benoit Heinrichs and John Severn for fruitful discussions. Many thanks are due to Peter Magusin and Eugene Oers for solid state NMR measurements, to Jos van Wolput for in-situ IR measurements, to Adelheid Elemans-Mehring for elemental analysis and to Peter Thune, Leon Coulier and Tiny Verhoeven for the XPS measurements. I am thankful also to Zhu Qingjun and Lu Gang for assistance with the catalytic tests. Many thanks as well to Wout van Herpen for technical support. Many thanks to all my colleagues from SKA for the warm ambiance during the work, lunch, borrel, and conferences.

I am indebted also to ing. Dick Klepper and especially to dr. Patricia Kooyman (National Centre for High Resolution Electron Microscopy - TU Delft) for TEM measurements. Many thanks also to ing. Nick Lousberg for EDX measurements and especially to dr. Arian Overweg (Interfacultair Reactor Insitute, Delft) for Mossbauer measurements. Prof. J.Th.M de Hosson (Groningen University) is acknowledged for assistance with FEG-SEM measurements.

Here is the place to express my sincere appreciation to my catalysis professors Ioan Sandulescu, Alfred Szabo, Emilian Angelescu and Vasile Parvulescu from University of Bucharest, Romania, who introduced me to the beautiful topic of catalysis.

Finally, I wish to express all my gratitude to my wife Monica and our daughter Andra for moral support and for their patience during the long evenings when I was working on my thesis.

Curriculum vitae

Nicolae Maxim was born on April 14th 1969 in Medias, Romania. He finished the high school ("Mathematics and Physics" High School, Suceava, Romania) in 1987. In 1988, he started his chemistry studies at the University of Bucharest, Romania. There, in the last year he worked in the group of prof.dr. Ioan Sandulescu on his graduation thesis "Aromatization of cyclohexane on Zn-ZSM-5 zeolites". He passed the graduation exam in June 1993 and received his University Diploma in Chemistry, specialty Catalysis. Afterwards, he worked as a researcher at the Laboratory of Chemical Technology and Catalysis, University of Bucharest.

In November 1998 he started his PhD thesis under supervision of prof.dr. R.A. van Santen in the Laboratory of Inorganic Chemistry and Catalysis at the Eindhoven University of Technology, which is a part of the Schuit Institute of Catalysis. The most important results of this work are described in this thesis.